

**ROLE OF A TOPOLOGICALLY CONSERVED  
ISOLEUCINE IN THE STRUCTURE AND FUNCTION OF  
GLUTATHIONE TRANSFERASES**

**Loren Fisher**

**A thesis submitted to the faculty of science, University of the Witwatersrand,  
Johannesburg, in fulfillment of the requirements for the degree of Master of  
Science.**

**Johannesburg, August 2005**

## **DECLARATION**

I declare that this thesis is my own, unaided work. It is being submitted for the degree of Master of Science in the University of the Witwatersrand, Johannesburg. It has not been submitted before for any degree or examination in any other University.

Loren Fisher

day of 2005.

I dedicate this work to those who have stood by me, who have made it worthwhile in the end.

To my parents, Nikki, Jo and Michelle

***”It is not so much that I have confidence in scientists being right, but that I have so much confidence in non-scientists being wrong”***

***Isaac Azimov***

## ABSTRACT

Proteins in the glutathione transferase family share a common fold. The close packing of secondary structures in the thioredoxin fold in domain 1 forms a compact hydrophobic core. This fold has a  $\beta\alpha\beta\alpha\beta\beta\alpha$  topology and most proteins/domains with this fold have a topologically conserved isoleucine residue at the N-terminus of  $\alpha$ -helix 3. Class Alpha glutathione transferases are one of 12 classes within the glutathione transferase family. To investigate the role of the conserved isoleucine residue in the structure, function and stability of glutathione transferases, homodimeric human glutathione transferase A1-1 (hGST A1-1) was used as a representative of the GST family. Ile71 was replaced with valine and the properties of I71V hGST A1-1 were compared with those of wildtype hGST A1-1. The spectral properties monitored using far-UV CD and tryptophan fluorescence indicated little change in secondary or tertiary structure confirming the absence of any gross structural changes in hGST A1-1 due to the incorporation of the mutation. Both wildtype and mutant dimeric proteins were determined to have a monomeric molecular mass of 26 kDa. The specific activity of I71V hGST A1-1 (130  $\mu\text{mol}/\text{min}/\text{mg}$ ) was three times that of wildtype hGST A1-1 (48  $\mu\text{mol}/\text{min}/\text{mg}$ ). I71V hGST A1-1 showed increased kinetic parameters compared to wildtype with a 10-fold increase in  $k_{\text{cat}}/K_{\text{m}}$  for CDNB. The increase in  $K_{\text{m}}$  of I71V hGST A1-1 suggests the mutation had a negative effect on substrate binding. The  $\Delta\Delta G$  for transition state stabilisation was  $-5.82$  kJ/mol which suggest the I71V mutation helps stabilise the transition state of the  $S_{\text{N}}\text{AR}$  reaction involving the conjugation of reduced glutathione (GSH) to 1-chloro-2,4-dinitrobenzene (CDNB). A 2-fold increase in the  $\text{IC}_{50}$  value for I71V hGST A1-1 (11.3  $\mu\text{M}$ ) compared to wildtype (5.4  $\mu\text{M}$ ) suggests that the most noticeable change due to the mutation occurs at the H-site of the active site. Conformational stability studies were performed to determine the contribution of Ile71 to protein stability. The non-superimposability of I71V hGST A1-1 unfolding curves and the decreased  $m$ -value suggest the formation of an intermediate state. The conformational stability of I71V hGST A1-1 (16.5 kcal/mol) was reduced when compared to that of the wildtype (23 kcal/mol). ITC was used to dissect the binding energetics of *S*-hexylglutathione to wildtype and I71V hGSTA1-1. The ligand binds 5-fold more tightly to wildtype hGST A1-1 (0.07  $\mu\text{M}$ ) than I71V hGST A1-1 (0.37  $\mu\text{M}$ ). The I71V mutant

displays a larger negative  $\Delta C_p$  than wildtype hGST A1-1 ( $\Delta\Delta C_p = -0.41$  kJ/mol/K). This indicates that a larger solvent-exposed hydrophobic surface area is buried for I71V hGST A1-1 than for wildtype hGST A1-1 upon the binding of *S*-hexylglutathione. Overall the results suggest that Ile71 conservation is for the stability of the protein as well as playing a pivotal indirect role in catalysis and substrate binding.

## ACKNOWLEDGEMENTS

I would like to thank the following people:

Professor Heini Dirr who has helped and encouraged me throughout my studies.

Dr. Jonathan Burke for his assistance, support and motivation.

The members of the Protein Structure-Function Research Programme, University of the Witwatersrand for all their assistance.

The University of the Witwatersrand and the South African National Research Foundation for financial support.

## TABLE OF CONTENTS

<b>ABSTRACT</b>	iv
<b>ACKNOWLEDGEMENTS</b>	vi
<b>ABBREVIATIONS</b>	x
<b>LIST OF FIGURES</b>	xii
<b>LIST OF TABLES</b>	xiv

### CHAPTER 1

#### INTRODUCTION

1.1 Protein folding and stability.....	1
1.2 Conserved residues in proteins.....	2
1.2.1 folding nucleus.....	3
1.2.2 hydrophobic cores.....	3
1.2.3 hydrophobic core residues.....	4
1.3 Thioredoxin superfamily.....	6
1.4 Glutathione transferase family.....	6
1.5 Thioredoxin fold.....	6
1.6 Environment of topologically conserved isoleucine.....	11
1.7 Human class alpha glutathione transferase A1-1.....	13
1.8 Catalytic mechanisms of hGST A1-1.....	13
1.9 Conformational stability of GSTs.....	17
1.10 Objectives.....	17

### CHAPTER 2

#### METHODS AND MATERIALS

Materials.....	19
Methods	
2.1 Verification of wild type and mutant pKHA1 plasmids.....	19
2.2 Expression and protein purification.....	20
2.3 Protein concentration determination.....	21

2.4 Spectroscopic studies	
2.4.1 Fluorescence spectroscopy.....	22
2.4.2 Far-UV circular dichroism spectroscopy.....	22
2.4.3 ANS fluorescence.....	23
2.5 Steady-state enzyme kinetics	
2.5.1 Standard CDNB conjugating assay.....	23
2.5.2 Kinetic parameters ( $K_m$ , $V_m$ , $k_{cat}$ , $k_{cat}/K_m$ ).....	24
2.5.3 Inhibition by G-site and H-site ligands.....	24
2.6 Unfolding/refolding and conformational stability studies	
2.6.1 Urea-induced equilibrium unfolding studies.....	25
2.6.2 Reversibility of unfolding.....	25
2.6.3 Analysis of the unfolding transition.....	25
2.7 Thermodynamic studies using isothermal titration calorimetry.....	27
2.7.1 Protein and ligand sample preparation.....	28
2.7.2 Correction of protein concentration due to light scattering effects.....	28
2.7.3 Thermodynamics of ligand binding to the active site of I71V hGST A1-1.....	28
2.7.4 Isothermal titration calorimetry data analysis.....	29

## CHAPTER 3

### RESULTS

3.1 Confirmation of the identities of wildtype and I71V pKHA1 plasmids.....	30
3.2 Expression and protein purification.....	30
3.3 Spectroscopic studies	
3.3.1 Fluorescence spectroscopy.....	32
3.3.2 Far-UV circular dichroism spectroscopy.....	34
3.3.3 ANS fluorescence.....	34
3.4 Steady-state enzyme kinetic properties	
3.4.1 Kinetic parameters ( $K_m$ , $k_{cat}$ , $k_{cat}/K_m$ ).....	38
3.4.2 Inhibition by G-site and H-site ligands.....	49
3.5 Conformational stability studies	
3.5.1 Reversibility of unfolding.....	49



3.5.2 Urea-induced equilibrium unfolding studies.....	53
3.6 Thermodynamic characterisation of <i>S</i> -hexylglutathione-hGST A1-1 binding ....	59

## **CHAPTER 4**

### **DISCUSSION**

4.1 Plasmid identity confirmation and assessment of protein purification.....	66
4.2 Verification of the structural integrity of I71V hGST A1-1 .....	66
4.3 Steady-state enzyme kinetic properties.....	68
4.4 Inhibition properties of the I71V and wildtype hGST A1-1.....	71
4.5 Conformational stability studies .....	73
4.6 Thermodynamic characterization of <i>S</i> -hexylglutathione binding to I71V hGST A1-1.....	75
4.7 Conclusion .....	79

## **CHAPTER 5**

<b>REFERENCES</b> .....	81
-------------------------	----

## ABBREVIATIONS

$\Delta C_p$	change in heat capacity
$\Delta G(H_2O)$	Gibbs free energy of unfolding in the absence of denaturant
$\Delta H$	change in enthalpy
$\Delta S$	change in entropy
$A_{280}$	Absorbance at 280 nm
Amp	ampicillin
ANS	8-anilino-1-naphthalene sulphonate
bp	base pairs
CD	circular dichroism
CDNB	1-chloro-2,4-dinitrobenzene
CM Sepharose	carboxymethyl sepharose
$C_m$	urea-induced midpoint of unfolding
EA	ethacrynic acid
EDTA	ethylenediaminetetra-acetic acid
GSH	reduced glutathione
G-site	glutathione binding site
$GSO_3^-$	glutathione sulphonate
GST	glutathione transferase
hGSTA1-1	human class alpha glutathione transferase with two type one subunits
H-site	hydrophobic electrophilic binding site
I	monomeric intermediate
I71V	replacement of wild-type isoleucine (I) with valine (V) at position 71
IPTG	isopropyl- $\beta$ -D-thio-galactoside
ITC	isothermal titration calorimetry
$K_a$	association constant
$k_{cat}$	catalytic constant
$K_d$	dissociation constant
kDa	kilodalton

$K_m$	Michaelis-Menten constant
LB	Luria-Bertani
L-site	non-substrate ligand binding site
$M_r$	relative molecular mass
$m$ -value	susceptibility of protein to denaturant i.e., co-operativity of unfolding transition
$N_2$	native folded dimer
NaCl	sodium chloride
OD	optical density
ORF	open reading frame
PDB	Protein Data Bank
rpm	revolutions per minute
SDS-PAGE	Sodium Dodecyl Sulphate polyacrylamide gel electrophoreses
U	unfolded monomer
UV	ultraviolet
v/v	volume by volume
$V_m$	maximum velocity
X	xenobiotic
$\epsilon_{280}$	molar extinction coefficient at 280 nm

The IUPAC-IUBMB one and three letter codes for amino acids are used

Enzyme: Glutathione Transferase (EC 2.5.1.18)

## LIST OF FIGURES

	<b>PAGE</b>
Figure 1. Sequence alignment	9
Figure 2. Thioredoxin fold in domain 1 of hGST A1-1	10
Figure 3. Environment of Isoleucine residue in the thioredoxin fold	12
Figure 4. Crystal structure of human glutathione transferase	14
Figure 5. GST catalysed S <sub>N</sub> AR reaction mechanism	16
Figure 6. Wildtype pKHA1 nucleotide sequence aligned with I71V pKHA1	30
Figure 7. (a) SDS PAGE analysis of wildtype and I71V hGST A1-1 (b) SDS PAGE calibration curve	31
Figure 8. Fluorescence emission spectra for excitation at 295 nm	33
Figure 9. Fluorescence emission spectra for excitation at 280 nm	35
Figure 10. Far-UV circular dichroism spectra	36
Figure 11. Fluorescence emission spectra of ANS in complex with hGST A1-1	37
Figure 12. Michaelis-Menten plot of velocity versus the substrate concentration (CDNB) for wildtype hGST A1-1.	39
Figure 13. Michaelis-Menten plot of velocity versus the substrate concentration (GSH) for wildtype hGST A1-1.	40
Figure 14. Michaelis-Menten plot of velocity versus the substrate concentration (CDNB) for I71V hGST A1-1.	41
Figure 15. Michaelis-Menten plot of velocity versus the substrate concentration (GSH) for I71V hGST A1-1.	42
Figure 16. Linear plots of velocity versus the substrate concentration (GSH) for wildtype hGST A1-1.	43
Figure 17. Linear plots of velocity versus the substrate concentration (CDNB) for wildtype hGST A1-1.	44
Figure 18. Linear plots of velocity versus the substrate concentration (GSH) for I71V hGST A1-1.	45

Figure 19.	Linear plots of velocity versus the substrate concentration (CDNB) for I71V hGST A1-1	46
Figure 20.	Inhibition of wildtype and I71V hGST A1-1 proteins with glutathione sulphonate	50
Figure 21.	Inhibition of wildtype and I71V hGST A1-1 proteins with ethacrynic acid.	51
Figure 22.	Urea-induced equilibrium unfolding of wildtype and I71V hGST A1-1 monitored by fluorescence	54
Figure 23.	Urea-induced equilibrium unfolding of wildtype and I71V hGST A1-1 monitored by circular dichroism.	55
Figure 24.	Urea-induced equilibrium unfolding of wildtype hGST A1-1 monitored by tryptophan fluorescence and CD	57
Figure 25.	Urea-induced equilibrium unfolding of I71V hGST A1-1 monitored by monitored by tryptophan fluorescence and CD including maximum wavelength emission	58
Figure 26.	A representative calorimetric titration profile of the binding of <i>S</i> -hexylglutathione to wildtype and I71V hGST A1-1.	61
Figure 27.	Calorimetric titration profiles of the binding of <i>S</i> -hexylglutathione to I71V hGST A1-1	62
Figure 28.	Temperature-dependence of the thermodynamic parameters for <i>S</i> -hexylglutathione binding to wildtype and I71V hGST A1-1	65

## LIST OF TABLES

		<b>PAGE</b>
Table 1.	Members of the thioredoxin-like superfamily	7
Table 2.	Summary of steady state kinetic properties of wildtype and I71V hGST A1-1	48
Table 3.	Summary of inhibition characteristics of wildtype and I71V hGST A1-1	52
Table 4.	Thermodynamic parameters for wild type and I71V hGST A1-1	56
Table 5.	Energetics of the interaction between wildtype and I71V hGSTA1-1 with <i>S</i> -hexylglutathione at different temperature.	63

# CHAPTER 1

## INTRODUCTION

### 1.1 Protein folding and stability

The question of how efficiently and reliably individual protein sequences achieve their native state following synthesis on the ribosome is one of the most challenging problems in structural biology (Dobson and Karplus., 1999). The folding of a protein into its unique three-dimensional conformation uses the information contained within its linear amino acid sequence (Anfinsen, 1973). The folding of a protein is crucial to its role in the cell since the biochemical character of a protein is determined by its three-dimensional state. Proteins have many different biological functions and play a crucial role in all biological functions. The genetic information of a cell is ultimately expressed as protein; in other words, proteins provide the functional flesh to genes. The gene encodes information specifying the proteins sequence of amino acids or the primary structure however the molecular mechanisms of protein folding, i.e., how the amino acid sequence directs the formation of the functional three-dimensional state, although extensively studied, is still unknown.

The principles that govern protein folding are not fully understood. The two most widely accepted explanations for the control of protein folding are the thermodynamic hypothesis proposed by the work of Anfinsen (1973) and the kinetic hypotheses based on calculations of Levinthal (1968). The thermodynamic hypothesis states that the three-dimensional state of the native protein represents the lowest Gibbs free energy state. This implies that the kinetic pathway taken results in the most stable product with the lowest Gibbs free energy.

The kinetic hypothesis proposed by Levinthal however assumes that the final product is formed via the fastest route possible and thus the final product may or may not be the most thermodynamically stable state. Levinthal calculated the number of different conformations about the polypeptide backbone that were possible before the final folded product was reached and showed that a polypeptide backbone of 100 residues would require  $4 \times 10^{72}$  years to sample each polypeptide conformation. Considering most

proteins manage to fold into their native state within seconds or minutes and therefore the thermodynamically most stable state may not be attained suggests that protein folding is kinetically controlled (Levinthal, 1968).

The complete folding pathway of a protein involves an initial unfolded state, possible stable intermediates and a final native or folded state. Proteins in biological environments can exist in a variety of different states and the state of a given protein under particular conditions depends on a complex series of thermodynamic and kinetic factors. The maintenance of the proteins three-dimensional state is dependent on the cooperative interactions of a large number of non-covalent forces such as hydrogen bonds and hydrophobic interactions. These interactions are thought to be the most dominant forces involved in stabilizing the folded state (Dill, 1990).

## **1.2 Conserved residues in proteins**

A particularly puzzling problem is how highly divergent sequences fold to give the same overall topology, as is the case with different proteins within a superfamily (Michnick *et al.*, 1998). Despite low sequence identity (<20%), proteins within a superfamily still have common structural features. Structurally related proteins have the necessary information embedded in their sequences for their common fold. Sequence comparisons of protein superfamily members with divergent sequences and functions can identify conserved amino acids that probably contribute to maintaining the fold. There are a number of reasons for the conservation of a residue. Conserved residues could either play a role in the structure and stability of a protein, where they are involved in long-range interactions to maintain the tertiary structure of a protein, or they could have a catalytic or binding function. Often conserved residues are found at a protein's active site and have a key role in the activity of the enzyme. Conserved residues may also be involved in the folding mechanism of a protein. It is not uncommon for structurally similar proteins to have only 10% sequence identity suggesting that many residues have no critical role in structure determination and that folding is determined by a limited number of residues (Friedberg *et al.*, 2001).



### 1.2.1 Folding nucleus

Natural selection conserves functionally important residues in proteins to preserve biological activity and likewise conserves residues critical to protein stability. Does evolution also maintain sequence to ensure folding? (Plaxco *et al.*, 2000). Both experimental (reviewed by Fersht (1997)) and theoretical (reviewed by Pande (1998)) studies suggest that protein folding occurs via the formation of a small region of native like structure that serves as a nucleus upon which further residues condense in a process that can be compared to a phase transition (Plaxco *et al.*, 2000). The formation of a nucleus in protein folding is known as the nucleation-condensation mechanism. An interesting aspect of this nucleation-condensation mechanism of protein folding is its relation to protein evolution. Mutation of residues making up the folding nucleus affect the folding rate to a much greater extent than elsewhere in a protein. It has thus been concluded that if there were evolutionary control of the folding rate, positive selection pressure would then be applied to residues within the folding nucleus. This evolutionary pressure is shown by the fact that folding nucleus residues are significantly more conserved than the non-folding regions (Mirny *et al.*, 2001). This does not mean that nucleus residues are the only conserved residues in any family of proteins. This also does not mean that folding nucleus residues are more conserved than other residues within the protein core since the nucleus is equally important for protein stability and for folding.

### 1.2.2 Hydrophobic cores

Generally in a globular protein the hydrophobic residues are found in the interior of a protein, whereas the hydrophilic residues are found on the exterior. It is the hydrophobic residues buried in protein interiors that form the hydrophobic cores. The burial of hydrophobic groups (the hydrophobic effect) serves as a primary source of stabilising energy in folded proteins. Core residues drive collapse through the hydrophobic effect and form stabilising van der Waals interactions through tight packing of the folded conformation (Di Nardo *et al.*, 2003). The hydrophobic effect is the energy of stabilisation provided by the transfer of hydrocarbon surfaces from solvent to the interior of a protein, which ranges between  $104 - 125 \text{ J mol}^{-1} \text{ \AA}^{-2}$  (Richards, 1977). The specific packing interactions within a core are important for maintaining the stability of the protein and it has been shown that these buried groups are packed as efficiently as

crystals of organic molecules (Richards, 1977). The inside of a typical protein contains side-chains that fit together with a striking complementarity, like pieces of a three dimensional jigsaw puzzle (Behe *et al.*, 1991). It is likely that such efficient packing originates in natural side chain complementarity, and indeed, the shapes of many residues do seem potentially complementary. For example the planar rings of aromatic residues – phenylalanine, tryptophan, and tyrosine - could stack like aromatic bases in nucleic acids (Behe *et al.*, 1991). It is commonly accepted that hydrophobic core residues of proteins are more conserved than non-core residues due to evolutionary and physicochemical constraints of side chain packing in the core (Kellis *et al.*, 1988; Dill, 1990).

### **1.2.3 Hydrophobic core residues**

In light of the previous statement on side chain complementarity, core residues could be conserved due to the fact that the packing environment within the core cannot tolerate any other residue besides those that complement the environment perfectly. Core residues drive hydrophobic collapse of the polypeptide chain and form stabilizing van der Waals interactions through tight packing in the folded conformation. Conserved clusters of hydrophobic residues without an obvious functional role are suggested to belong to the folding nucleus of the proteins (Mirny *et al.*, 2001).

Some core randomisation studies have shown that hydrophobic cores can tolerate drastic changes in composition without losing the ability to fold or function. Studies have shown that many mutations introduced into protein sequences have little effect on the proteins activity (Rennell *et al.*, 1991; Suckow *et al.*, 1996) or stability (Milla *et al.*, 1994). Most mutations that had an effect were located either in the hydrophobic core or the proteins functional sites. The core residues where conservations seemed to be important, were mostly hydrophobic, but their identity was not crucial and different hydrophobic residues could replace one another without affecting the structure (Lim *et al.*, 1989; Bowie *et al.*, 1990). These results imply that mere hydrophobicity is a sufficient requirement for core composition (Di Nardo *et al.*, 2003).

While it has been shown that some protein folds can tolerate drastic substitutions to their core and still function, specific packing interactions appear to be crucial for the

maintenance of maximal stability (Di Nardo *et al.*, 2003) and proper core packing interactions are important determinants of the proteins precise structure and stability (Ventura *et al.*, 2004). It is true that improving the packing of the core does not necessarily increase the stability of proteins. Mutagenesis studies involving the substitution of one amino acid with another smaller amino acid within a core generally creates cavities, which reduce the stability to an extent that has been found to be proportional to the loss in van der Waals contacts (Di Nardo *et al.*, 2003). Also small to large mutations often decrease the stability due to the introduction of strains and/or unfavourable van der Waals contacts (Lim *et al.*, 1989; Baldwin *et al.*, 1993).

When choosing suitable changes for folding studies, it is especially important to use nondisruptive mutations to introduce as small a change as possible and not affect the overall structure of the protein (Kellis *et al.*, 1988). Side chain truncation substitutions have been studied in a number of proteins containing hydrophobic cores (Kellis *et al.*, 1988; Eriksson, 1992). Side chain truncations such as the substitution of an isoleucine to a valine, involve the removal of a methyl (CH<sub>2</sub>) group, which decreases the number of van der Waals contacts that may be important in the stability of a protein. The removal of van der Waals contacts decreases the hydrophobic effect in the cavity and decreases the protein stability. The contribution of hydrophobic interactions to protein stability on small ribonuclease from *Bacillus amyloliquefaciens* was measured by truncating the hydrophobic side chains at an  $\alpha$  helix/ $\beta$  sheet interface. Mutations included an Ile  $\rightarrow$  Val, Ile  $\rightarrow$  Ala and Phe  $\rightarrow$  Leu. It was reported that the removal of a CH<sub>2</sub> group destabilized the enzyme by 4.6 kJ/mol (Kellis *et al.*, 1988).

The effects of mutations underscore the uniquely important role of interactions involving the mutated residue in molecular stability and catalysis. The thermodynamic and structural consequences of mutations depend, however, on the exact location within the hydrophobic core and vary from virtually no structural movement, which is usually coupled to maximum destabilization, to almost complete collapse of surrounding atoms into the cavity along with some compensation of the loss of free energy of stabilisation (Eriksson, 1992; Buckle *et al.*, 1996).

### 1.3 Thioredoxin superfamily

The thioredoxin fold has been identified in a large number of proteins and these proteins are grouped into the thioredoxin-like superfamily. There are at least 12 different protein families within the thioredoxin superfamily and these families are tabulated (Table 1). Although functions differ and sequence identity to thioredoxin is low (7%-28%), all members of the thioredoxin superfamily maintain the same characteristic fold in domain 1 (Holmgren *et al.*, 1975). Of these the Glutathione transferase (GST) family is the subject of this investigation.

### 1.4 Glutathione transferase family

The GSTs make up a supergene family of detoxification enzymes. GSTs catalyse the nucleophilic addition of reduced glutathione (GSH) to a wide range of compounds such as alkyl- and aryl halides, lactones, epoxides and esters (Mannervik *et al.*, 1988) and also display a ligand-binding function. GSTs have dimeric quaternary structures (molecular mass ( $M_r$ )  $\approx$  50 000) and exist as either homo- or heterodimeric structures (Cameron, 1995; Wallace *et al.*, 1999). The GST family is grouped into at least 12 classes: Alpha, Beta, Delta, Mu, Phi, Pi, Theta, Kappa, Sigma, Tau, Omega and Zeta (for review see (Sheehan, 2001)). Recently glutaredoxin-2 (Grx2) (Xia *et al.*, 2001), yeast prion protein Ure2p (Bousset, 2001) and chloride intracellular channel (Clic1) (Harrop *et al.*, 2001) protein have also been classified as members of the GST structural family by virtue of the fact that they possess the archetypal thioredoxin fold in domain 1 and contain an alpha helical domain 2. Generally GSTs within a class share greater than 60% sequence identity but between classes there is between 20 – 30% identity (Sheehan, 2001). Despite a low sequence identity proteins in the GST family have the same overall fold (Wallace *et al.*, 1999).

### 1.5 Thioredoxin fold

As stated, all members of the GST family contain the thioredoxin fold in domain 1 (for review see Sheehan (2001)). The thioredoxin fold comprises about 80 residues and is characterised by a  $\beta\alpha\beta\alpha\beta\beta\alpha$  topology (Holmgren *et al.*, 1975; Dirr, 1994; Martin, 1995). A mixed 4-strand  $\beta$  sheet, in the order 4312 with strand 3 antiparallel to the others is sandwiched between two layers of  $\alpha$ -helices. The fold is subdivided into an

**Table 1.** Members of the thioredoxin-like superfamily .

Glutathione S-transferase N-terminal domain (GST)
Protein disulphide isomerase (PDI)
Calsequestrin
Disulphide-bond formation facilitator (DsbA)
Thioltransferase
Phosducin
Endoplasmic reticulum ERP29
Splicesomal protein U5-15 kd
Disulphide bond isomerase C-terminal
Glutathione peroxidase-like
Thioredoxin-like 2Fe-2S ferredoxin
Arsenate reductase ArsC

Classification of the thioredoxin superfamily according to the Structural Classification Of Proteins server website at <http://scop.mrc-lmb.cam.ac.uk/scop> (Murzin *et al.*, 1995)

N-terminal  $\beta\alpha\beta$  motif and a C-terminal  $\beta\beta\alpha$  motif connected by a loop of residues that incorporates a third helix (Martin, 1995). The packing of secondary structures in the thioredoxin fold form a compact hydrophobic core. Alpha helices 1 and 3 as well as beta strands 1, 2 and 4 make up the hydrophobic core of the fold due to the packing of the alpha helices 1 and 3 against the one side of the beta sheet (Martin, 1995).

Although superimposed subunit structures indicate a great degree of similarity between the structures of domain 1 from the various GST classes, it is clearly apparent that the gene classes are characterised by specific structural features (Dirr, 1994). Class Mu has an extended and mobile loop called the Mu loop. This loop occurs in the connecting sequence between  $\beta 2$  strand and  $\alpha 2$  helix (Ji *et al.*, 1992). Alpha class enzymes are characterised by an additional 15 amino acid C-terminal  $\alpha$  helix,  $\alpha 9$  helix that has been shown to be crucial for catalysis (Board *et al.*, 1991). The recently determined structure for class Kappa enzymes show that domain 2 is inserted into the thioredoxin fold-containing domain 1. The all-alpha helical domain 2 is inserted between  $\alpha 2$  helix and  $\beta 3$  strand of the fold, yet the archetypal thioredoxin fold is still present (Ladner *et al.*, 2004). Figure 1 (A and B) show structure-based sequence alignments of representatives of the 12 classes in the GST family as well as Grx2, Ure2p and Clic1. Only the thioredoxin-like domain 1 of the proteins was aligned. The alignment shows that certain residues are conserved throughout the family, with 3 residues being conserved within the thioredoxin fold of domain 1.

There are five highly conserved amino acids that have been identified in all known GST sequences. The five conserved residues are Pro56, Asp61, Ile71, Gly150 and Asp157, numbered according to the Alpha class GST. Pro56, Asp61, Ile71 are all found within domain 1. Proline-56 has been determined to play an important role in the binding of glutathione to the G-site (Wang *et al.*, 1992). Ile71, Gly150 and Asp157 are found in the interior of the protein and may be necessary for determining and maintaining the fold and stability of the protein (Wilce *et al.*, 1994). Figure 2 is a representative structure of the thioredoxin fold to show the positioning of the conserved isoleucine residue (Ile71). This residue is situated in the hydrophobic core of the thioredoxin fold and, as mentioned, could have a possible role in the stability of the protein since core residues drive the

A) Alpha ag----vefeekfik-----sae**dl**d--klr**nd**gyLm-fqqvPMVeId-gmklVqtraIlnyIaskynly  
 Beta Sg----kdf**tlvs**Vd**l**mk**k**---r**len**g----dd**Y**fa--v**N**p-kGqV**PA**Ll**l**dd**gt**ll**t**egva**Im**qy**LAd**s**v**pd**r**  
 Delta Vg----ve**Ln**kl**I**n**l**ma-----g**eh**mk**pe**Fl**k**--i**N**p-qhcIP**TL**v**D**n-gfalwe**Sra**I**cty**La**eky**g**k**d  
 Mu yt**d**----ss**ye**ekr**Y**amgda--pdy**dr**s**q**W**l**--n**ek**fk**l**g**L**d-fpnLP**YL**id**g**-sr**kit**g**sna**I**m**ry**Lark**h**h**l  
 Phi e**K**n----ld**fel**vh**Vel**kd-----g**eh**k**ke**p**Fl**s--r**N**p-fGqV**PA**Fed**g**-dl**kl**fe**Sra**I**tqy**I**ah**ry**en**q  
 Pi Lad**q**g----q**sw**keev**Vt**-----v**et**wq**e**g**s**l**ka**--s**C**l-ygqLP**k**F**q**d**g**-dl**tly**q**snt**I**lrh**L**grt**l**gly**  
 Theta Ak**kn**g----Ip**Le**l**rt**V**d**l**vk**-----g**qh**k**s**ke**Fl**q--i**n**s-lGkLP**TL**k**d**g-d**fil**t**essa**I**liy**L**sck**y**q**T**p**  
 Kappa vl**cry**q**hl**wn**Ik**L**kl**r**pa**ll**ag**im**kd**s**gn**q-ppamv**ph**k**g**q-----y**ile**I**pl**l**k**q**l**f**q**V**p**  
 Sigma Fay**l**d----i**qy**ed**hr**I**e**-----q**ad**w**p**--e**ik**s--t**L**p-fgkIP**I**Le**vd**-g**lt**l**h**q**sla**I**ary**L**t**k**nt**d**la**  
 Tau g----lsy**ed**ve**E**d**ly**-----k**k**s**e**ll**l**k--s**N**pvhkkIP**V**L**I**h**n**-g**ap**v**ce**S**mi**I**l**q**y**I**dev**f**ast**  
 Omega g----ir**he**vin**In**l**k**-----n**k**p**ew**F**fk**--k**N**p-fGL**VP**l**en**s**q**q**l**iy**e**S**ai**T**c**  
 Zeta l**k**g----id**y**kt**vp**in**l**ik-----d**g**G**q**f**s**kd**F**q**a**--l**N**p-mkqVP**TL**k**I**d-g**it**ih**g**Sl**a**I**ey**Le**et**r**pt**  
 bbbb bbbb bbbb aaaaaaaaaa

B) Alpha r**M**e**s**Tr**w**l**L**aa**ag**ve**fe**ek**f**ik**s**ae-**dl**d**kl**rn**d**gyLm**f**qqv**PM**Ve**I**dg---m**k**l**V**q**t**ra**I**ln**y**I**a**sk**y**n--ly**g**k**d**-  
 Clic1 f**S**qr**L**fm**v**L**w**l**k**g**vt**fn**v**tt**V**d**t**kr**rt**---e**t**V**q**kl**C**pg**ge**l**P**F**L**ly**gt**---e**vh**t**d**tn**k**I**ee**f**Le**av**l**cp  
 Grx2 y**C**lk**A**rm**I**F**g**l**K**n**ip**v**el**h**v**ll**nd**--d**a**et**P**tr--m**V**g**q**k**g**VP**I**L**q**k**d**--d**s**ry**mp**e**S**md**I**v**h**y**VD**k**l**d**g**k**p**ll**t**g**k**r  
 Ure2p n**G**fk**V**aiv**L**se**L**g**fh**ynt**if**L**d**fn**l**G**eh**r**ap**e**F**v**s**v**N**pnar**v**P**AL**I**d**h**gm**dn**l**s**i**w**e**s**ga**l**ll**h**V**ln**ky**y--k**et**g**n**-  
 aaaaaaaaaa bbbb aaa a bbbb bbbb aaaaaaaaaa

**Figure 1.** Structure based sequence alignment of domain 1 of representatives of the glutathione transferase family whose 3D structures have been determined. Alignment was done using the COMPARER online server (Sali and Blundell, 1990). The results are shown in JOY format and the key for the alignment is shown below. Secondary structural elements are indicated, alpha helices (a) in red and beta strands (b) in blue. The conserved isoleucine residue (numbered according to human class alpha GST A1-1) and the topologically equivalent residues are shown in green.

A) Structure based sequence alignment of representatives of the 12 classes within the glutathione transferase family

B) Structure based sequence alignment of representatives of the glutathione transferase family. Class Alpha is used as a representative of the 12 classes within the family and other proteins in the alignment are glutaredoxin-2 (Grx2), chloride intracellular channel protein (clic1) and yeast prion protein Ure2p. These proteins show similar folds as hGST A1-1 but do not have glutathione conjugation activity.

JOY format key:			
solvent inaccessible UPPER CASE	X	hydrogen bond to other sidechain tilde	x~
solvent accesible lower case	x	hydrogen bond to mainchain amide <b>bold</b>	<b>x</b>
positive <i>italic</i>	x	hydrogen bond to mainchain carbonyl underline	<u>x</u>
<i>cis</i> -peptide breve	x	ç disulphide bond cedilla	ç
□ helix <b>red</b>	<b>x</b>	□ strand <b>blue</b>	<b>x</b>
310-helix <b>maroon</b>	x		

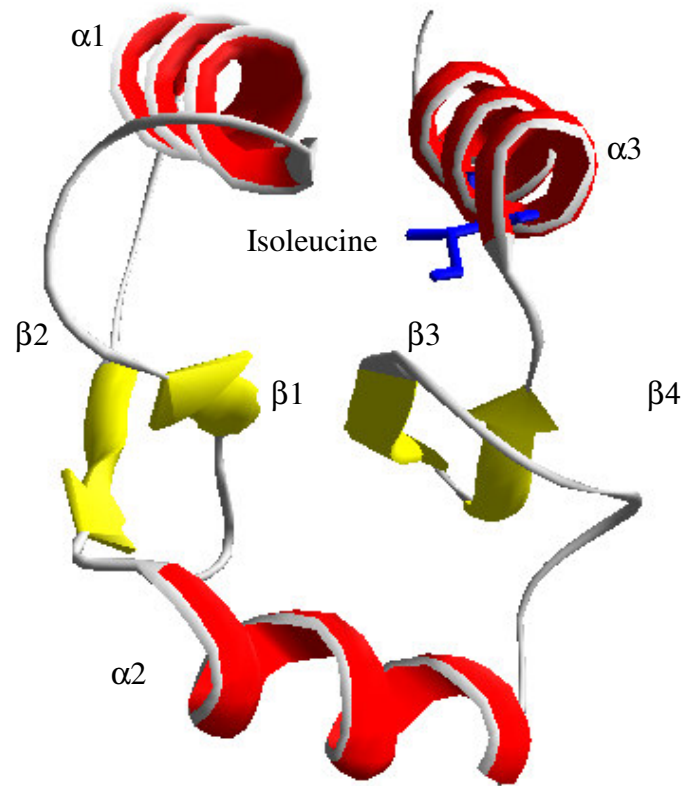


**Figure 2.** Ribbon representation of the thioredoxin fold in domain 1 of hGST A1-1. Alpha helices are shown in red and beta-strands in yellow. The topologically conserved isoleucine residue is indicated in blue. The figure was generated with Swiss-pdb Viewer (Guex *et al.*, 1997) using PDB file 1GUH (Sinning *et al.*, 1993).



hydrophobic collapse and form stabilizing van der Waals interactions through tight packing in the folded conformation (Kellis *et al.*, 1988; Dill, 1990). This conserved isoleucine residue is the subject for this study.

The topologically conserved isoleucine residue is present in 11/12 of the sequences aligned. In the sequence for Omega, where the topologically equivalent residue is not an isoleucine, comparisons show that this residue has been replaced with a threonine. Comparing the structures of the two amino acids, there is little difference in the bulk of the side chains and thus, in this sense, can be considered a conservative replacement. Given that proteins in the GST family have the same general structure human class Alpha glutathione transferase A1-1 (hGST A1-1) has been chosen to represent the 12 classes of GSTs to investigate the role of this highly conserved isoleucine.

### **1.6 Environment of the topologically conserved isoleucine**

When analysing the role of a conserved residue it is important to consider the residue type as well as its context within the environment of the protein. The question to ask is whether the residue is conserved for a specific function such as catalytic or structural, or due to physiochemical and evolutionary constraints? Figure 3 shows the isoleucine environment in domain 1 of hGST A1-1. The residues shown in red are those that form hydrophobic-hydrophobic contacts with the isoleucine. From Figure 3 it can be seen that isoleucine fits into a hydrophobic pocket formed by the surrounding hydrophobic residues in the interior of the hydrophobic core. It is important to note that the hydrophobic core of the thioredoxin fold is formed by  $\alpha$ -helices 1 and 3 and  $\beta$ -strands 1,3 and 4. The isoleucine as well as the hydrophobic residues packed around the isoleucine are all located within the hydrophobic core.

From the positioning of the isoleucine residue within its environment one can hypothesise that the residue is conserved due to evolutionary and physiochemical constraints of side chain packing. It could be that the isoleucine is conserved because the pocket in which it is found is conserved such that any other residue besides isoleucine would not complement the packing environment and thus not allow for the correct folding of the protein therefore rendering the protein enzymatically functionless.

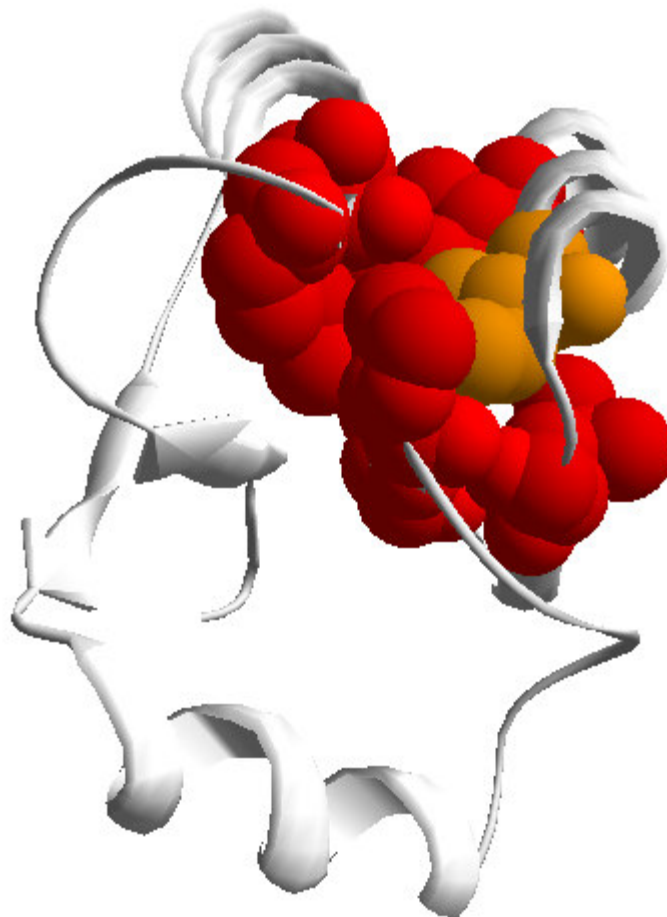


**Figure 3.** Spacefill representation of the isoleucine environment in domain 1 of hGST A1-1. The thioredoxin fold (grey) has been included to show the positioning of the isoleucine residue within the fold. Isoleucine is coloured orange. Residues that form hydrophobic-hydrophobic contacts with isoleucine are shown in red. The figure was generated with Swiss-pdb Viewer (Guex *et al.*, 1997) using PDB file 1GUH (Sinning *et al.*, 1993).

### **1.7 Human class Alpha glutathione transferase A1-1**

Human GSTs are named with respect to the class in which they fall and their subunit composition. Therefore hGST A1-1 refers to human class Alpha GST that is a dimer of two type 1 subunits (Armstrong, 1997). Human class Alpha glutathione transferase A1-1 (hGST A1-1) is the major isoenzyme found in human liver where it represents about 2 % of the cytosolic protein (Allardyce *et al.*, 1999). The homodimeric glutathione transferase A1-1 contains 221 amino acid residues per subunit and each subunit is composed, as is typical of GSTs, of two structurally distinct domains with hydrophobic cores (Figure 4). Domain 1 is a small thioredoxin-like N-terminal domain and domain 2 is a larger all-alpha-helical domain (Allardyce *et al.*, 1999; Wallace *et al.*, 1999). The subunits are related by a two-fold axis and each subunit contains one active site consisting of two adjacent substrate-binding sites; a specific glutathione binding site (G-site) and a less specific hydrophobic binding site (H-site) (Allardyce *et al.*, 1999; Wallace *et al.*, 1999). The conserved isoleucine residue under investigation is Ile71 in hGST A1-1 and the position of Ile71, located at the N-terminal of alpha helix 3, within the hGST A1-1 structure is shown in Figure 4.

### **1.8 Catalytic mechanisms of hGST A1-1**

Glutathione transferases catalyse the reaction that involves the  $S_NAR$  reaction of reduced glutathione (GSH) to a variety of electrophilic compounds. The catalytic mechanism involves a ternary complex formed by sequential addition of reduced glutathione and the electrophilic substrate to the active site of the enzyme (Armstrong, 1991). Class Alpha GST has a tyrosyl hydroxyl group that acts as a hydrogen bond donor to the sulphur atom of GSH. This lowers the  $pK_a$  of the thiol group in the enzyme•GSH complex so that it exists as an ionised form ( $GS^-$ ) at physiological pH. (Kolm *et al.*, 1992; Wang *et al.*, 1992; Armstrong, 1997). Class Alpha GST also incorporates an interaction between the  $N^\epsilon$  of Arg15 and the sulphur atom of GSH. The presence of this interaction is proposed to further promote the stabilisation energy of the thiolate and assist in lowering the  $pK_a$  of the tyrosyl hydroxyl group, thereby making it a better hydrogen bond donor (Sinning *et al.*, 1993; Bjornestedt *et al.*, 1995; Armstrong, 1997). The role of the C-terminal region of hGST A1-1 in catalysis has been proposed by several authors to contribute to the chemical step of the reaction as well (Nilsson *et al.*, 2002).

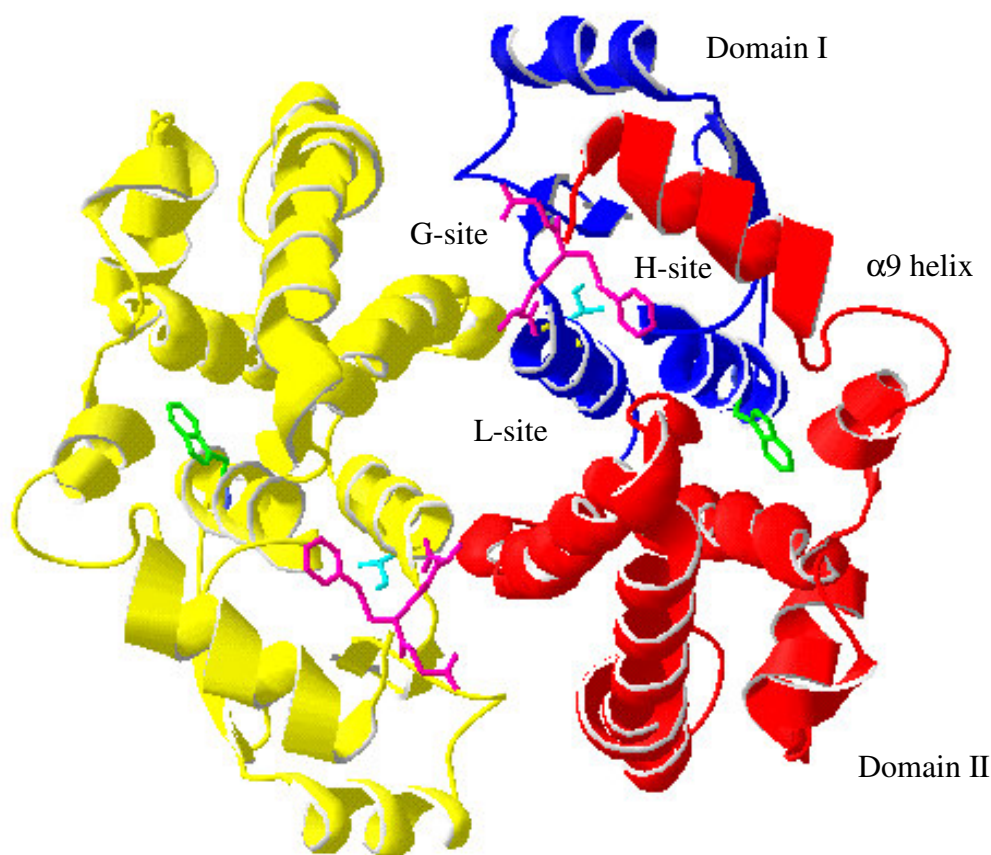


**Figure 4.** A ribbon diagram of the crystal structure of human glutathione transferase hGST A1-1 in complex with *S*-benzylglutathione, viewed parallel to the two-fold axis. One subunit is shown in yellow, the other indicating the two domains. Domains 1 ( $\alpha/\beta$ ) and 2 (all  $\alpha$  helical) are shown in blue and red respectively. The *S*-benzylglutathione (ball and stick) locates the G-site (occupied by glutathione) and the H-site (occupied by the benzyl moiety) and the L-site is unoccupied. *S*-benzyl glutathione is shown in pink. Trp20 is indicated in green and Ile71 in light blue. The alpha-9 helix forms a lid over the occupied active site and is also shown. This figure was generated using Swiss-pdb Viewer (Guex *et al.*, 1997) and the PDB file 1GUH was used (Sinning *et al.*, 1993).

The sequential mechanism of the S<sub>N</sub>AR reaction may be represented as follows:



where E is GST, R-X is the hydrophobic electrophilic substrate, GSH is reduced glutathione and GS<sup>-</sup> is the highly reactive thiolate anion. Due to the high GSH concentration in the cell (1-10 mM) it is likely that reduced GSH is complexed to the enzyme G-site before the arrival of the H-site substrate (Dirr, 1994). An example of such a reaction is shown in Figure 5.

GSTs are involved in S<sub>N</sub>AR reactions, example shown in Figure 5. The GSH/CDNB (1-chloro-2,4-dinitrobenzene) conjugation reaction is commonly used for assaying GST enzymatic activity and is therefore of crucial importance in understanding the kinetic mechanisms of these enzymes. The S<sub>N</sub>AR of this nitro-substituted aryl chloride proceeds via the formation of 1-chloro-1-(S-glutathionyl)-2,4-dinitrobenzene, an unstable Meisenheimer complex that is a transition state analogue (Graminski *et al.*, 1989).

With many nucleophiles and leaving groups, the formation of this Meisenheimer complex is the rate-limiting step of the reaction however the GSTs active site is able to stabilise the formation of this dead-end Meisenheimer complex for efficient S<sub>N</sub>AR reactions (Graminski *et al.*, 1989; Bico *et al.*, 1994). It has been said that the ability of the enzyme to stabilise a Meisenheimer complex is related to its ability to stabilise the transition state for formation of a Meisenheimer complex intermediate. Therefore the transition state for this reaction must in some sense resemble the Meisenheimer complex (Graminski *et al.*, 1989). The better an enzyme can stabilise the transition state of the reaction, the more efficient the reaction will be (Graminski *et al.*, 1989).

Although conserved throughout the GST superfamily, the role of Ile71 in catalysis has not yet been investigated. Due to the location of the residue within the hydrophobic core of the thioredoxin fold and its position close to the active site, one hypothesis is that this

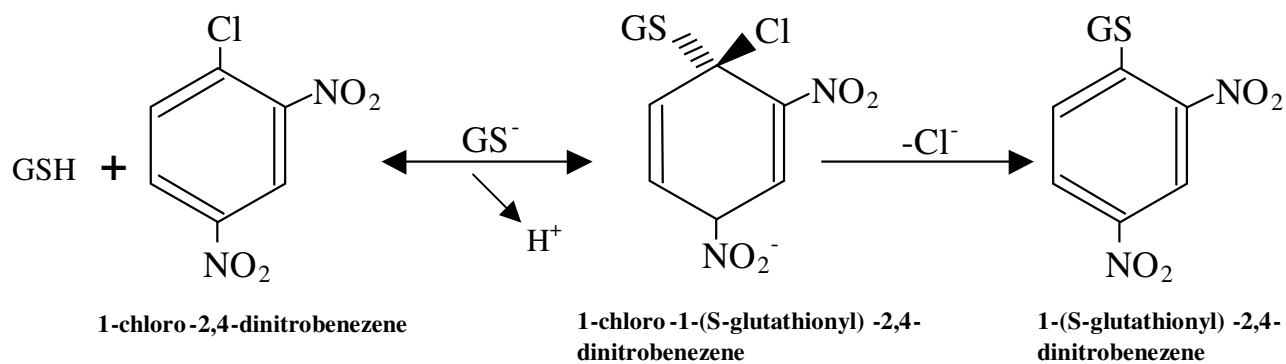


**Figure 5.** Schematic diagram showing the GST catalysed  $S_NAR$  reaction mechanism between CDNB and GSH, adapted from Graminski *et al.* (1989).

residue could, indirectly, play an important role in the catalytic mechanism of this enzyme by maintaining the positions of crucial active site residues.

### **1.9 Conformational stability of GSTs**

Differences in the conformational stabilities of the various GST classes have been observed. The equilibrium unfolding studies performed on class Alpha (Wallace *et al.*, 1998b), Pi (Erhardt *et al.*, 1995) and *Schistosoma japonicum* glutathione transferases (Kaplan *et al.*, 1997) are consistent with a highly cooperative two-state unfolding process involving the native dimer and unfolded monomer. The class Mu (Hornby *et al.*, 2000), Sigma (Stevens *et al.*, 1998) and Beta (Sacchetta *et al.*, 1993) however, display a multi-step equilibrium pathway involving stable monomeric intermediates, with class Mu enzymes displaying enhanced conformational stability compared to class sigma and beta enzymes. In contrast to equilibrium unfolding studies, stopped-flow kinetic studies of hGST A1-1 unfolding have indicated the existence of a three-state kinetic unfolding mechanism involving the folded dimer and unfolded monomer. Kinetic refolding study of the same enzyme showed the presence of structured monomers with native-like structures (Wallace *et al.*, 1998b; Wallace *et al.*, 1999).

### **1.10 Objectives**

Highly conserved residues in a particular group of structurally related enzymes become obvious candidates for playing crucial folding, structural and/or functional roles. The objective of this present study was to establish the role of a topologically conserved isoleucine residue located within a hydrophobic core of the GST family. A representative, hGST A1-1, of the thioredoxin-like superfamily was used to conduct the study. The investigation was carried out by studying the effects of mutating the conserved isoleucine to a valine (I71V). This residue is one of five highly conserved residues in hGST A1-1 and therefore determining the reasons for its conservation is of importance in understanding fully the structural and catalytic mechanisms of this protein. The results also add to our knowledge of structure and folding in general.

The hypothesis upon which this study was based was that, due to the hydrophobic nature of the Ile71 and its close packing within a hydrophobic environment, this residue plays a

role in the structure of the catalytic site and stabilisation of the enzyme. The questions posed were what effect does an Ile71 → Val mutation have on the catalytic activity, stability and folding of GST proteins? The prediction was that there would be a decrease in the stability of the protein due to the incorporation of an Ile71 → Val mutation. The extent of the destabilisation is predicted to be 1.1 kcal/mol or 4.6 kJ/mol, proportional to the removal of van der Waals contacts due to the removal of a methyl group. The result of this study will not only be relevant to the glutathione transferase family but to the members of the thioredoxin-like superfamily as well.



## CHAPTER 2

### EXPERIMENTAL PROCEDURES

#### Materials

The overexpression vector, pKHA1 encoding wildtype hGST A1-1 was a kind donation from Prof B. Mannervik (Department of Biochemistry, University of Uppsala, Sweden) (Stenberg *et al.*, 1992). The pKHA1 vector containing the open reading frame (ORF) sequence for the mutant protein, I71V hGST A1-1 was a gift from Dr. J. Burke (Protein Structure Function Research Programme, University of the Witwatersrand). Restriction enzymes *Sma*I, *Pvu*II and *Hind*III were purchased from Amersham Life Sciences (Sweden). Reduced glutathione (GSH) and 1-chloro-2,4-dinitrobenzene (CDNB) were purchased from Sigma Aldrich (USA). Ultrapure urea was purchased from Merck (Darmstadt, Germany). All other reagents were of analytical grade.

#### Methods

##### 2.1 Verification of wildtype and mutant pKHA1 plasmids

*Escherichia coli* BL21 DE3 cells transformed with the pKHA1 plasmid, which confers ampicillin resistance, were plated on Luria-Bertani (LB) agar plates containing 100 µg/ml ampicillin to select for successfully transformed cells. Overnight cultures of selected colonies were grown at 37°C in 2 ml LB liquid media (1% tryptone, 0.5% yeast extract, 0.5% NaCl and 100 µg/ml Amp). The plasmid DNA was isolated using a FlexiPrep kit (Amersham Biosciences, Sweden). Purified wildtype plasmid DNA was digested with *Sma*I, *Pvu*II and *Hind*III for 2 hours at 37°C. Mutant plasmid DNA was digested with *Sma*I to detect a translationally silent mutation engineered into the mutant plasmid and not present in the wildtype plasmid, for 6 hours at 30°C. Digested DNA together with an undigested control was analysed on a 1% (w/v) agarose gel (made up with TBE buffer comprising Tris, Borate and EDTA, pH 8.3) stained with 0.2% ethidium bromide. The sizes of the fragments were compared to a standard 1 kilobase DNA marker (GibcoBRL, USA).

## 2.2 Expression and protein purification

The pKHA1 encoded hGST A1-1 ORF is transcribed under the control of the pTac promoter, resulting in the translation of the hGST A1-1 protein. A structural analogue of allolactose, isopropyl- $\beta$ -D-thiogalactoside (IPTG), was used to induce hGST A1-1 ORF transcription. Optimal growth conditions for heterologous protein expression for both wildtype and mutant protein have previously been determined. The method was as follows; *Escherichia coli* BL21 cells transformed with wildtype and mutant plasmid were grown overnight in LB liquid media containing 100  $\mu$ g/ml ampicillin and 100  $\mu$ g/ml chloroamphenicol. Chloroamphenicol was only used for the mutant cultures since the BL21 cells transformed with the mutant plasmid also contain the pLys plasmid which confers chloroamphenicol resistance. A 50 times dilution of the culture was inoculated into LB broth with the same concentration of antibiotics and grown at 37°C with a shaker rotation of 250 rpm until mid exponential phase (0.3 – 0.6 OD<sub>600</sub>). At this point the transcription of hGST A1-1 was induced with 1 mM IPTG and 0.2 mM IPTG for wildtype and mutant plasmid respectively, for the overexpression of the protein. Cultures were incubated overnight. These cells were then pelleted by centrifugation for 20 minutes at 5000 xg. The pellets were resuspended in equilibration buffer (10 mM sodium phosphate, 1 mM EDTA, 0.02% sodium azide, pH 7.45) and frozen at - 20°C for at least 2 hours to promote cell lyses. Cells were lysed at 4°C by pulse sonicating for 60 seconds. The lysate was centrifuged at 13 000 xg for 30 minutes at 4°C.

The resulting supernatant was subjected to CM-Sepharose cation exchange chromatography (Wallace *et al.*, 1999). Supernatant was collected and diluted 1.5 times with equilibration buffer (10 mM sodium phosphate, 1 mM EDTA, 0.02% sodium azide, pH 7.45) to ensure efficient binding of the protein to the column. The diluted supernatant was loaded onto a CM-Sepharose column (50 ml volume) pre-equilibrated with 500 ml equilibration buffer. The column was washed with at least 10 column volumes of equilibration buffer until the absorbance reading of column eluent at 280 nm was zero, indicating all unbound protein was eluted. hGST A1-1 was eluted off the column using a 200 ml linear salt gradient of 0-300 mM NaCl prepared in 10 mM sodium phosphate, 1 mM EDTA, 0.02% sodium azide, pH 7.45. Fractions of 3 ml of the eluent were collected.

The absorbance at 280 nm of each fraction was measured using a Jasco V-550 UV/VIS spectrophotometer. Samples of 10 µl each were taken from fractions with an  $A_{280}$  higher than 0.1 and analysed by discontinuous sodium dodecyl sulphate polyacrylamide gel electrophoresis (SDS-PAGE) using a 4% acrylamide stacking gel and a 15% acrylamide separating gel (Laemmli, 1970). Fractions containing pure protein were pooled and concentrated by ultrafiltration through an Amicom PM-10 membrane to a volume of less than 10 ml. The concentrated protein solution was then buffer exchanged using a Sephadex G-25 column equilibrated with sodium phosphate buffer (20 mM sodium phosphate, 1 mM EDTA, 0.02% sodium azide, pH 6.5). Fractions of 5 ml were collected and those with an  $A_{280}$  higher than 0.1 were pooled and the protein solution was stored at 4°C. The purity and molecular mass of the protein subunits were assessed by SDS-PAGE. Low Molecular Mass standards (Amersham Biosciences, Vienna, Austria) were electrophoresed together with the protein samples to determine the molecular mass. Pure fractions were pooled and filtered using a 0.22 µM filter.

### 2.3 Protein concentration determination

The concentrations of purified hGST A1-1 proteins was determined spectrophotometrically using a molar extinction coefficient at 280 nm calculated by the method described by Perkins (1986):

$$\epsilon = 5550\sum\text{Trp} + 1340\sum\text{Tyr} + 150\sum\text{Cys} \quad (1)$$

where the coefficients ( $\epsilon$ ) for the specific residue is multiplied by the number occurring in the protein sequence. The extinction coefficient was calculated to be  $38200 \text{ M}^{-1} \text{ cm}^{-1}$ . To calculate protein concentration the molar extinction coefficient and the absorbance reading at 280 nm were used in the Beer-Lambert equation:

$$A = \epsilon cl \quad (2)$$

where  $A$  is the absorbance at 280 nm,  $\epsilon$  is the molar extinction co-efficient,  $c$  is the concentration of the protein in the sample and  $l$  is the path length of light through a cuvette, measured in cm.

## 2.4 Spectroscopic studies

### 2.4.1 Fluorescence spectroscopy

Fluorescence spectroscopy is a technique used for assessing the tertiary structure of proteins. The aromatic residues; tryptophan, tyrosine and phenylalanine are the main intrinsic fluorophores and these residues are used to probe the conformational dynamics of a protein since the emission wavelength is dependent on the polarity of the local solvent environment around the fluorophore (Eftink *et al.*, 1991; Lakowicz, 1999). A Perkin Elmer LS-50B Luminescence Spectrophotometer (Perkin Elmer, South Africa) was used to monitor all fluorescence measurements. A protein concentration of 2  $\mu\text{M}$  for both wildtype and I71V hGST A1-1 was used throughout. All samples were in 20 mM sodium phosphate, 1 mM EDTA, 0.02% sodium azide, pH 6.5 buffer and 3 scans were accumulated for each sample, using a path length of 1 cm and an excitation and emission bandwidth of 5 nm at 20°C. Spectra were collected under native and unfolded conditions for wildtype and I71V hGST A1-1. Unfolded samples were left in 8 M urea for 1 hour to unfold. The fluorescence emission spectra for tryptophan alone (excitation at 295 nm) as well as for tryptophan and tyrosine (excitation at 280 nm) were measured. Emission spectra were obtained over the wavelength range 280-450 nm.

### 2.4.2 Far-UV circular dichroism spectroscopy

Circular dichroism (CD) is a technique used for assessing the secondary structure of proteins in solution. Far-UV (190-250 nm) CD spectra due to peptide bond absorption give information about the secondary structures of the proteins (Woody, 1995). A Jasco J-810 spectropolarimeter was used to collect CD spectra. A protein concentration of 2  $\mu\text{M}$  was used for both wildtype and I71V hGST A1-1. All samples were in 20 mM sodium phosphate, 1 mM EDTA, 0.02% sodium azide, pH 6.5, filtered using a 2  $\mu\text{M}$  filter. A 2 mm path length cuvette was used and values for the spectra between 207-250 nm were averaged from 10 accumulations. Spectra were collected under native and unfolded conditions at 20°C. Unfolded samples were left in 8 M urea for 1 hour to unfold. Averaged CD signals, corrected for solvent, were converted to mean residue ellipticity  $[\Theta]$ ,

$$[\Theta] = \frac{100 \times \Theta}{\text{Cnl}} \quad (3)$$

where  $C$  is the protein concentration in millimolar,  $\Theta$  is the measured ellipticity in millidegree,  $n$  is the number of residues (221 in this case) and  $l$  is the path length (cm) (Woody, 1995).

### **2.4.3 ANS fluorescence**

8-Anilino-1-naphthalene sulphonate (ANS) fluorescence is a technique used to monitor changes in hydrophobic surface area of proteins upon folding and refolding. A Perkin Elmer LS-50B Luminescence Spectrophotometer was used measure ANS fluorescence. A protein concentration of 2  $\mu$ M for both wildtype and I71V hGST A1-1 was used. A final concentration of 200  $\mu$ M ANS was used. All samples were in 20 mM sodium phosphate, 1 mM EDTA, 0.02% sodium azide, pH 6.5 buffer and 3 scans were accumulated for each sample, using a path length of 1 cm and an excitation and emission bandwidth of 5 nm at 20°C. An excitation wavelength of 390 nm was used and emission spectra were obtained over the wavelength range 400-600 nm.

## **2.5 Steady-state enzyme kinetic properties**

### **2.5.1 Standard CDNB conjugating assay**

Steady-state enzyme kinetics (to determine specific activity) for wildtype and I71V hGST A1-1 proteins were performed spectrophotometrically in 0.1 M sodium phosphate, 1 mM EDTA, pH 6.5 (Habig and Jakoby., 1981). The enzyme activity was monitored at an absorbance of 340 nm by measuring the formation of 1-(*S*-glutathionyl)-2,4-dinitrobenzene (extinction co-efficient of 9600  $M^{-1}cm^{-1}$ ), the product of the GST catalysed conjugation of reduced glutathione (GSH) to 1-chloro-2,4-dinitrobenzene (CDNB) (Habig and Jakoby., 1981). Assays contained a final concentration of 1 mM GSH and 1 mM CDNB in 3% (v/v) ethanol with a final enzyme concentration of between 1-7 nM, and reactions were followed as linear progress curves for 1 minute at 20°C on a Hewlett Packard model 8452A-diode array spectrophotometer interfaced with a Vectra CS computer. All non-enzymatic reaction rates were measured using the same experimental protocol as described above, and subtracted from the final data to correct for any non-enzymatic activity.

### 2.5.2 Kinetic parameters ( $K_m$ , $V_m$ , $k_{cat}$ , $k_{cat}/K_m$ )

Standard assay conditions were modified in order to obtain a detailed kinetic profile for I71V hGST A1-1. The concentrations of the two substrates (GSH and CDNB) were varied from 0.5 mM to 6 mM and 0.2 mM to 2 mM, respectively. Initial reaction velocities (determined as in section 2.5.1) were plotted against substrate concentration in order to generate Michaelis-Menten plots using the following equation:

$$v_o = \frac{V_{max} [S]}{[S] + K_m} \quad (4)$$

$K_m$  values were then determined graphically.

All non-enzymatic reaction rates were subtracted from the assays containing enzyme. The catalytic efficiency ( $k_{cat}/K_m$ ) values for both CDNB and GSH variations were calculated from the slope of the linear plot of velocity versus substrate concentration:

$$v_o = (k_{cat}/K_m)[E]_t[S] \quad (5)$$

where  $[E]_t$  is the GST subunit concentration. Three concentrations of enzyme were used, 4 nM, 5 nM and 6 nM. The measured slope of the plots was then divided by the respective enzyme concentrations to give values for  $k_{cat}/K_m$ .

The turnover number ( $k_{cat}$ ) was determined using the data obtained for the Michaelis-Menten plots using the  $V_{max}$  and the amount of enzyme added together with the following equation.

$$V_{max} = k_{cat}[E]_t \quad (6)$$

### 2.5.3 Inhibition by G-site and H-site ligands

Determination of the concentration of inhibitor at which 50% enzyme activity was retained ( $IC_{50}$ ) was performed using standard assay conditions as in 2.5.1 together with the addition of either glutathione sulphonate ( $GSO_3^-$ ), a G-site ligand or ethacrynic acid (EA), an H-site ligand. Assays were performed using a final concentration of 2 nM enzyme, 1 mM CDNB and 1 mM GSH in 0.1 mM sodium phosphate, 1 mM EDTA, pH 6.5. The concentrations of the inhibitors ( $GSO_3^-$  and EA) were varied from 10  $\mu$ M to 170  $\mu$ M and 0.6  $\mu$ M to 70  $\mu$ M, respectively. The percentage activity for each concentration of inhibitor was plotted against the inhibitor concentration and the  $IC_{50}$  was determined from the plot. All non-enzymatic reaction rates were measured using the same

experimental protocol as described above, and subtracted from the final data to correct for any non-enzymatic activity.

## **2.6 Unfolding/refolding and conformational stability studies**

### **2.6.1 Urea-induced equilibrium unfolding studies**

Equilibrium unfolding studies measure the level of cooperativity of folding and stability of a protein. Tryptophan fluorescence and far-UV CD were used as structural probes to obtain unfolding data. Equilibrium unfolding was performed at 20°C in 20 mM sodium phosphate, 1 mM EDTA, 0.02% sodium azide buffer, pH 6.5. Unfolding reactions were set up using a concentration of 2 µM wildtype and I71V hGST A1-1 which were unfolded in 0-8 M urea for 1 hour at 20°C. The extent of urea-induced unfolding was monitored by tryptophan fluorescence (excitation at 295 nm) and far-UV CD (ellipticity at 222 nm), where spectra were obtained as described in section 2.4.1 and 2.4.2, respectively. Rayleigh scattering was assessed using excitation and emission wavelengths set at 295 nm to monitor protein aggregation.

### **2.6.2 Reversibility of unfolding**

To calculate thermodynamic parameters from unfolding experiments, the reversibility of the unfolding process must be demonstrated (Pace *et al.*, 1986). For both wildtype and I71V hGST A1-1 the reversibility of unfolding was monitored by fluorescence spectroscopy and enzyme activity. The refolding of protein was initiated by a 10-fold dilution of unfolded 10 µM protein in 8 M urea into assay buffer. A 1 µM native protein sample with the same final concentration (0.8 M urea) was set up and fluorescence spectra for both were obtained. Enzyme activities for the proteins were determined as in 2.5.1.

### **2.6.3 Analysis of the unfolding transition**

The absence of any thermodynamically unstable intermediates yield a single sigmoidal transition for both the wildtype and mutant proteins and thus allows the unfolding curves to be analysed according to the two-state assumption (Pace *et al.*, 1989). Equilibrium unfolding was studied by solvent denaturation using urea. In the two-state assumption

only the native (N) and unfolded (U) states are considered to exist in significant concentrations within the equilibrium unfolding transition region i.e  $N_2 \leftrightarrow 2U$ .

Any measured property ( $Y_{OBS}$ ) was converted to the fraction of protein populated in the unfolded form ( $F_U$ ). The fraction of the protein in the folded ( $F_N$ ) and the unfolded ( $F_U$ ) conformational states can be represented by:

$$F_N + F_U = 1 \quad (7)$$

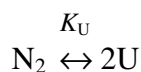
The observed property at any point in the equilibrium-unfolding curve is therefore:

$$Y_{OBS} = Y_N F_N + Y_U F_U \quad (8)$$

where  $Y_N$  and  $Y_U$  are the values of the folded and unfolded conformational states, respectively. The  $Y_F$  and  $Y_U$  values were estimated from the linear extrapolation of the pre- and post- transition baselines observed in the equilibrium unfolding curves. The pre- and post- transition baselines can be described by the straight line equations  $Y_F = ax + c$  and  $Y_U = ax + c$ , respectively. By combining these equations, we get:

$$F_U = (Y_N - Y_{OBS}) / (Y_N - Y_U) \quad (9)$$

For the two-state model for dimeric proteins (Pace, 1989) the equilibrium constant,  $K_U$ , was calculated using each point in the transition region of the denaturation curve:



$$K_U = [U]^2/[N_2] = 2P_t[F_U^2/(1-F_U)] \quad (10)$$

where  $P_t$  is the protein concentration of the monomer,  $F_U$  is the fraction-unfolded protein, and N and U represent the native and unfolded forms, respectively.

The free energy change was calculated according to the linear free energy model as described by Pace *et al.* (1989). The linear dependence of Gibbs free energy on unfolding is described as:

$$\Delta G = -RT \ln K_U \quad (11)$$



If a linear dependence is assumed for Gibbs free energy of unfolding on the concentration of denaturant (urea) in the transition region (Myers *et al.*, 1995), then

$$\Delta G = \Delta G(\text{H}_2\text{O}) - m [\text{denaturant}] \quad (12)$$

where  $\Delta G(\text{H}_2\text{O})$  is the Gibbs free energy difference between the native and unfolded state in the absence of denaturant and  $m$  is the susceptibility of the protein to urea (the  $m$ -value) (Green and Pace., 1974). The  $\Delta G(\text{H}_2\text{O})$  and  $m$ -value were calculated using equations 10, 11 and 12 together with Sigma Plot v. 8.0 (Systat Software Inc., California, USA).

## 2.7 Thermodynamic studies using isothermal titration calorimetry (ITC)

Isothermal titration calorimetry (ITC) is used to obtain a detailed thermodynamic profile of molecular associations. ITC is capable of directly measuring the heat evolved or absorbed during any molecular reaction and is therefore used to determine thermodynamic parameters; standard Gibbs free energy change, ( $\Delta G$ ), the binding constant ( $K_a$ ), the enthalpy change ( $\Delta H$ ), the entropy change ( $\Delta S$ ) as well as the stoichiometry ( $N$ ) of the binding interaction. Calorimetric studies were conducted using a VP-ITC MicroCalorimeter from MicroCal Incorporated (Northampton, MA, USA). ITC is also used to measure the heat capacity change ( $\Delta C_p$ ) of protein-ligand binding reactions by performing identical experiments at different temperatures.

The standard Gibbs free energy change ( $\Delta G$ ) of a binding reaction is related to the equilibrium binding constant ( $K_a$ ) using the equation:  $\Delta G = -RT \ln K_a$ , where  $R$  is the universal gas constant (1.987 cal/mol/K or 8.314 J/mol/K) and  $T$  is the absolute temperature. The free energy change ( $\Delta G$ ) is associated with the enthalpy ( $\Delta H$ ) and entropy ( $\Delta S$ ) changes as follows:

$$\Delta G = \Delta H - T\Delta S. \quad (13)$$

In this way, ITC provides valuable information about the binding events of protein-ligand, antigen-antibody, enzyme-substrate or enzyme-inhibitor complexes as well as the binding of metal ions to proteins.

### **2.7.1 Protein and ligand sample preparation**

Wildtype and I71V hGST A1-1 samples were dialysed extensively at 4°C against 20 mM sodium phosphate buffer, pH 6.5 containing 1 mM EDTA and 0.02% sodium azide. Proper dialysis is of fundamental importance in obtaining reliable ITC results. Dialysis tubing with a molecular weight cut-off of 3500 Da was used. Protein samples (40 ml) were dialysed for a minimum of 6 hours per change of dialysis buffers (2 litres/change) with at least three consecutive changes of dialysis buffer. Ligand samples were prepared with dialysis buffer from the final dialysis change. Certificates of analyses from the suppliers indicated that the ligands used in this study were chemically pure. Therefore, no further purification of the ligands was attempted.

### **2.7.2 Correction of protein concentration due to light scattering effects**

Protein concentrations were measured spectrophotometrically at 280 nm using the extinction coefficients reported earlier (section 2.3). Corrections due to light scattering effects were taken into account according to Winder (1971). A spectrum of the protein sample was obtained from 370 nm to 240 nm. The absorbance from 370 nm to 320 nm was measured at 5 nm intervals. Between these wavelengths protein does not absorb light and therefore data obtained is due to aggregation. Using this information, a plot of wavelength versus absorbance (for the range 370 – 320 nm) yielded straight lines with the equation:  $y = ax + c$ , where  $y$  is the absorbance value,  $x$  is the wavelength and  $a$  and  $c$  are obtained from the linear regression curve fit. By substituting  $x = 280$  into the above equation, the value of  $y$  is obtained. This value represents the contribution due to the light scattering effects of the protein sample. Subtraction of the calculated  $y$ -value from the absorbance value at 280 nm of the protein sample yields a corrected  $A_{280}$  value. This value is, therefore, used to calculate the corrected protein concentration of the sample.

### **2.7.3 Thermodynamics of ligand binding to the active site of I71V mutant**

The dialysed wildtype and I71V hGST A1-1 proteins were prepared to give a monomeric protein concentration of ~ 0.025 mM. The ligand, *S*-hexylglutathione, was prepared at a concentration of 0.5 mM. In all the experiments performed, the ligand was injected in 3 µl increments into the ITC sample cell containing the protein until complete saturation had occurred (~ 50-60 injections). The reference power was set to 15 µcal/sec and the

initial delay was 60 seconds. The stirring speed was kept constant at 310 rpm and the spacing between injections was set to 240 seconds. In order to determine the heat capacity of the binding reaction, identical experiments were performed at different temperatures in the range of 5-25°C. To correct for heat of dilution effects, the averaged heat of the post-saturation injections was subtracted from each injection. All data analysis was performed using the computer software package (ORIGIN 5) supplied with the VP-ITC calorimeter.

#### **2.7.4 ITC data analysis**

The raw data obtained from the calorimetric experiments were collected and integrated using the ORIGIN 5 software. All data were corrected for the contribution due to heat of dilution effects. Where necessary, the baseline was adjusted manually before correcting the raw data. The integrated data all fit well to a single site/independent-binding model per monomer. The most basic parameters that define a calorimetric titration are the concentrations of the interacting species (i.e., protein and ligand). The ideal protein concentration depends to a large extent on the binding constant of the reaction. The shape of the binding isotherm is described by the *c*-value (Wiseman *et al.*, 1989). This is a unitless value that is obtained as follows:  $c = [M] K_a$ , where  $[M]$  is the molar protein concentration and  $K_a$  is the binding constant with units of  $M^{-1}$ . The *c*-value for the binding interaction between *S*-hexylglutathione and I71V hGST A1-1 was between 10 and 20. The recommended *c*-values range from 1-1000 (Wiseman *et al.*, 1989). The heat capacity change of the interaction was determined by the slope of the linear dependence of the binding enthalpy of the reaction over a temperature range of 5 – 25°C.

## CHAPTER 3

### RESULTS

#### 3.1 Confirmation of the identities of wildtype and I71V pKHA1 plasmids

The pKHA1 plasmid contains a single restriction site for both *PvuII* and *HindIII*, but does not contain a restriction site for *SmaI*. A *SmaI* restriction site was incorporated close to the mutation in I71V pKHA1 plasmid for plasmid selection. The coding region for I71V hGST A1-1 was sequenced to verify the mutation was present and that no additional mutations had been introduced. Figure 6 shows a portion of the wildtype pKHA1 nucleotide sequence aligned with the equivalent portion of I71V pKHA1 nucleotide sequence. The results confirmed the presence of the Ile71 → Val codon change and showed that no additional mutations had been introduced into either the wildtype or I71V plasmids (results not shown).

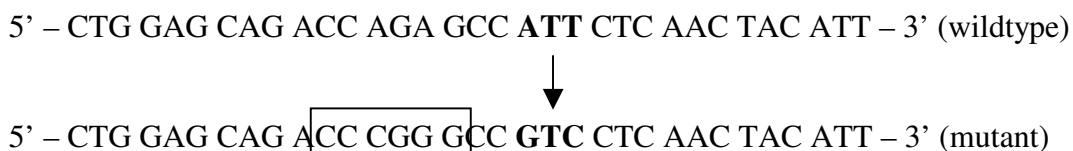


**Figure 6.** A portion of the wildtype nucleotide sequence (top row) encoding hGST A1-1 (Stenberg *et al.*, 1992) with isoleucine-71 ATT codon in bold. Below is the equivalent portion of I71V pKHA1 nucleotide sequence containing the I71V mutation. The replacement of the isoleucine codon at position 71 with valine codon is indicated (ATT → GTC). The boxed nucleotides represent the translationally silent mutation for the *SmaI* restriction site (CCCGGG).(Pace, 1989)

#### 3.2 Expression and protein purification

Wildtype and I71V hGST A1-1 was expressed according to established methods (Wallace *et al.*, 1998b). SDS-PAGE analysis was used to assess the size and homogeneity of wildtype and I71V hGST A1-1 proteins (Figure 7). SDS-PAGE separates proteins based on size differences between denatured proteins and is therefore used to determine the subunit size of proteins. To determine the subunit size of I71V hGST A1-1 an SDS-PAGE molecular mass standard marker mass was analysed on the same gel as samples of

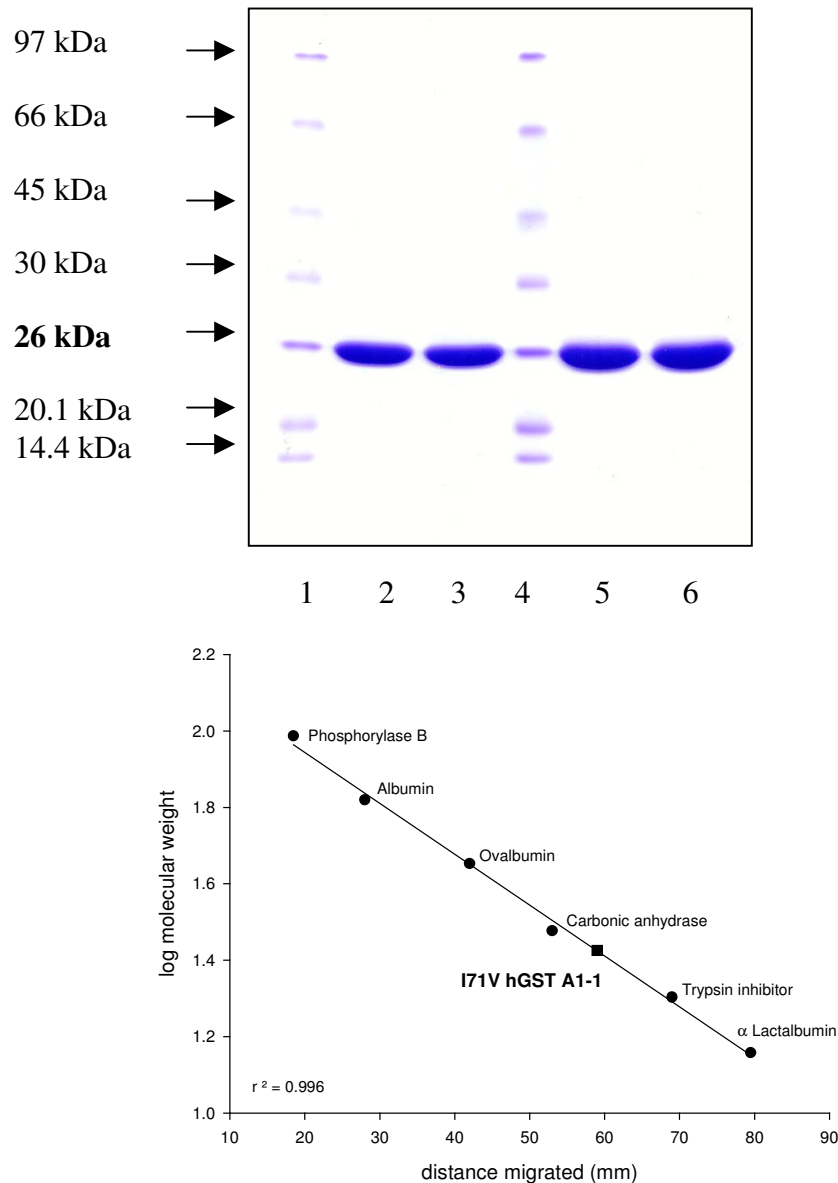


**Figure 7. (a)** SDS-PAGE analysis of CM-Sepharose purified wildtype and I71V hGST A1-1 proteins obtained using methods in section 2.2. Lanes 1 and 4 are low molecular mass markers (sizes indicated by arrows), lanes 2 and 3 are wildtype hGST A1-1 protein and lanes 5 and 6 are I71V hGST A1-1 protein samples. **(b)** SDS-PAGE calibration curve. The log of the molecular mass of the standards from lane 2 in Figure 7a were plotted against the distance migrated of each protein and by means of a linear regression, a straight line was fitted to the data. The R squared value for the fit is 0.99. The ■ indicates the migration coordinate for wildtype and I71V hGST A1-1.

purified wildtype and I71V hGST A1-1 (Figure 7a). Using the distance migrated by the molecular mass standards, a calibration curve (Figure 7b) was constructed and the subunit molecular mass of the I71V hGST A1-1 was calculated to be 26 kDa.

Wildtype hGST A1-1 protein sample was electrophoresed on the same gel so as to check the molecular mass of I71V hGST A1-1 against wildtype hGST A1-1. Both proteins migrated as single bands, the same distance on the gel (Figure 7a). The migration coordinate for wildtype and I71V hGST A1-1 proteins corresponds to subunit size of approximately 26 kDa. For one-litre of culture, on average, 245 mg of protein was purified for I71V hGST A1-1 and 90 mg for wildtype. The results therefore indicate that purification yielded pure homogenous protein samples of the correct molecular mass.

### **3.3 Spectroscopic studies**

#### **3.3.1 Fluorescence spectroscopy**

Intrinsic tryptophan fluorescence is a useful spectroscopic technique used to measure the conformational stability of proteins. Tryptophan is the most highly fluorescent amino acid due to its indole side chain and is widely used as an intrinsic reporter group in protein structural studies (Eftink and Anusiem., 1991). The indole side chain is highly sensitive to its local environment and thus provides a useful technique of probing for local and global conformational changes. Tryptophan can be selectively excited at 295 nm but greater absorption and fluorescence occur when it is excited at 280 nm. Excitation at 280 nm also results in excitation of the side chains of the tyrosine residues but, because of the close proximity of the residues, resonance energy transfer can occur between the tyrosine and tryptophan residues (Lakowicz, 1983). hGST A1-1 was excited at 295 nm and 280 nm to probe for changes in tertiary structure as a result of the I71V mutation. Figure 8 shows the emission spectra for 2  $\mu$ M concentration of wildtype and I71V hGST A1-1, measured between 300-400 nm, for both their native and denatured states. All spectra of denatured protein were of protein denatured in 8 M urea. Upon denaturation there is a red shift of about 30 nm in the spectra for both proteins, and a 9% increase in fluorescence intensity for the I71V hGST A1-1.

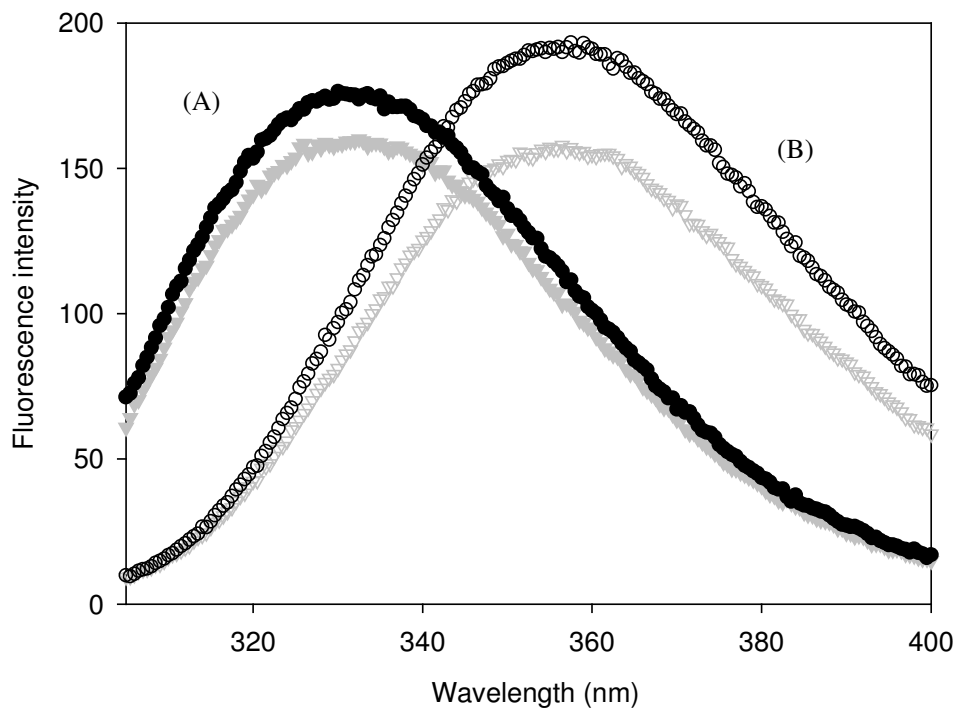


**Figure 8.** Fluorescence emission spectra for wildtype (black) and I71V (grey) hGST A1-1. The lone tryptophan residue was selectively excited at 295 nm and the wavelength emission spectra monitored. All spectra are for 2  $\mu$ M protein in sodium phosphate buffer (20 mM sodium phosphate, 1 mM EDTA, 0.02% NaN<sub>3</sub>, pH 6.5) at 20°C. (A) Represents the spectra for the native proteins in the absence of urea (B) Represents the spectra for the denatured proteins in the presence of 8 M urea.

Spectra of native wildtype and I71V hGST A1-1 exhibit an emission maximum of 330 nm. Spectrum of denatured proteins showed similar emission wavelength maxima of 356 nm and 357 nm for wildtype and I71V hGST A1-1, respectively.

Figure 9 shows the emission spectra for wildtype and I71V hGST A1-1 excited at 280 nm. Spectra of denatured wildtype and I71V hGST A1-1 are red shifted about 30 nm with respect to spectra of the native protein, and show a decrease in fluorescence intensity. Wildtype and I71V mutant both show an emission maximum of 330 nm for the native sample and 356 nm for the denatured sample. Spectra of the denatured samples show an additional peak at 310 nm when excited at 280 nm.

### **3.3.2 Far-UV circular dichroism spectroscopy**

The secondary structural content of native and denatured wildtype and I71V hGST A1-1 was analysed using far-UV CD as a probe. This was done to monitor any secondary structural changes due to the I71V mutation. Spectra were determined between 210 nm and 250 nm (Figure 10). CD buffer-corrected spectra for native wildtype and I71V hGST A1-1 exhibited two troughs in molar ellipticity minima at 210 and 222 nm, typical spectrum for a predominantly alpha-helical protein (Woody, 1995). This is consistent with the crystal structure of hGST A1-1, which reports that the protein is about 60% alpha-helical (Sinning *et al.*, 1993; Cameron, 1995). Spectra of protein in 8 M urea showed a loss of secondary structure indicated by the lack of the characteristic high alpha helical content spectrum shown for the native samples. Spectra obtained for both native and denatured wildtype and I71V hGST A1-1 were superimposable indicating there were no changes in gross secondary structure caused by the I71V mutation.

### **3.3.3 ANS fluorescence**

The organic anion ANS is an amphipathic fluorescent dye used to probe for changes in the hydrophobic surfaces of a protein. ANS has a fluorescence emission maximum of 530 nm in water that is blue-shifted when the dye binds to protein (Lakowicz, 1999). Fluorescence emission spectra of ANS binding to hGST A1-1 are seen in Figure 11. Monitoring the enhancement or quenching of the dye is an indication of the degree of exposure of hydrophobic surfaces of the protein being studied to the surrounding



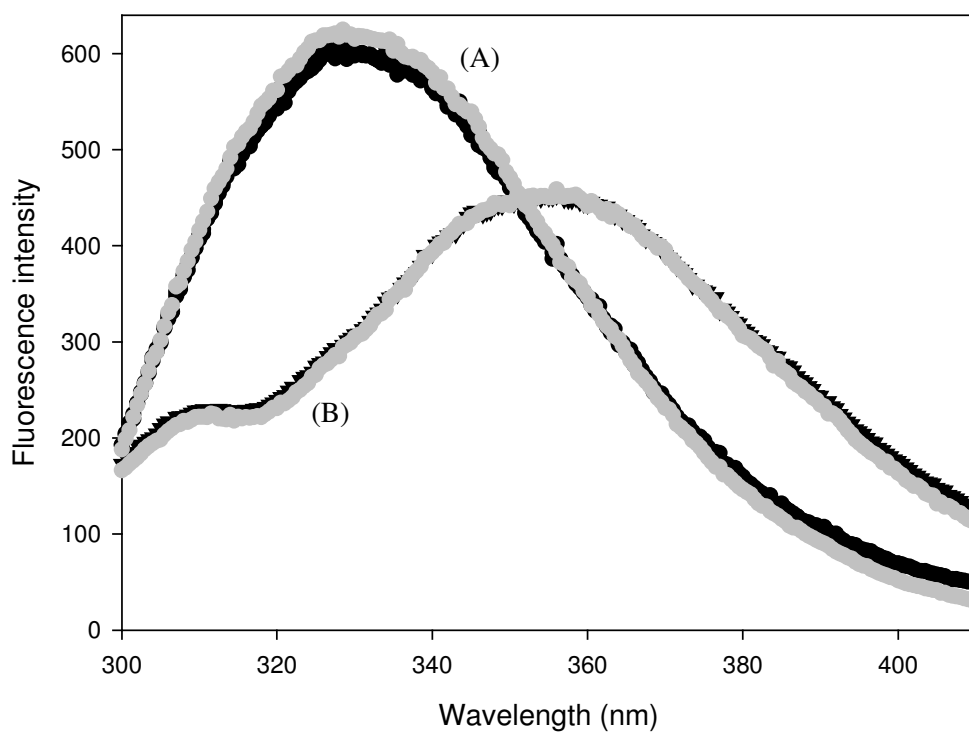


**Figure 9.** Fluorescence emission spectra for wildtype (black) and I71V (grey) hGST A1-1. Tryptophan and tyrosine residues were selectively excited at 280 nm and the wavelength emission spectra monitored. All spectra are for 2  $\mu$ M protein in sodium phosphate buffer (20 mM sodium phosphate, 1 mM EDTA, 0.02% NaN<sub>3</sub>, pH 6.5) at 20°C. **(A)** Represents the spectra for the native proteins in the absence of urea. **(B)** Represents the spectra for the denatured proteins in the presence of 8 M urea.

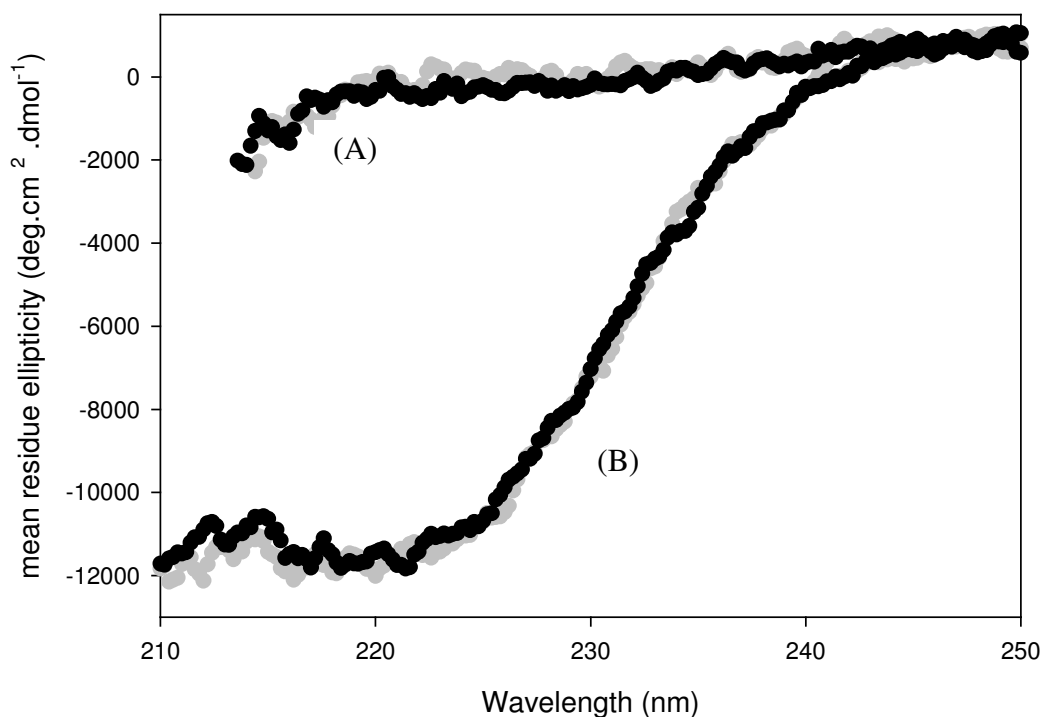


**Figure 10.** Far-UV CD spectra for wildtype (black) and I71V hGST A1-1 (grey). **(A)** Represents spectra for the native proteins in the absence of urea. **(B)** Represents spectra for the denatured proteins in the presence of 8 M urea. A 2  $\mu$ M concentration of protein in sodium phosphate buffer (20 mM sodium phosphate, 1 mM EDTA, 0.02%  $\text{NaN}_3$ , pH 6.5) was used for all samples at 20°C. Each spectrum represents an average of 10 accumulations. Spectra for native samples are superimposable as are spectra for denatured proteins. Both proteins exhibit molar ellipticity minima at 210 and 222 nm.

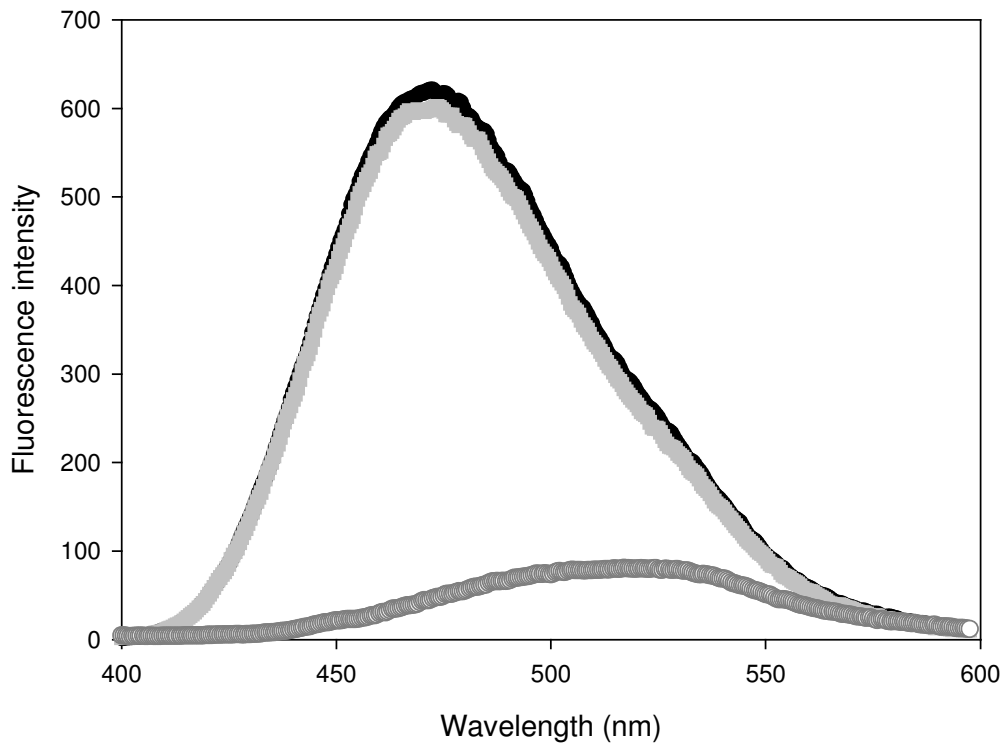


**Figure 11.** Fluorescence emission spectra of ANS in buffer (dark grey), ANS in complex with wildtype protein (black) and I71V hGST A1-1 (grey). Experiments were performed by adding 200  $\mu\text{M}$  ANS in 20 mM sodium phosphate buffer, pH 6.5, to 2  $\mu\text{M}$  wildtype and I71V hGST A1-1. ANS was selectively excited at 390 nm and the emission spectra were measured in the wavelength range 400-600 nm.

environment. The change or shift in the ANS fluorescence emission spectrum is determined by the polarity of the environment in which it binds, binding at a low polarity site results in a greater blue-shift than binding at a high polarity site (Lakowicz, 1999). It has previously been shown that ANS binds the non-polar H-site of the active site (Dirr *et al.*, 2005).

Fluorescence emission spectra of ANS binding to the wildtype and I71V hGST A1-1 proteins are shown in Figure 11. In the absence of protein, ANS was observed to have an emission maximum at 530 nm. When bound to the wildtype and I71V hGST A1-1 proteins, a blue-shift of about 65 nm in emission maxima was observed together with an increase in the emission intensity. The emission maxima for wildtype and I71V hGST A1-1 occurred at 475 nm.

### **3.4 Steady-state enzyme kinetic properties**

#### **3.4.1 Kinetic parameters ( $K_m$ , $k_{cat}$ , $k_{cat}/K_m$ )**

Enzymatic analysis is used to detect any small structural changes, induced by a mutation, close to the active site of a protein. hGST A1-1 catalyses the conjugation of reduced glutathione (GSH) to the non-polar substrate 1-chloro-2,4-dinitrobenzene (CDNB) producing a chromogenic glutathione dinitrobenzene (Habig and Jakoby, 1981). Kinetic properties of wildtype and I71V hGST A1-1 proteins were monitored to establish the impact of the I71V mutation on the function of hGST A1-1 and the results are shown in Table 2.

The wildtype and mutant enzymes both obeyed Michaelis-Menten kinetics. Figures 12 and 13 show the graphical plots of the data used to determine the  $K_m$  of wildtype protein, and Figures 14 and 15 are the graphical plots used to determine the  $K_m$  of I71V hGST A1-1 protein. Initial velocity of linear progress curves versus substrate concentration were plotted to obtain the Michaelis-Menten plots. Saturation was reached in all cases. For an explanation on how the parameters were determined see section 2.5.2. Figures 16 and 17 show the graphical plots of the data used to determine the  $k_{cat}/K_m$  of wildtype protein, and Figures 18 and 19 are the graphical plots used to determine the  $k_{cat}/K_m$  of the I71V hGST A1-1 protein. Linear progress curves were obtained for low

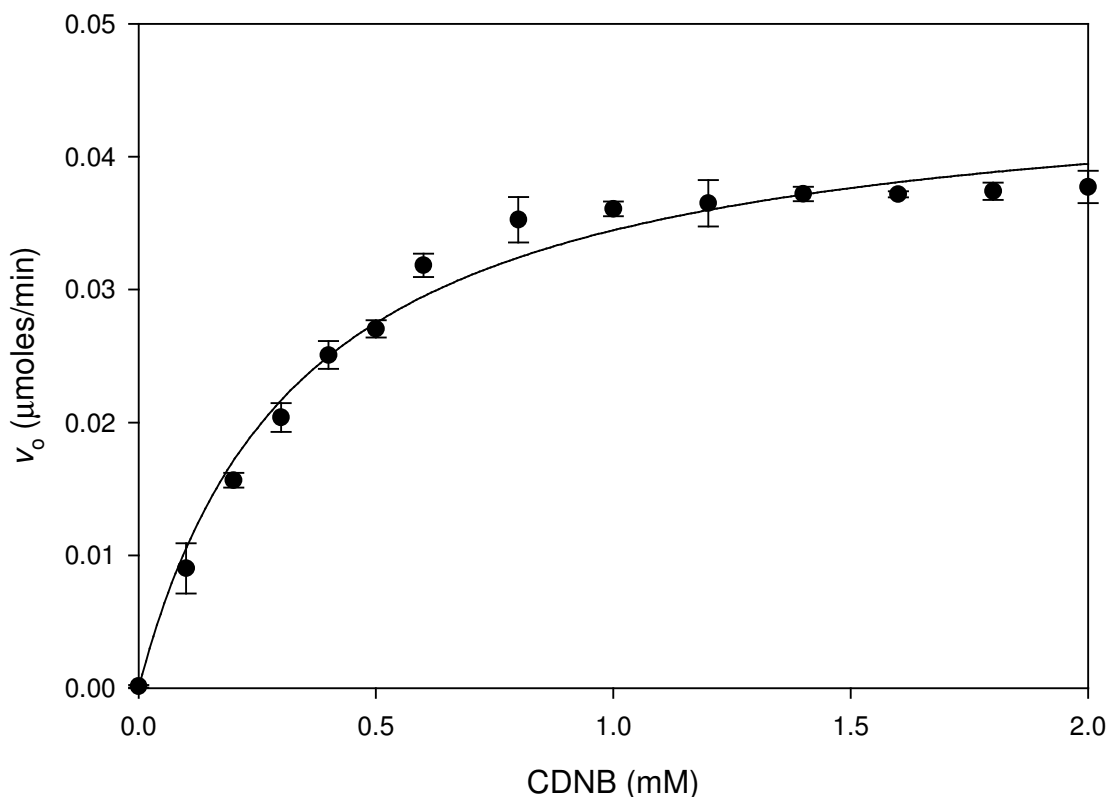


**Figure 12.** A Michaelis-Menten plot of velocity versus the substrate concentration (CDNB) for wildtype hGST A1-1. Enzyme kinetics were monitored spectrophotometrically at 340 nm in 100 mM sodium phosphate, 1 mM EDTA, pH 6.5 at 20°C by measuring the formation of *S*-2,4-dinitrophenyl glutathione ( $\epsilon = 9600 \text{ M}^{-1} \text{ cm}^{-1}$ ). The  $K_m$  for CDNB was determined using a final concentration of reduced glutathione (GSH) of 5 mM and varying the concentration of CDNB from 0 – 2 mM. A final enzyme concentration of 4 nM was used. Data was fitted to a hyperbolic curve using Sigma Plot v. 8.0, with a non-linear regression analysis in order to obtain kinetic parameters. The average of three data sets were plotted and error bars are shown.

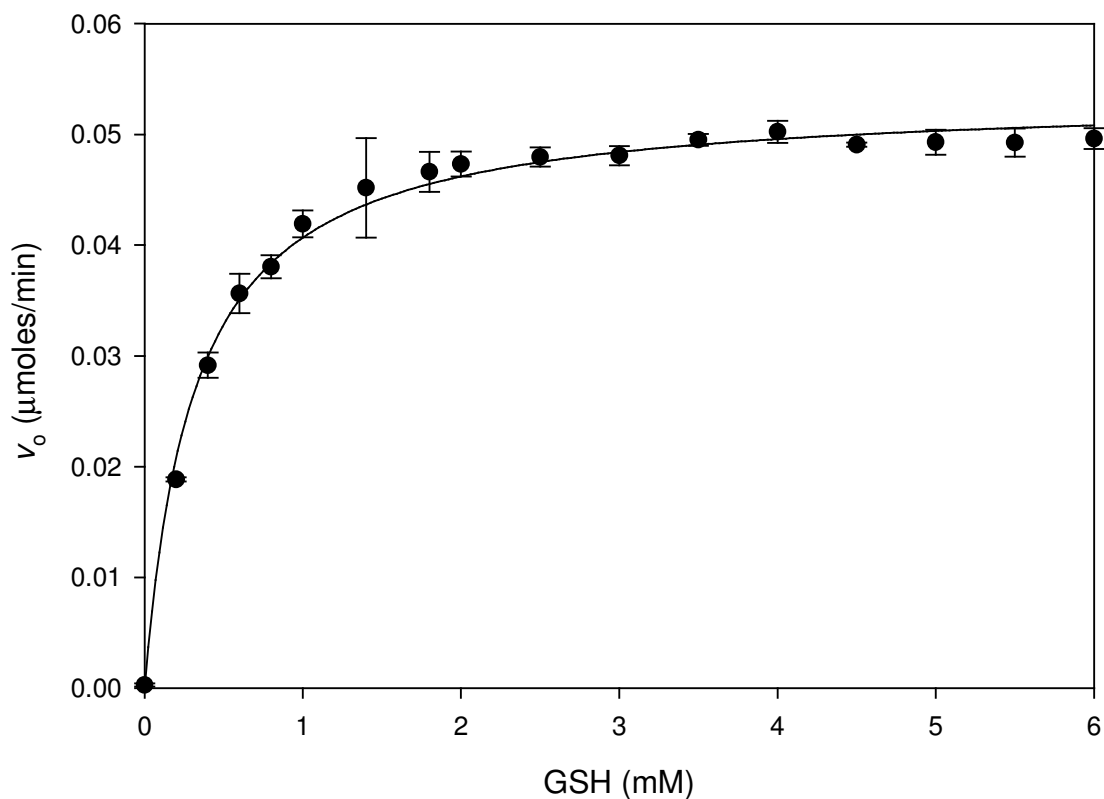


**Figure 13.** A Michaelis-Menten plot of velocity versus the substrate concentration (GSH) for wildtype hGST A1-1. Enzyme kinetics were monitored spectrophotometrically at 340 nm in 100 mM sodium phosphate, 1 mM EDTA, pH 6.5 at 20°C by measuring the formation of *S*-2,4-dinitrophenyl glutathione ( $\epsilon = 9600 \text{ M}^{-1}\text{cm}^{-1}$ ). The  $K_m$  for GSH was determined using a final concentration of CDNB of 1.6 mM and varying the concentration of GSH from 0 – 6 mM. A final enzyme concentration of 4 nM was used. Data was fitted to a hyperbolic curve using Sigma Plot v. 8.0, with a non-linear regression analysis in order to obtain kinetic parameters. The average of three data sets were plotted and error bars are shown.

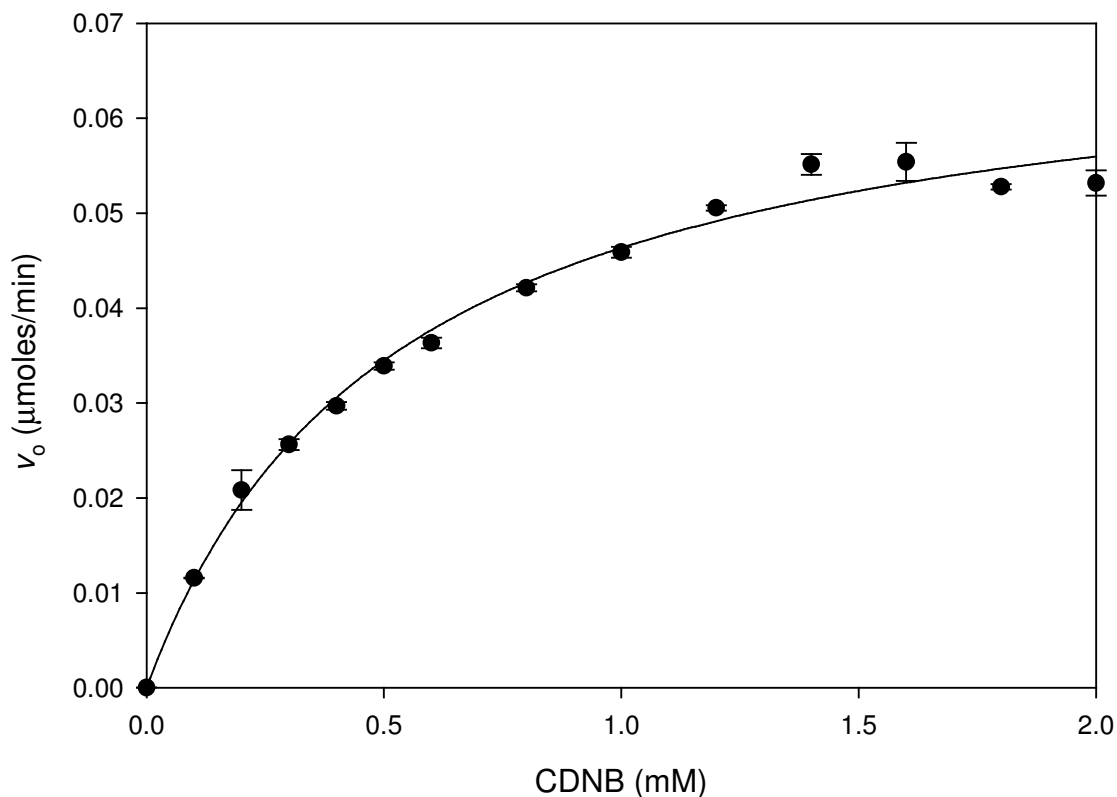


**Figure 14.** A Michaelis-Menten plot of velocity versus the substrate concentration (CDNB) for I71V hGST A1-1. Enzyme kinetics were monitored spectrophotometrically at 340 nm in 100 mM sodium phosphate, 1 mM EDTA, pH 6.5 at 20°C by measuring the formation of *S*-2,4-dinitrophenyl glutathione ( $\epsilon = 9600 \text{ M}^{-1} \text{ cm}^{-1}$ ). The  $K_m$  for CDNB was determined using a final concentration of reduced glutathione (GSH) of 5 mM and varying the concentration of CDNB from 0 – 2 mM. A final enzyme concentration of 4 nM was used. Data was fitted to a hyperbolic curve using Sigma Plot v. 8.0, with a non-linear regression analysis in order to obtain kinetic parameters. The average of three data sets were plotted and error bars are shown.

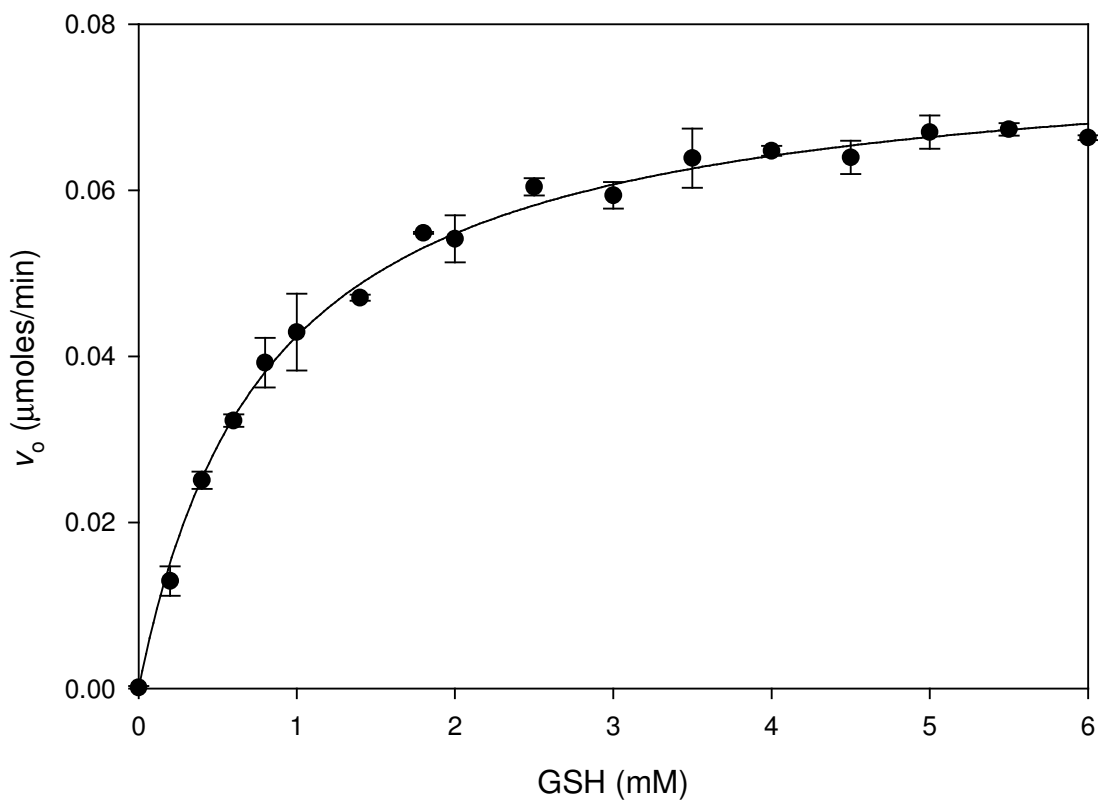


**Figure 15.** A Michaelis-Menten plot of velocity versus the substrate concentration (GSH) for I71V hGST A1-1. Enzyme kinetics were monitored spectrophotometrically at 340 nm in 100 mM sodium phosphate, 1 mM EDTA, pH 6.5 at 20°C by measuring the formation of *S*-2,4-dinitrophenyl glutathione ( $\epsilon = 9600 \text{ M}^{-1}\text{cm}^{-1}$ ). The  $K_m$  for GSH was determined using a final concentration of CDNB of 1.6 mM and varying the concentration of GSH from 0 – 6 mM. A final enzyme concentration of 4 nM was used. Data was fitted to a hyperbolic curve using Sigma Plot v. 8.0, with a non-linear regression analysis in order to obtain kinetic parameters. The average of three data sets were plotted and error bars are shown.



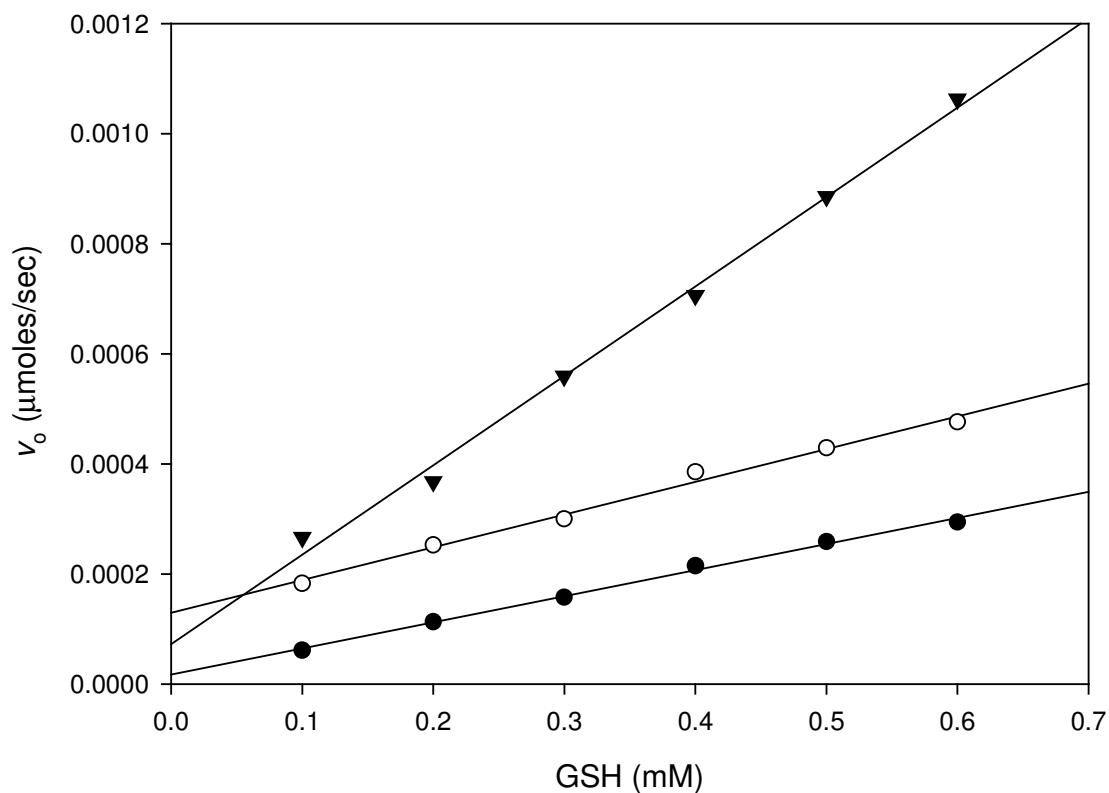


**Figure 16.** Linear plots of velocity versus the substrate concentration (GSH) for wildtype hGST A1-1. Enzyme kinetics were monitored spectrophotometrically at 340 nm in 100 mM sodium phosphate, 1 mM EDTA, pH 6.5 at 20°C by measuring the formation of *S*-2,4-dinitrophenyl glutathione ( $\epsilon = 9600 \text{ M}^{-1}\text{cm}^{-1}$ ). The  $k_{\text{cat}}/K_m$  for GSH was determined using a final concentration of CDNB of 1.6 mM and varying the concentration of GSH from 0.1 – 0.6 mM. Three final enzyme concentrations were used; 4 nM (solid circle), 5 nM (open circle) and 6 nM (triangle). A linear regression was fitted to the data using Sigma Plot v. 8.0, in order to obtain kinetic parameters.

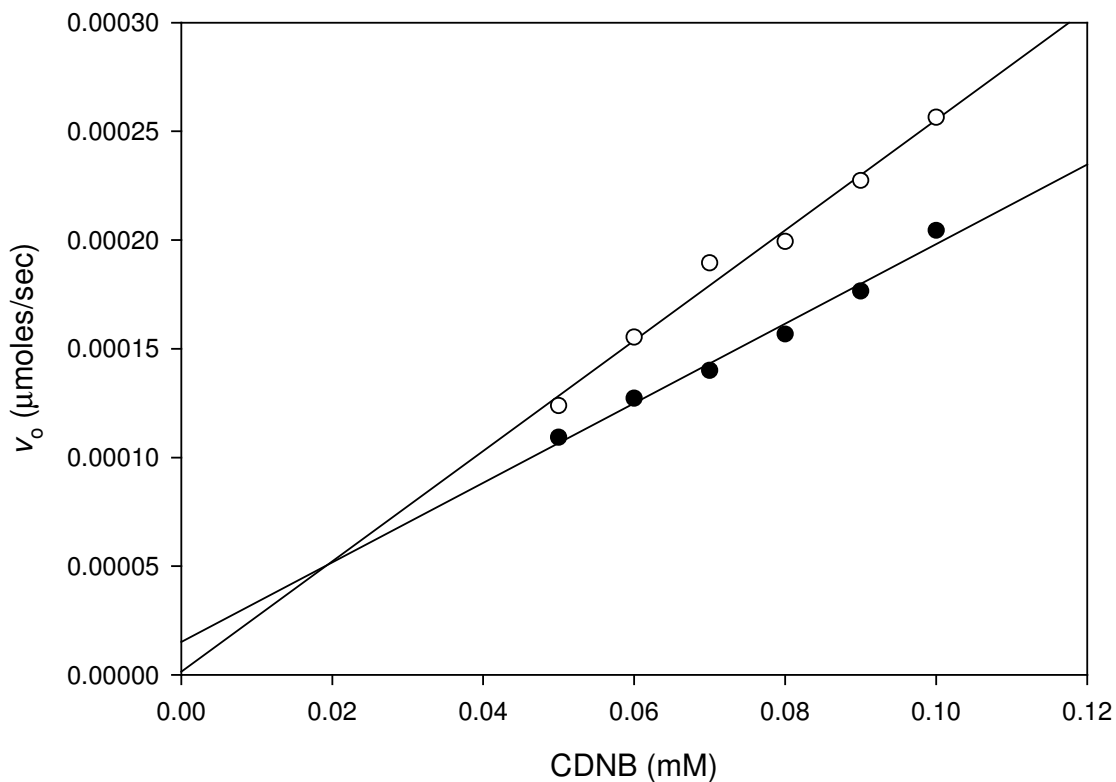


**Figure 17.** Linear plots of velocity versus the substrate concentration (CDNB) for wildtype hGST A1-1. Enzyme kinetics were monitored spectrophotometrically at 340 nm in 100 mM sodium phosphate, 1 mM EDTA, pH 6.5 at 20°C by measuring the formation of *S*-2,4-dinitrophenyl glutathione ( $\epsilon = 9600 \text{ M}^{-1}\text{cm}^{-1}$ ). The  $k_{\text{cat}}/K_m$  for CDNB was determined using a final concentration of GSH of 5 mM and varying the concentration of CDNB from 0.05 – 0.1 mM. Two final enzyme concentrations were used; 5 nM (solid circle) and 6 nM (open circle). A linear regression was fitted to the data using Sigma Plot v. 8.0, in order to obtain kinetic parameters.

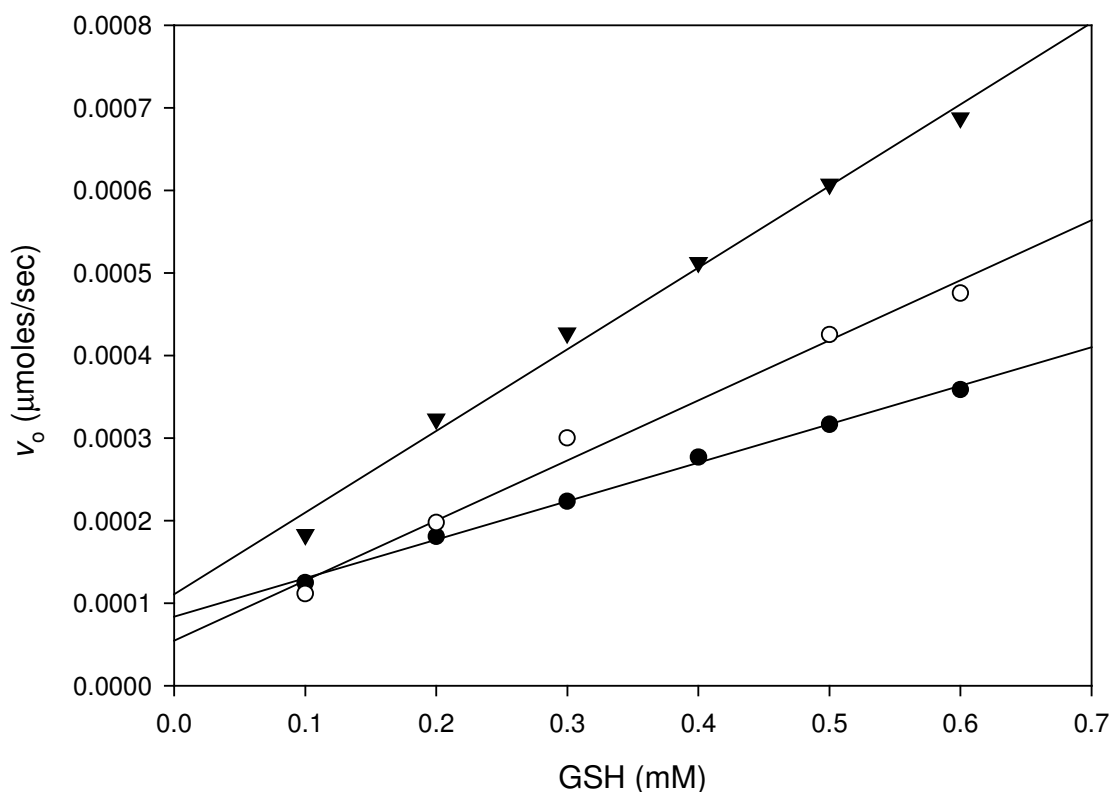


**Figure 18.** Linear plots of velocity versus the substrate concentration (GSH) for I71V hGST A1-1. Enzyme kinetics were monitored spectrophotometrically at 340 nm in 100 mM sodium phosphate, 1 mM EDTA, pH 6.5 at 20°C by measuring the formation of *S*-2,4-dinitrophenyl glutathione ( $\epsilon = 9600 \text{ M}^{-1}\text{cm}^{-1}$ ). The  $k_{\text{cat}}/K_m$  for GSH was determined using a final concentration of CDNB of 1.6 mM and varying the concentration of GSH from 0.1 – 0.6 mM. Three final enzyme concentrations were used; 4 nM (solid circle), 5 nM (open circle) and 6 nM (triangle). A linear regression was fitted to the data using Sigma Plot v. 8.0, in order to obtain kinetic parameters.

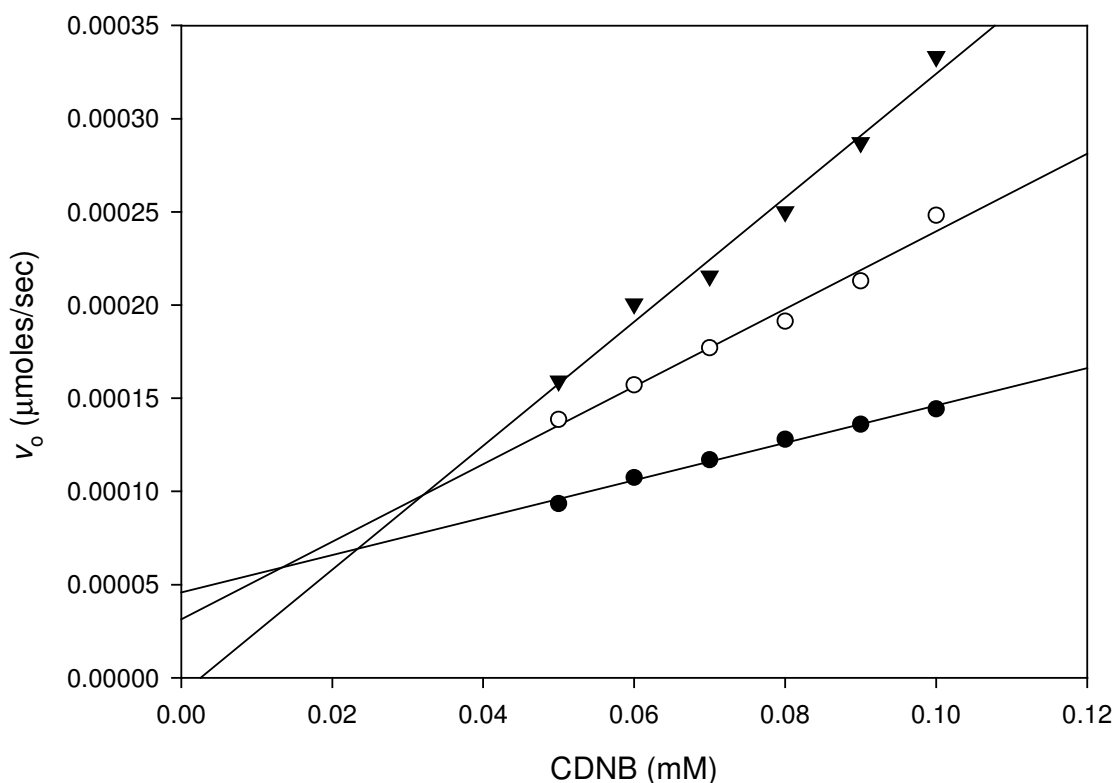


**Figure 19.** Linear plots of velocity versus the substrate concentration (CDNB) for I71V hGST A1-1. Enzyme kinetics were monitored spectrophotometrically at 340 nm in 100 mM sodium phosphate, 1 mM EDTA, pH 6.5 at 20°C by measuring the formation of *S*-2,4-dinitrophenyl glutathione ( $\epsilon = 9600 \text{ M}^{-1}\text{cm}^{-1}$ ). The  $k_{\text{cat}}/K_m$  for CDNB was determined using a final concentration of GSH of 5 mM and varying the concentration of CDNB from 0.05 – 0.1 mM. Three final enzyme concentrations were used; 4 nM (solid circle), 5 nM (open circle) and 6 nM (triangle). A linear regression was fitted to the data using Sigma Plot v. 8.0, in order to obtain kinetic parameters.

concentrations of substrate and the initial velocity was determined. Initial velocity was plotted against substrate concentration and data was fitted with a linear regression yielding an equation with an  $m$  value equal to  $k_{cat}/K_m [E_t]$ . For an explanation on how the parameters were determined see section 2.5.2.

The specific activity of I71V hGST A1-1 was three times that of the wildtype hGST A1-1 (Table 2). To determine whether this was due to structural alterations at the G-site or the H-site more kinetic parameters were determined for the wildtype and I71V hGST A1-1 proteins. The results of the kinetic analysis are summarised in Table 2. The plots in Figures 12 – 19 were used to obtain the kinetic parameters presented in Table 2. As shown in Table 2 the I71V mutation caused an increase in  $K_m$  for GSH and CDNB as well as an increase in the catalytic efficiency for both substrates, with a much larger increase seen for CDNB. The  $k_{cat}$  for I71V hGST A1-1 was increased one and a half times that of wildtype hGST A1-1  $k_{cat}$ . The I71V hGST A1-1  $K_m$  for CDNB was increased by almost one and a half times that of the wildtype and  $K_m$  for GSH was almost three times greater than the wildtype  $K_m$ . For both substrates the  $k_{cat}/K_m$  was increased for the I71V hGST A1-1. The most evident change due to the mutation, in all parameters determined, was the increase in the  $k_{cat}/K_m$  for the substrate CDNB. The mutant shows a 10-fold increase in  $k_{cat}/K_m^{CDNB}$  over that of the wildtype.

The catalytic efficiency ( $k_{cat}/K_m$ ) relates to the free energy of the transition state and can be used as a measure of the stabilising effect contributed by an enzyme (Nilsson *et al.*, 2002). The difference in free energy change for formation of the corresponding transition states in wildtype and I71V hGST A1-1 ( $\Delta\Delta G$ ) is calculated from the equation (Fersht, 1999)

$$\Delta\Delta G = -RT \ln \frac{k_{cat}/K_m^{mutant}}{k_{cat}/K_m^{wildtype}} \quad (14)$$

The  $\Delta\Delta G$  for transition state stabilisation for the reaction used is  $-5.82$  kJ/mol.

**Table 2.** Summary of steady state enzyme kinetic properties of wildtype and I71V hGST A1-1

<b>Parameter</b>	<b>Wildtype</b>	<b>I71V hGST A1-1</b>
<b>Specific activity</b> ( $\mu\text{mol min}^{-1}\text{mg}^{-1}$ )	48 $\pm$ 4	130 $\pm$ 3
$K_m^{\text{CDNB}}$ (mM)	0.34 $\pm$ 0.02	0.50 $\pm$ 0.03
$K_m^{\text{GSH}}$ (mM)	0.32 $\pm$ 0.006	0.82 $\pm$ 0.082
$k_{\text{cat}}/K_m^{\text{CDNB}}$ ( $\text{mM}^{-1} \text{s}^{-1}$ )	39 $\pm$ 4	408 $\pm$ 52
$k_{\text{cat}}/K_m^{\text{GSH}}$ ( $\text{mM}^{-1} \text{s}^{-1}$ )	114 $\pm$ 8	143 $\pm$ 24
$k_{\text{cat}}$ ( $\text{s}^{-1}$ )	74 $\pm$ 0.6	108 $\pm$ 3

The values of the parameters as well as the standard deviations were determined by non-linear regression analysis. Parameters were derived from Figures 12 – 19.

### 3.4.2 Inhibition by G-site and H-site ligands

To further characterise the effect of the I71V mutation, competitive inhibition studies were performed using glutathione sulphonate ( $\text{GSO}_3^-$ ) and ethacrynic acid as inhibitors. These inhibitors and substrate analogues compete with the substrate for the active site. Inhibition studies yield an  $\text{IC}_{50}$  value; the concentration of inhibitor that causes a 50% decrease in enzyme activity. The inhibition studies were performed to determine whether one or both parts of the active site were affected by the mutation. From Figure 20 as well as data shown in Table 3 it can be seen that the inhibition curve for the CDNB-conjugating activity of I71V hGST A1-1 is similar to that of wildtype with the mutant enzyme being only slightly less competitively inhibited by  $\text{GSO}_3^-$ . The inhibitor ethacrynic acid, which binds to the H-site of the enzyme binds in a non-productive mode in the absence of the substrate glutathione (Cameron *et al.*, 1995). I71V hGST A1-1 showed about a 2-fold increase in the  $\text{IC}_{50}$  value for ethacrynic acid (Table 3 and Figure 21).

## 3.5 Unfolding/refolding and conformational stability studies

### 3.5.1 Reversibility of unfolding

Reversibility and equilibrium are required for the determination of thermodynamic parameters, thus the reversibility of the urea-induced equilibrium unfolding for wildtype and I71V hGST A1-1 had to be measured (Pace, 1986). The reversibility of unfolding was assessed by a 10-fold dilution of the 8 M urea unfolded sample into native buffer followed by monitoring refolding using two probes. These probes were a structural probe, tryptophan fluorescence at 295nm, and a functional probe, specific activity. The unfolding of wildtype hGST A1-1 has been established to be highly reversible (Wallace *et al.*, 1998b). this was confirmed in this study: refolded wildtype regained 98% of its catalytic activity (results not shown). I71V hGST A1-1 recovered 92% of its enzymatic activity. An analysis of the maximum fluorescence intensity values after excitation at 295 nm of the refolded mutant protein showed 96.6% recovery of its original value implying reversible unfolding (results not shown). Since the unfolding reaction was shown to be highly reversible, the calculation of thermodynamic parameters from the urea-induced unfolding curves was possible.

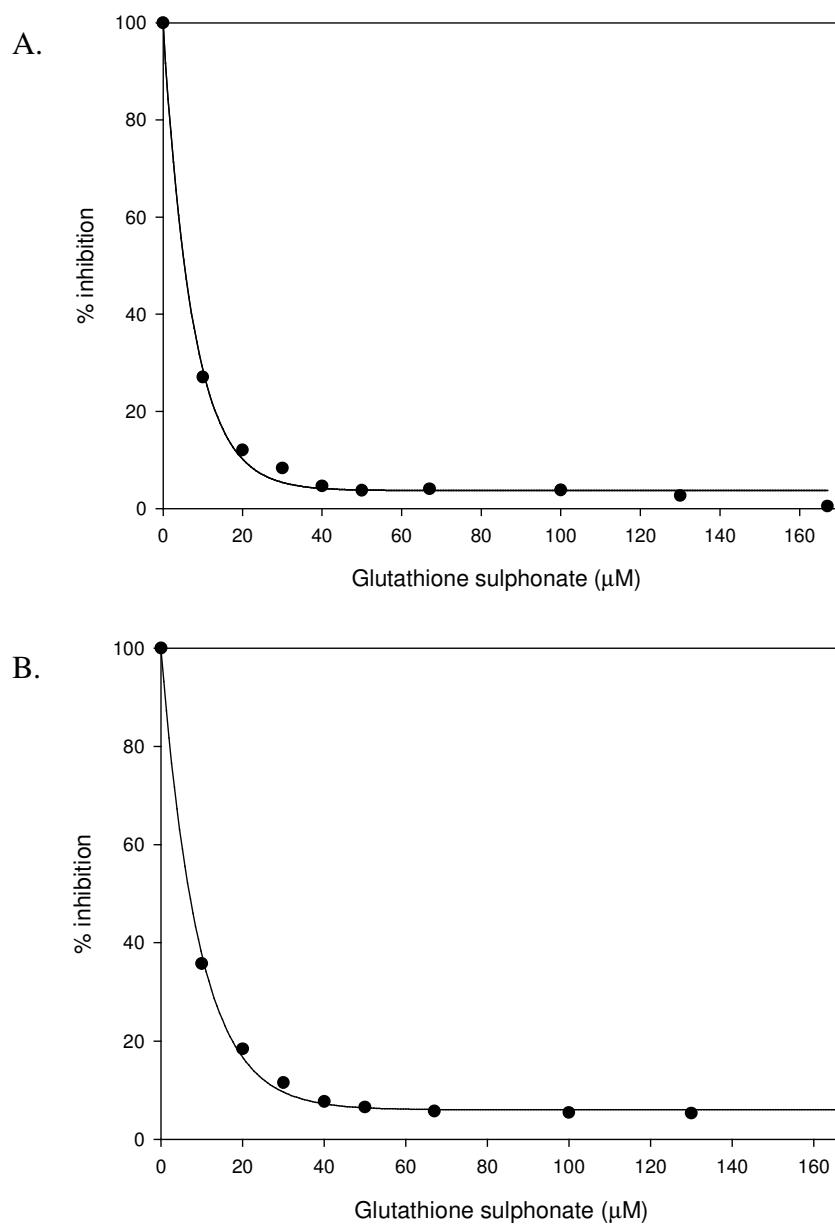


**Figure 20.** Inhibition of wildtype and I71V hGST A1-1 with glutathione sulphonate. Standard GSH/CDNB assay conditions were used (1 mM reduced glutathione (GSH), 1 mM 1-chloro-2,4-dinitrobenzene (CDNB)) with increasing amounts of glutathione sulphonate added (0 – 170 µM final concentration). The *S*-conjugating activity of the enzyme was assessed by measuring the concentration of the ligand required to inhibit 50 % of the enzyme activity. (A) wildtype hGST A1-1 ( $R^2 = 0.99$ ). (B) I71V mutant hGST A1-1 ( $R^2 = 0.99$ ).



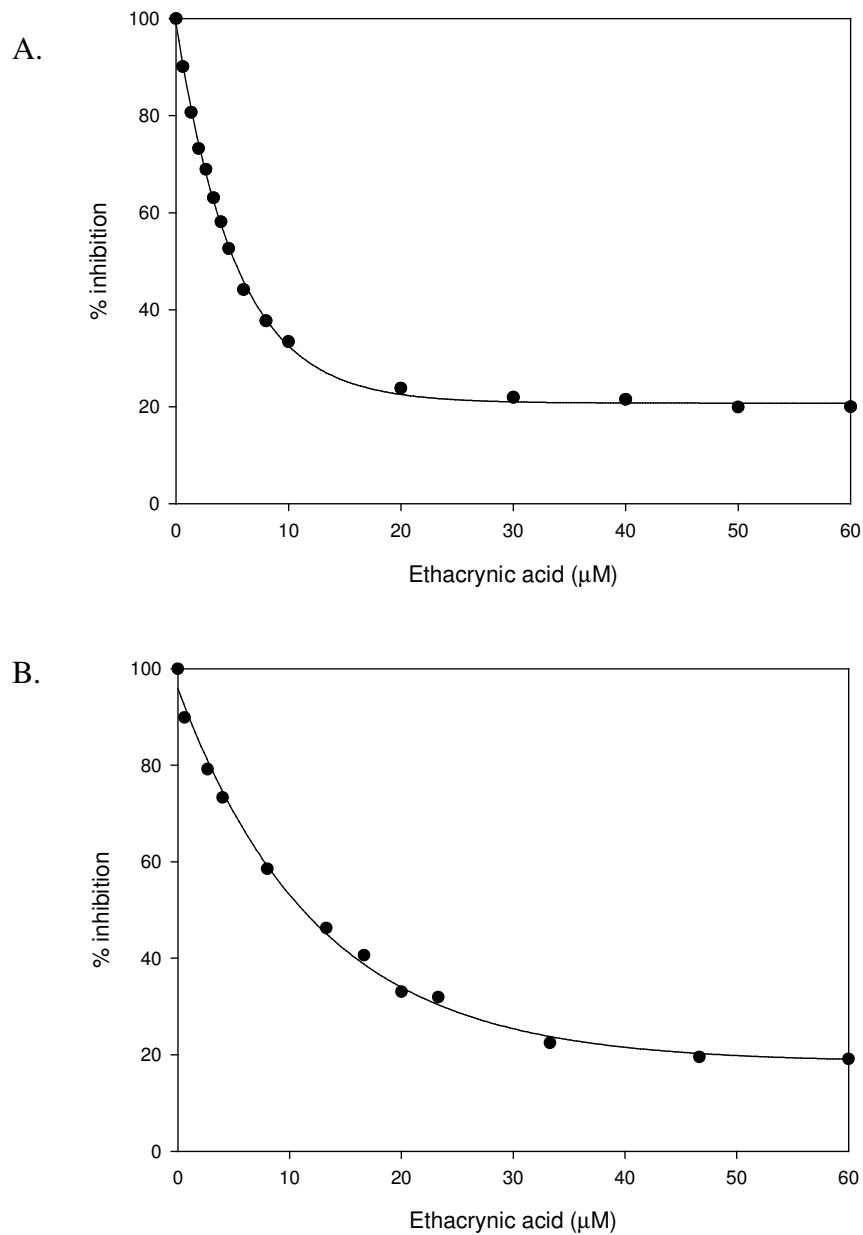


**Figure 21.** Inhibition of wildtype and I71V hGST A1-1 with ethacrynic acid. Standard GSH/CDNB assay conditions were used (1 mM GSH, 1 mM CDNB) with increasing amounts of ethacrynic acid added (0 – 60 μM final concentration). The S-conjugating activity of the enzyme was assessed by measuring the concentration of the ligand required to inhibit 50 % of the enzyme activity. (A) wildtype hGST A1-1 ( $R^2 = 0.99$ ). (B) I71V mutant hGST A1-1 ( $R^2 = 0.99$ ).

**Table 3.** Summary of inhibition characteristics of wildtype and I71V hGST A1-1

<b>Inhibitor</b>	<u>IC<sub>50</sub> (μM)</u>	
	<b>Wildtype</b>	<b>I71V hGST A1-1</b>
Glutathione sulphonate	5.4 ± 0.4	6.9 ± 1
Ethacrynic acid	5.1 ± 0.5	11.3 ± 1.8

IC<sub>50</sub> values were determined as the inhibitor concentration causing 50% inhibition at constant glutathione (1 mM), 1-chloro-2,4-dinitrobenzene (1 mM) and 2 nM enzyme concentrations

### 3.5.2 Urea-induced equilibrium unfolding studies

Urea-induced equilibrium unfolding of wildtype and I71V hGST A1-1 was monitored using tryptophan fluorescence and ellipticity at 222 nm as probes as shown in Figures 22 and 23 respectively. The unfolding curves were used to obtain the thermodynamic parameters shown in Table 4. The unfolding transition curves of both proteins are characterised by single-phase sigmoidal curves. Although both sigmoidal, the unfolding curves of wildtype and I71V hGST A1-1 are not superimposable. The differences in the unfolding curves when comparing I71V hGST A1-1 to wildtype protein include changes in the unfolding transition mid-point ( $C_m$ -value), as well as differences in the slope of the transition regions.

The curves from Figures 22 and 23 were analysed according to the linear extrapolation method of Pace (1986). The normalised data was fitted to a two-state dimer model using Sigma Plot v. 8.0. As previously described, wildtype hGST A1-1 unfolds via a two-state transition (Wallace *et al.*, 1998b). The non-superimposability of wildtype and I71V hGST A1-1 equilibrium unfolding transitions, together with the decreased  $m$ -value of the I71V unfolding transitions indicate that the two-state fit is not suitable for I71V hGST A1-1.

Figures 24 and 25 show fluorescence and CD equilibrium unfolding curves, combined in one Figure, for wildtype and I71V hGST A1-1, respectively. Figure 25 includes the maximum emission wavelength for I71V hGST A1-1 for each urea concentration used to obtain the urea-induced unfolding curve. The maximum emission wavelength was obtained by reading the wavelength value which gave the maximum fluorescence intensity for each sample at the different urea concentrations. Figures 24 and 25 show that wildtype unfolding transitions, obtained using different probes, are slightly more superimposable than I71V hGST A1-1 unfolding transitions. The decreased  $m$ -value for I71V hGST A1-1 indicates an intermediate although the unfolding transitions do not clearly show the presence of a possible intermediate.

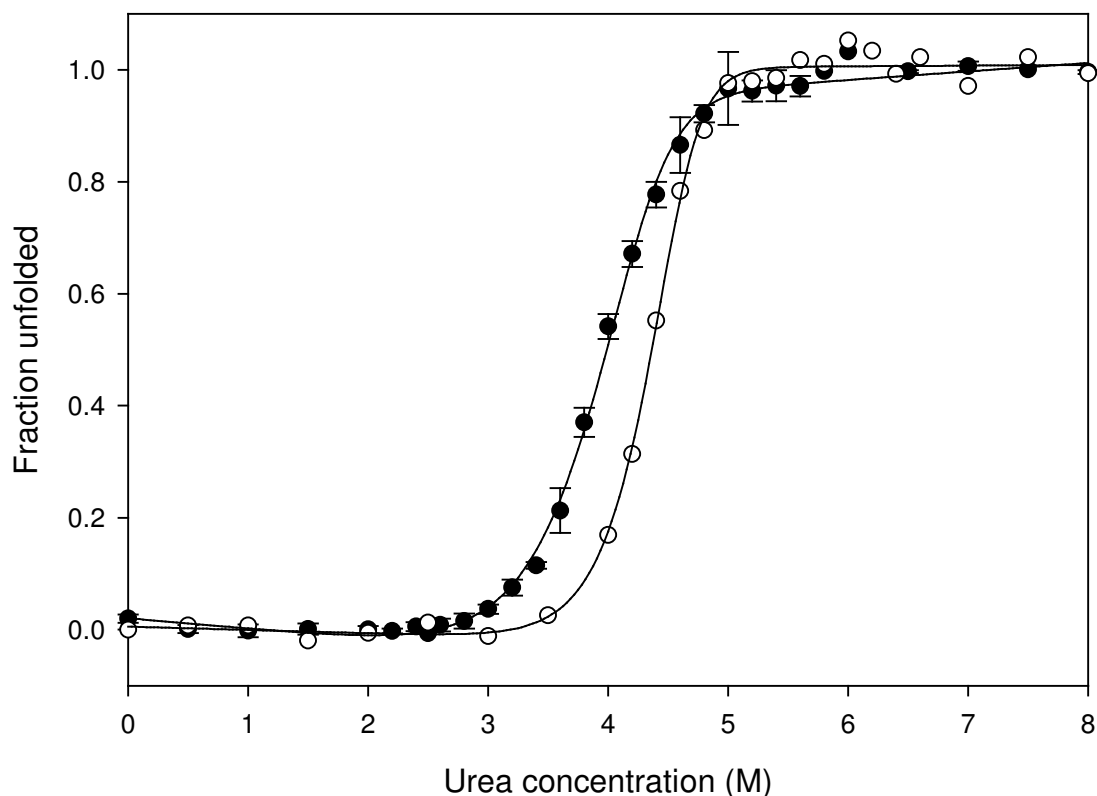


**Figure 22.** Urea-induced equilibrium unfolding of wildtype (open circle) and I71V (solid circle) hGST A1-1 monitored by fluorescence. Experiments were performed at 20°C using a 2  $\mu$ M concentration of protein, 20 mM sodium phosphate buffer, 1 mM EDTA, 0.02%  $\text{NaN}_3$ , pH 6.5. Trp-20 was selectively excited at 295 nm. The emission intensities at 330 nm (folded protein) and 355 nm (unfolded protein) were measured and normalization of the equilibrium unfolding curves was performed according to the method of Pace *et al.* (1989). Data was fitted to a two-state transition model (shown as the solid black line), with a non-linear regression analysis in order to obtain thermodynamic parameters (Pace *et al.*, 1989). For both wildtype and I71V hGST A1-1 the average of three data sets were plotted.

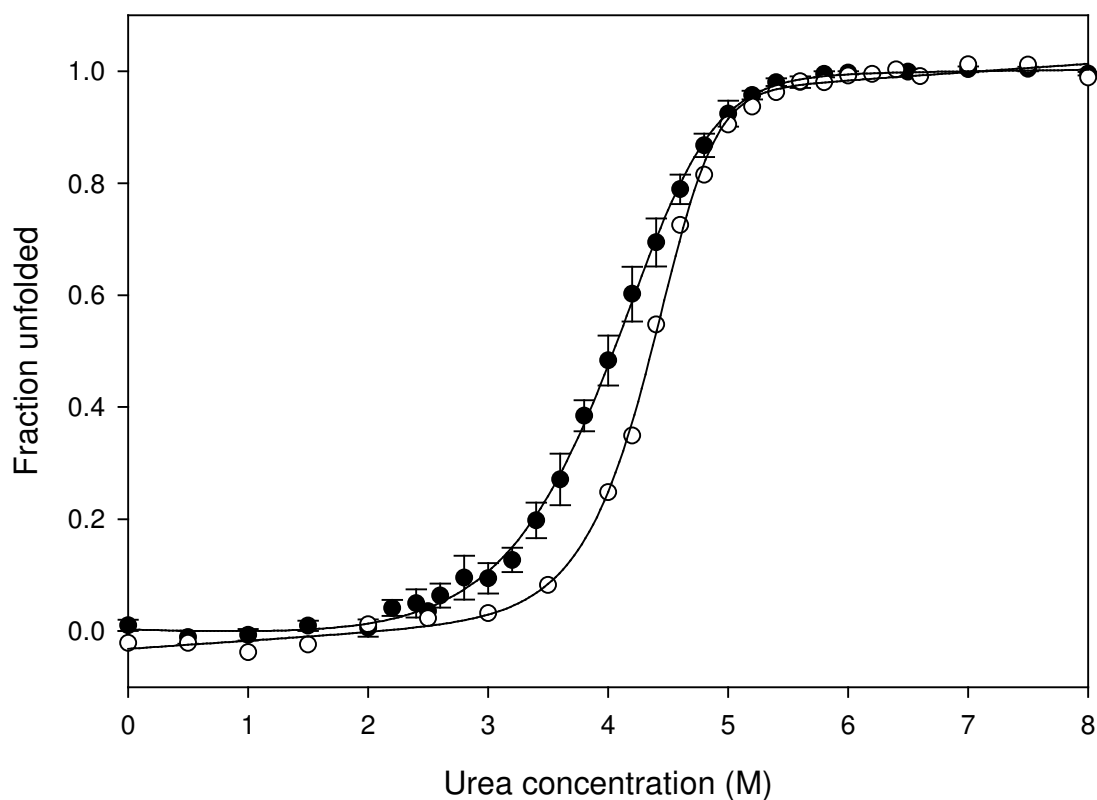


**Figure 23.** Urea-induced equilibrium unfolding of wildtype and I71V hGST A1-1 monitored by circular dichroism. Experiments were performed at 20°C using a 2  $\mu$ M concentration of protein, 20 mM sodium phosphate buffer, 1 mM EDTA, 0.02%  $\text{NaN}_3$ , pH 6.5. Ellipticity was measured at 222 nm. Data was fitted to a two-state transition model (shown as the solid black line) and normalization of the equilibrium unfolding curves was performed according to the method of Pace *et al.* (1989). For I71V hGST A1-1 the average of three data sets were plotted and error bars are shown.

**Table 4.** Thermodynamic parameters for wildtype and I71V hGST A1-1

Parameter	$\Delta G(\text{H}_2\text{O})$ (kJ/mol)	<i>m</i> -value (kJ/mol/M urea)	<i>C<sub>m</sub></i> (M urea)
Wildtype hGST A1-1			
Fluorescence	100 ± 0.4184	16 ± 0.3	4.5
Circular Dichroism	92 ± 1.25	14 ± 0.21	4.5
I71V hGST A1-1			
Fluorescence	75 ± 2.4	12 ± 0.7	4
Circular Dichroism	63 ± 2.3	8 ± 0.7	4

Parameters obtained from data in Figure 22 and 23. Parameters for both fluorescence and CD unfolding curves are tabulated. Refer to section 2.6.3 for the methods in obtaining the tabulated parameters.

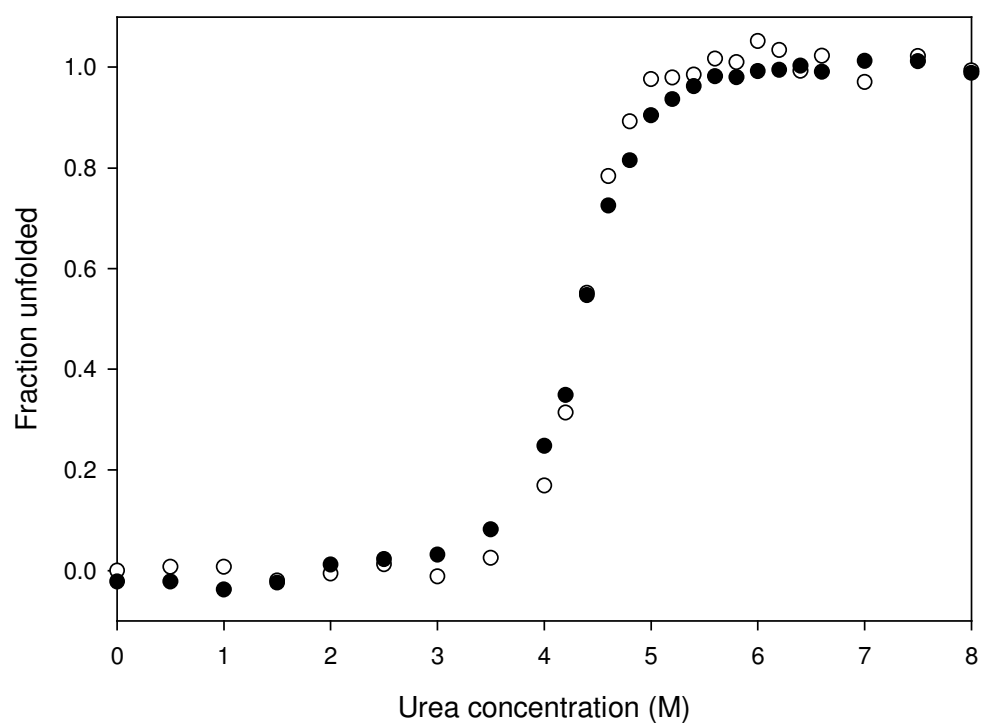


**Figure 24.** Urea-induced equilibrium unfolding of wildtype hGST A1-1 monitored by tryptophan fluorescence (open circle) and CD (solid circle). Experiments were performed at 20°C using a 2  $\mu$ M concentration of protein, 20 mM sodium phosphate buffer, 1 mM EDTA, 0.02% NaN<sub>3</sub>, pH 6.5.

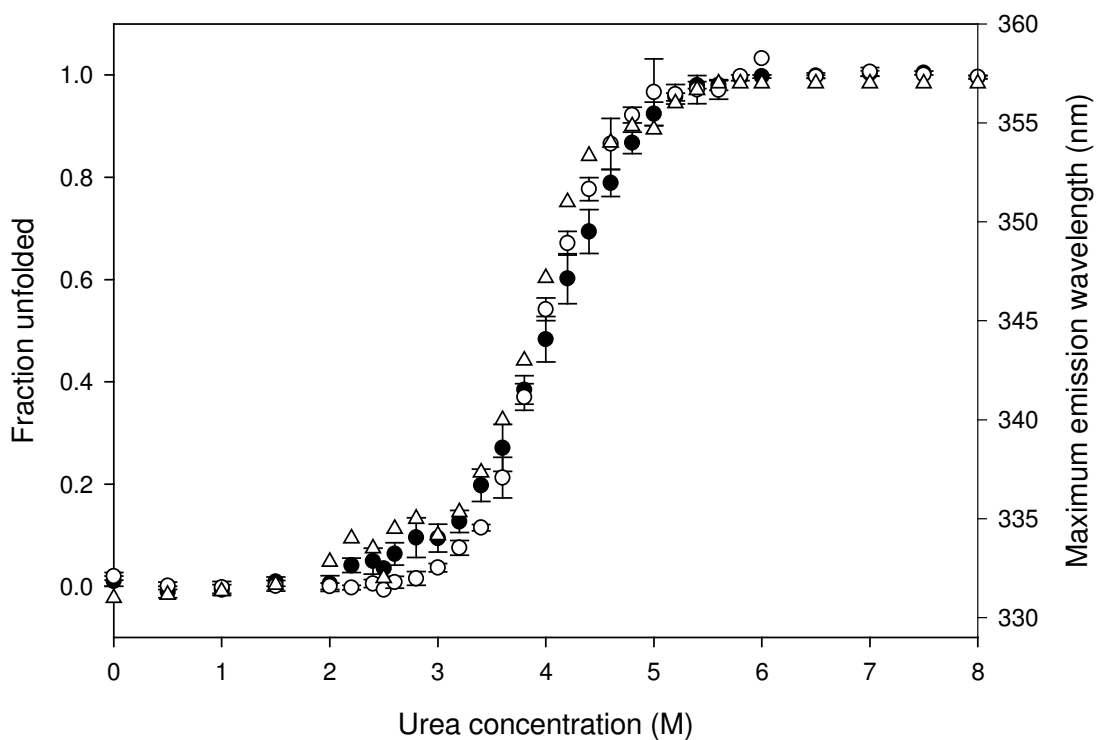


**Figure 25.** Urea-induced equilibrium unfolding of I71V hGST A1-1 monitored by tryptophan fluorescence (open circle) and CD (solid circle). The maximum emission wavelength (open triangle) is shown and was obtained by reading the wavelength value which gave the maximum fluorescence intensity for each sample at the different urea concentrations. Experiments were performed at 20°C using a 2  $\mu$ M concentration of protein, 20 mM sodium phosphate buffer, 1 mM EDTA, 0.02%  $\text{NaN}_3$ , pH 6.5. The average of three data sets were plotted for both fluorescence and CD unfolding transitions and error bars are shown.



The thermodynamic parameters shown in Table 4 were calculated using the unfolding curves (Figures 22 and 23) assuming a two-state unfolding process.  $\Delta G(\text{H}_2\text{O})$ , the free energy change in the absence of denaturant, was calculated to be 96 kJ/mol and 69 kJ/mol for wildtype and I71V hGST A1-1 respectively. The  $m$  value for I71V mutant was estimated to be 9.6 kJ/mol/M urea, a 36% decrease compared to that of 15 kJ/mol/M urea for the wildtype. The transition midpoint ( $C_m$  value) for the I71V hGST A1-1 unfolding curve showed a decrease of 0.5 M urea in comparison to the wildtype.

### **3.6 Thermodynamic characterization of *S*-hexylglutathione-hGST A1-1 binding by isothermal titration calorimetry**

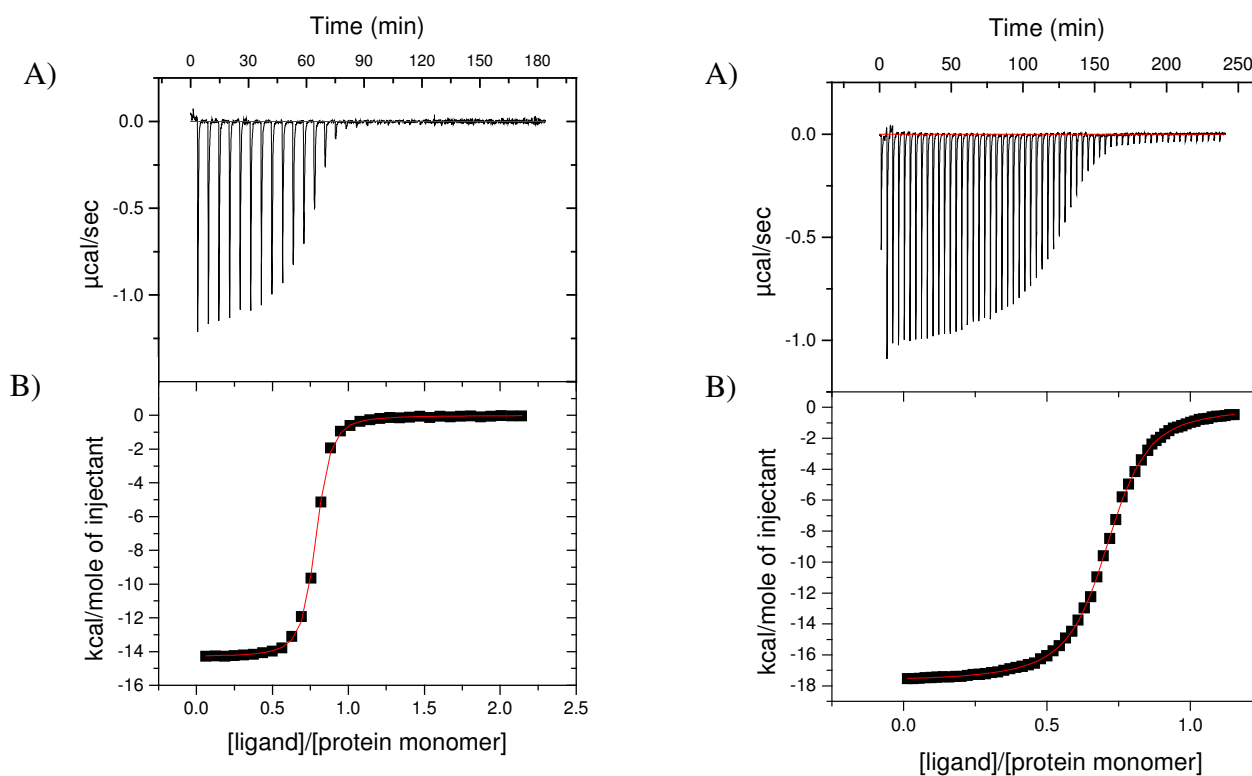
Isothermal titration calorimetry is used to obtain detailed thermodynamic profiles of molecular associations. ITC is capable of directly measuring heat evolved or absorbed during any molecular reaction and is therefore used to determine thermodynamic parameters. The independent parameters are the stoichiometry ( $N$ ) of the binding interaction, the binding constant ( $K_a$ ) and the enthalpy change of the binding interaction ( $\Delta H$ ). The dependent parameters are the standard Gibbs free energy change ( $\Delta G$ ) and the entropy ( $\Delta S$ ) of the binding interaction.

Figure 26 shows the raw and normalised integrated titration profile of binding of *S*-hexylglutathione to wildtype and I71V hGST A1-1 performed at 25°C. Figure 27 shows the raw and normalised integrated titration profile of binding of *S*-hexylglutathione to I71V hGST A1-1 performed at 5 - 20°C. The most notable feature of the binding isotherms at high temperatures (20 - 25°C) is binding of *S*-hexylglutathione to I71V hGST A1-1 is exothermic. However at lower temperatures (15°C and below) the binding isotherm starts off exothermic and becomes endothermic, seen by the positive peaks for the last 20 or 30 injections. These endothermic injections, attributed to the heats of dilution at lower temperatures, are corrected for before determining any thermodynamic parameters. All binding isotherms for wildtype protein are exothermic (Kuhnert *et al.*, 2005). For I71V hGST A1-1 as is the case for wildtype hGST A1-1, the integrated data for *S*-hexylglutathione binding fit well to a single-site binding model per monomer. At higher temperatures, the titration curve exhibits a decrease in the exothermic heat of binding after each successive injection. The reaction is, therefore, characterised by a

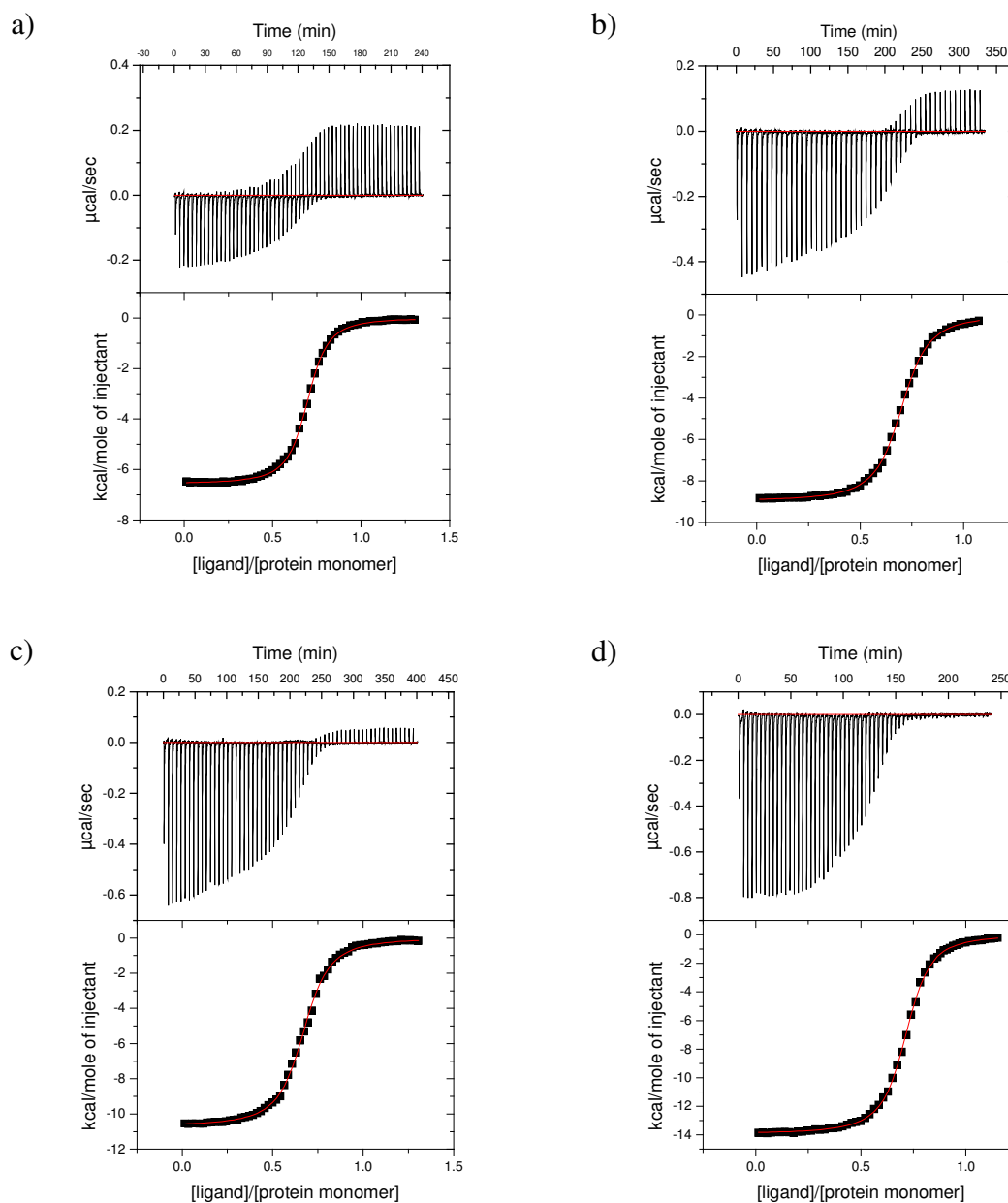
series of negative peaks representative of a favourable enthalpy change. To obtain the heat evolved from each injection, the averaged heats of the post saturation peaks were subtracted from the raw data. The  $\Delta H$  is obtained by integrating the area under each peak and dividing this by the moles of ligand added. The  $\Delta H$  for the wildtype and I71V hGST A1-1, at 25°C, is shown in panel B (Figure 26).

Table 5 summarises the experimental parameters obtained for the binding of *S*-hexylglutathione to wildtype (Table 5A) (Kuhnert *et al.*, 2005) and I71V (Table 5B) hGST A1-1 proteins. The binding stoichiometry indicated that one *S*-hexylglutathione molecule binds to each active site (i.e. one molecule per subunit). The binding strength of the inhibitor (*S*-hexylglutathione) to the proteins is seen in terms of the dissociation constant ( $K_d$ ) where the lower the  $K_d$  the tighter the binding. The results in Table 5 show the  $K_d$  for wildtype (0.071  $\mu\text{M}$ ) is lower than that of I71V hGST A1-1 (0.37  $\mu\text{M}$ ) by a factor of about 5. Also, the binding strength is greater at lower temperatures and decreases as the temperature increases, for both wildtype and I71V hGST A1-1.

For all *S*-hexylglutathione-binding experiments performed, an increase in temperature resulted in an increase in the binding enthalpy of the reaction, as well as a decrease in the binding entropy (both parameters became more negative with increasing temperature). The free energy of complex formation ( $\Delta G$ ) however is practically insensitive to temperature due to the compensatory effects of enthalpy and entropy (Lumry and Rajender., 1970), both of which are temperature dependent. The enthalpy of complex formation ( $\Delta H$ ) is exothermic throughout the temperature range studied (5 – 25°C) while the entropy of complex formation ( $\Delta S$ ) is favourable (positive) only at temperatures of 10°C and below. At higher temperatures the unfavourable  $\Delta S$  are compensated for by favourable  $\Delta H$ . The entropy term ( $T\Delta S$ ) at 25°C of *S*-hexylglutathione binding to wildtype hGST A1-1 (-19kJ/mol) (Kuhnert *et al.*, 2005) is more negative than that of I71V hGST A1-1 (-63kJ/mol).



**Figure 26.** A representative calorimetric titration profile of the binding of *S*-hexylglutathione to the wildtype (left) and I71V mutant (right) hGST A1-1 protein. The experiment was performed at 25<sup>o</sup>C. The conditions were: 0.05 mM protein monomer concentration and 0.05 mM *S*-hexylglutathione in 20 mM sodium phosphate buffer, pH 6.5, containing 1 mM EDTA, 0.02% sodium azide. Panel A shows the raw exothermic heats associated with the injection of *S*-hexylglutathione into the ITC sample cell containing the I71V mutant protein. Panel B shows the integrated and fitted binding isotherm (corrected for heats of dilution) corresponding to the data in panel A. The solid line through the data represents the best fitted curve obtained using the ORIGIN software.



**Figure 27.** Calorimetric titration profiles of the binding of *S*-hexylglutathione to I71V hGST A1-1. The experiments were performed at 5°C (a) , 10°C (b) , 15°C (c) and 20°C (d). The conditions were: 0.05 mM protein monomer concentration and 0.05 mM *S*-hexylglutathione in 20 mM sodium phosphate buffer, pH 6.5, containing 1 mM EDTA, 0.02% sodium azide. The top panel shows the raw exothermic heats associated with the injection of *S*-hexylglutathione into the ITC sample cell. The bottom panel shows the integrated binding isotherm (corrected for heats of dilution) corresponding to the data in the top panel.

**Table 5.** Energetics of the interaction between (A) wildtype and (B) I71V hGSTA1-1 with *S*-hexylglutathione at different temperatures. All the values are based on a single experiment and the errors were obtained by fitting the titration data using the ITC software programme (ORIGIN 5.0).

A.

Temperature (Kelvin)	N	$K_d$ ( $\mu\text{M}$ )	$\Delta H$ (kJ/mol)	$\Delta S$ (kJ/mol/k)	$T\Delta S$ (kJ/mol)	$\Delta G$ (kJ/mol)
278	$0.79 \pm 0.001$	$0.049 \pm 0.01$	$-26.1 \pm 0.08$	0.046	12.79	-38.89
283	$0.78 \pm 0.001$	$0.048 \pm 0.01$	$-36.6 \pm 0.09$	0.019	5.377	-41.97
288	$0.77 \pm 0.001$	$0.063 \pm 0.08$	$-41.27 \pm 0.12$	-0.005	-1.44	-39.83
293	$0.76 \pm 0.002$	$0.085 \pm 0.08$	$-50.56 \pm 0.19$	-0.037	-10.84	-39.72
298	$0.76 \pm 0.001$	$0.071 \pm 0.06$	$-59.84 \pm 0.14$	-0.064	-19.07	-40.77

Data presented in the above Table were obtained by Diane Kuhnert and have been included in this thesis with her permission. This data has previously been published (Kuhnert *et al.*, 2005).

B.

Temperature (Kelvin)	N	$K_d$ ( $\mu\text{M}$ )	$\Delta H$ (kJ/mol)	$\Delta S$ (kJ/mol/k)	$T\Delta S$ (kJ/mol)	$\Delta G$ (kJ/mol)
278	$0.70 \pm 0.001$	$0.25 \pm 0.08$	$-27.48 \pm 0.04$	0.028	7.78	-35.26
283	$0.70 \pm 0.001$	$0.32 \pm 0.06$	$-37.5 \pm 0.05$	-0.008	-0.23	-37.27
288	$0.67 \pm 0.001$	$0.40 \pm 0.08$	$-44.73 \pm 0.12$	-0.033	-9.50	-35.23
293	$0.71 \pm 0.001$	$0.25 \pm 0.08$	$-58.28 \pm 0.08$	-0.07	-20.51	-37.77
298	$0.71 \pm 0.001$	$0.37 \pm 0.02$	$-74.1 \pm 0.05$	-0.125	-37.25	-36.85

The heat capacity change ( $\Delta C_p$ ) upon binding of *S*-hexylglutathione to wildtype and I71V hGST A1-1 was determined by performing the calorimetric experiments at different temperatures under the same pH and buffer conditions.  $\Delta C_p$  is associated with the protein-ligand complex formation and estimated from the slopes of the linear curves (Figure 28A and B). The temperature dependence yields a  $\Delta C_p$  value of  $-1.71$  kJ/mol/K for wildtype hGST A1-1 (Kuhnert *et al.*, 2005) and  $-2.12$  kJ/mol/K for I71V hGST A1-1. The difference in heat capacity between wildtype and I7V hGST A1-1 is  $-0.41$  kJ/mol/K.

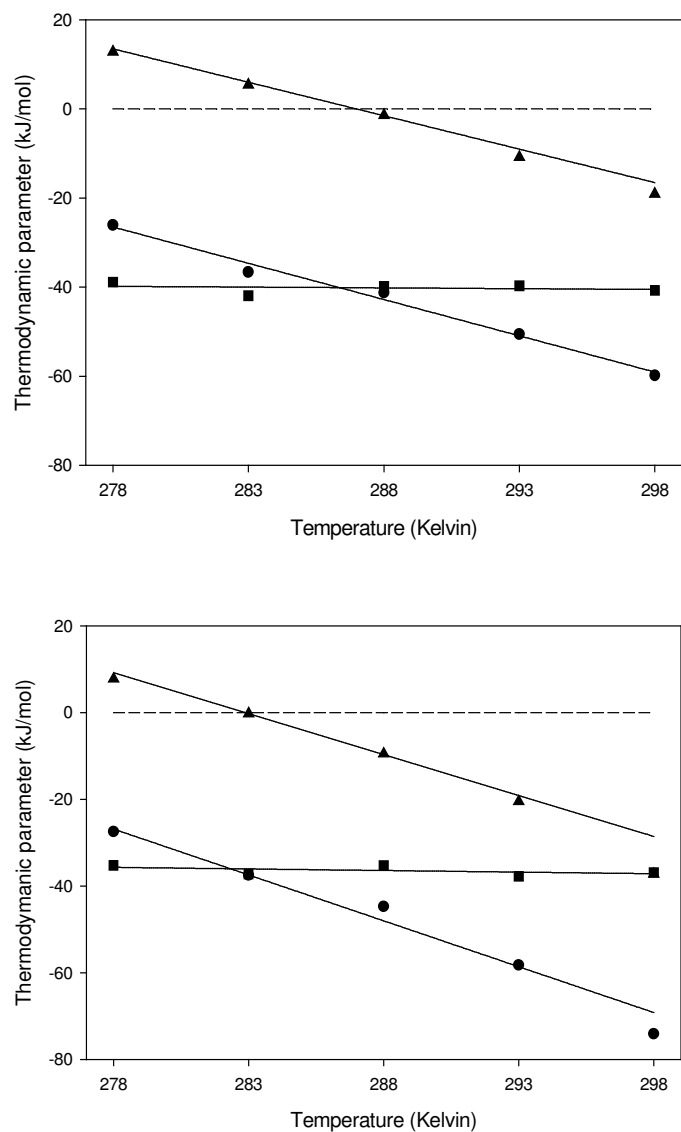


**Figure 28.** Temperature-dependence of the thermodynamic parameters for *S*-hexylglutathione binding to wildtype (top) (Kuhnert *et al.*, 2005) and I71V (bottom) hGST A1-1. The circles, triangles and squares represent  $\Delta H$ ,  $T\Delta S$  and  $\Delta G$  respectively. The data are summarised in Table 5. The solid line through the points is the linear regression fit to the data. From the plot of  $\Delta H$  versus temperature, the slope of the linear regression yields the change in heat capacity ( $\Delta C_p$ ) upon ligand binding to each of the proteins. The correlation coefficient for the plot of  $\Delta H$  versus temperature for (A) and (B) is 0.99 and 0.98, respectively.

## CHAPTER 4

### DISCUSSION

#### 4.1 Plasmid identity confirmation and assessment of protein purification

DNA sequencing confirmed the presence of wildtype and I71V hGST A1-1 coding sequences, which also showed that no additional mutations had been introduced into either wildtype or I71V hGST A1-1 plasmid (Figure 6).

Purification methods for both wildtype and I71V hGST A1-1 had previously been determined. The protocol (section 2.3) was followed and purification of both wildtype and I71V hGST A1-1 was successful. The proteins were purified using a CM-Sepharose column that separates protein according to charge. SDS PAGE analysis showed that purification yielded pure homogenous protein samples. The physical properties of I71V hGST A1-1, such as electrophoretic mobility and  $M_r$  are indistinguishable from those of the wildtype. Both proteins were determined to have a  $M_r$  of 26 000, consistent with the predicted weight of hGST A1-1.

#### 4.2 Verification of the structural integrity of I71V hGST A1-1

For the work undertaken, the gross secondary and tertiary structure of I71V hGST A1-1 must be comparable to wildtype hGST A1-1. Intrinsic tryptophan fluorescence is a useful spectroscopic technique used to measure the conformational stability of proteins. The indole side chain of the tryptophan residue is highly sensitive to its local environment. As such, the number as well as the location of this residue within a protein, provides a useful means of probing for local or global conformational changes. hGST A1-1 has one tryptophan residue (Trp-20) per monomer. The indole side chain of Trp20 protrudes from domain 1 into domain 2 and forms a series of hydrophobic interactions with the side chains of Ile158, Glu162 and Tyr165 (in  $\alpha$ -helix 6) and Val194 and Phe197 in  $\alpha$ -helix 8. In the native state of the protein, the indole side chain of Trp20 is inaccessible to solvent (solvent accessible surface area  $\sim 4 \text{ \AA}^2$ ; (Wallace *et al.*, 1998a). Based on these characteristics, the location of Trp-21 can serve as a local reporter of events occurring at the interdomain interface.



Tryptophan fluorescence emission spectra indicate the overall tertiary structure of I71V hGST A1-1 is similar to wildtype hGST A1-1. The emission maxima of the native conformations were identical at 330 nm (Figure 8), consistent with the burial of the Trp-20 residue in the native state of the protein (Lakowicz, 1983); Wallace *et al.*, 1998a; Wallace *et al.*, 1998b). The absence of any shift in wavelength suggests that the mutations did not impact upon the environment of the tryptophan residue in hGST A1-1. Similarly, the spectra for both denatured sample proteins show an emission maximum of 357 nm when excited at either 280 nm or 295 nm. The red shift upon denaturation is indicative of the exposure of the Trp20 residue to solvent. Excitation at 280 nm shows an additional emission peak at 310 nm for the spectrum of both denatured wildtype and I71V hGST A1-1. This is due to the fact that as hGST A1-1 protein unfolds, the energy transfer from the tyrosine's to the tryptophan is decreased due to the increase in distance between the residues upon unfolding, and the tyrosine residues therefore emit light as well, giving the additional peak. The additional peak is accompanied by a decrease in the intensity of the spectra for the same reason; energy is no longer transferred from the tyrosine to the tryptophan resulting in a decrease in the light emitted from the tryptophan (Lakowicz, 1983). Similar emission spectrum for both wildtype and I71V hGST A1-1 show that there are no apparent changes in hGST A1-1's global structure upon incorporation of the I71V mutation. Furthermore, these similarities are indicative of the tertiary structure of I71V hGST A1-1 being equivalent to that of wildtype hGST A1-1.

The far-UV circular dichroism spectral properties show that the overall secondary structure conformation of wildtype and I71V hGST A1-1 are similar. Both proteins showed molar ellipticity minima at 210 and 222 nm, a spectra characteristic of proteins predominantly composed of  $\alpha$ -helices. This is consistent with the crystal structure of hGST A1-1, which reports that the protein is about 60% alpha-helical (Sinning *et al.*, 1993; Cameron, 1995). Following denaturation the distinctive troughs observed in the spectra of native protein were no longer evident (Figure 10). Therefore, the secondary structure is completely disrupted as the protein unfolds in 8 M urea. From these results it is evident that the I71V mutation did not adversely affect the secondary structural content of hGST A1-1.

Changes or shifts in ANS fluorescence emission spectrum are determined by the polarity of the environment in which it finds itself (Lakowicz, 1999; Sayed *et al.*, 2002). Fluorescence enhancement as well as the blue shift in the emission maximum wavelength of ANS on binding wildtype and I71V hGST A1-1 is indicative of the dye binding a more hydrophobic or more non-polar environment. The extent of the blue-shift in emission maximum is determined by the polarity of the ANS binding site; the lower the polarity, the greater the blue-shift (Lakowicz, 1999; Sayed *et al.*, 2002). Recent studies have shown that ANS binds the non-polar H-site of the active site (Dirr *et al.*, 2005). The binding site of ANS to wildtype and I71V mutant hGST A1-1 is not strictly hydrophobic in nature, however, as compared with an emission maximum intensity of ANS (454 nm) when bound to a highly hydrophobic site in apomyoglobin for example (Stryer, 1965). The spectral blue shift of each hGST A1-1 protein was accompanied by an enhanced fluorescence intensity (Figure 11). Because ANS fluorescence is quenched by water, the fluorescence intensity of protein-bound ANS is highly dependent on its accessibility to water (Kirk *et al.*, 1996; Matulis *et al.*, 1998). Relative to other lipid-binding proteins, the fluorescence enhancement of ANS bound to hGST A1-1 is low, indicating a greater exposure of ANS to solvent in the protein (Sayed *et al.*, 2002). Overall the polarity and degree of solvent exposure of the ANS binding site in I71V hGST A1-1 is unchanged compared to the wildtype protein.

Overall, the structural analysis confirms the absence of any changes in the proteins gross structural properties due to the incorporation of the I71V mutation. Thus the wildtype and I71V hGST A1-1 can be compared, with respect to their unfolding and enzyme kinetics.

### **4.3 Steady-state enzyme kinetic properties**

Analysis of the kinetic properties of I71V hGST A1-1 shows that the introduction of the mutation impacts considerably on the activity of the enzyme. The results in Table 2 show that the specific activity of I71V hGST A1-1 is three times that of the wildtype hGST A1-1. This result suggests some kind of local structural change at or near the active site that affected the catalysis of the enzyme and possibly substrate binding, however this change was not detected by low resolution probes such as CD and tryptophan fluorescence. It is difficult to identify the exact point of change within the enzyme by enzymatic analysis

alone, since one needs to determine which part of the active site is affected, either the G-site or the H-site or both.

GSTs are involved in nucleophilic substitution reactions ( $S_NAR$ ). An example of this reaction is shown in Figure 5. The  $S_NAR$  of this nitro-substituted aryl proceeds via the formation of 1-chloro-1-(*S*-glutathionyl)-2,4-dinitrobenzene, an unstable Meisenheimer complex transition state (Graminski *et al.*, 1989) which is the rate-limiting step of the reaction. It has been said that the ability of the enzyme to stabilise a Meisenheimer complex is related to its ability to stabilise the transition state for formation of a Meisenheimer complex intermediate. Therefore the transition state for this reaction must in some sense resemble the Meisenheimer complex (Graminski *et al.*, 1989). The increase in the I71V hGST A1-1 activity suggests that the introduction of valine at position 71 in the thioredoxin fold could have directly or indirectly affected the enzymes ability to stabilise the transition state or it could have altered the on/off rates of substrate binding. The better an enzyme can stabilise the transition state of the reaction, the more efficient the reaction will be (Graminski *et al.*, 1989). The efficiency of the reaction taking place is seen by the greater specific activity, as well as the increased catalytic efficiency.

The results obtained from the standard GSH/CDNB conjugation assay suggest that tertiary structural changes occurred at or near the active site of I71V hGST A1-1. Small structural changes are predicted since the mutation of isoleucine with valine results in a small cavity due to the truncation of the isoleucine side chain and although the residue is not directly involved in the active site, the position of the Ile71 is such that it is found close to the active site. The removal of the methyl group from the side chain of isoleucine resulted in the loss of van der Waals contacts and this affects the catalytic mechanism of the enzyme.

$K_m$ , the Michaelis constant, relates to the substrate concentration for an enzyme to reach half its maximum velocity. Although the increases in  $K_m$  for I71V hGST A1-1 are slight, these results show that the  $K_m$  is definitely affected to some extent. The increase in  $K_m$  tells us that the I71V mutation induces a conformational change that affects the binding

of the substrate to the enzyme, indicating loss of affinity for the substrates. In a previous mutational study on Alpha class, a R15K mutant demonstrated a seven fold increase in  $K_m$  for GSH which indicated loss of affinity for GSH (Bjornestedt *et al.*, 1995). The  $K_m$  can be determined by both physical and chemical events referring to binding and catalysis. It is difficult, however, to distinguish between the two by enzyme kinetics alone and tell which event is affected. The catalytic efficiency ( $k_{cat}/K_m$ ) relates to the free energy of the transition state and can be used as a measure of the stabilising effect contributed by an enzyme (Nilsson *et al.*, 2002). The increase in  $k_{cat}/K_m$  for both substrates (GSH and CDNB) suggests that the I71V mutation helps attain or stabilise the transition state. Other studies on hGST A1-1 have shown that mutations of residues important in catalysis show an increase in  $K_m$  and a decrease in  $k_{cat}/K_m$  as well as a greatly reduced specific activity (Stenberg *et al.*, 1991; Bjornestedt *et al.*, 1995; Allardyce *et al.*, 1999; Sayed *et al.*, 2000; Nilsson *et al.*, 2002; Mosebi *et al.*, 2003; Nathaniel *et al.*, 2003; Dirr *et al.*, 2005). Non-productive binding of a substrate is expected to decrease both  $k_{cat}$  and  $K_m$  by the same factor, leaving  $k_{cat}/K_m$  unchanged (Fersht, 1999). On a study of a Y9F mutation in hGST A1-1 the effects of  $k_{cat}$  and  $K_m$  for GSH suggested that GSH was bound in a catalytically unproductive mode in the mutant (Pettersson *et al.*, 2001). In the present study both  $k_{cat}$  and  $K_m$  were increased for both substrates for I71V hGST A1-1 resulting in an increase in the  $k_{cat}/K_m$  as well, confirming that the binding of the substrates has been altered, together with an alteration in the stabilisation of the transition state.

The  $\Delta\Delta G$  for transition state stabilisation is  $-5.82$  kJ/mol, indicative of a greater stabilisation of the transition state on incorporation of the I71V mutation. A previous study involving a D209G mutation in wildtype hGST A1-1 resulted in  $\Delta\Delta G$  for transition state stabilisation of  $0.4$  kJ/mol, indicating a lower stabilisation of the transition state on disruption of the conserved N-capping motif in helix 9 (Dirr *et al.*, 2005). Taking into consideration the increased specific activity of I71V hGST A1-1 as well as the increase in the  $k_{cat}$  and  $K_m$ , it is apparent that the I71V mutation increases the stabilisation of the transition state allowing for a more efficient enzyme.

When a residue is mutated and the resulting kinetic parameters reflect an increase in  $K_m$  and a decrease in  $k_{cat}$ , the residue is said to be important for both substrate binding and catalysis (Allardyce *et al.*, 1999). In the present study, the mutation has a small effect on substrate binding as seen by the small increase in the  $K_m$  value for I71V hGST A1-1 and a larger effect on the catalysis of the enzyme, as seen by the increase in specific activity and  $k_{cat}$  value. The increase in  $k_{cat}$  suggests the I71V mutation results in product release being more facile as is the case with the F220A and F220T mutants in the work by Nilsson *et al.* (2002) where the more open active site is responsible for the better product release. It is difficult to say whether the active site is more open for the I71V mutant however, since the crystal structure is not available.

Without the crystal structure of I71V hGST A1-1 the exact reasons for the increased stabilisation of the transition state as well as changes in binding of the substrates cannot be determined. The kinetic data together with the location of Ile71 suggests that the mutation causes a less favourable active site for the binding of substrates, as indicated by the lower  $K_m$ . The increase in  $K_m$  together with the increase in specific activity could be a reflection of a gain of function with respect to reaction intermediates stabilisation. Ile71, although an unlikely residue to participate directly in the catalytic mechanism has a side chain that may serve an important role that directs other residues in the active site to assume optimal position for efficient catalysis.

#### **4.4 Inhibition properties of the I71V and wildtype hGST A1-1**

To further characterise the effect of the I71V mutation, competitive inhibition studies were performed using glutathione sulphonate ( $GSO_3^-$ ) and ethacrynic acid as inhibitors. Inhibition studies yield an  $IC_{50}$  value (the concentration of inhibitor causing a 50% decrease in enzyme activity). One would predict that if a mutation causes a structural change that does not favour substrate binding there would be an increase in the  $IC_{50}$  value compared to that of the wildtype, as is the case with the I219A substitution in hGST A1-1 (Mosebi *et al.*, 2003). The activity of the enzyme was only 28% of that of the wildtype and inhibition studies showed a 6-fold increase in the  $IC_{50}$  values for inhibition with  $GSO_3^-$  (Mosebi *et al.*, 2003).

Inhibition studies are used to determine which part of the active site is affected by the mutation; the G-site, the H-site or both.  $\text{GSO}_3^-$  is an analogue of the G-site substrate GSH and therefore used as a competitive inhibitor of the G-site and binds the G-site of the active site located on each subunit (i.e. one molecule of  $\text{GSO}_3^-$  per protein monomer) (Reinemer *et al.*, 1991). Molecular recognition of glutathione (or its analogues) bound at the G-site involves a network of specific polar interactions between the tripeptide and a number of protein moieties in domain 1 of one subunit and domain 2 of the other subunit in the dimer (Dirr, 1994). Values in Table 3 show that the CDNB-conjugating activity of the I71V mutant is similar to that of the wildtype with the mutant enzyme being only slightly less competitively inhibited by  $\text{GSO}_3^-$ . This gives an indication that the G-site is only slightly altered by the I71V mutation.

Ethacrynic acid binds in a non-productive mode in the absence of the co-enzyme glutathione (Cameron, 1995). The crystal structure of hGST A1-1 determined by Cameron (1995) shows that this substrate exhibits a weaker mode of binding and exclusively occupies the H-site (Cameron, 1995). The replacement of isoleucine with valine resulted in about a 2-fold increase in the  $\text{IC}_{50}$  value for the ethacrynic acid (Table 3 and Figure 21). Considering there was little change in the  $\text{IC}_{50}$  value for  $\text{GSO}_3^-$  and a 2-fold increase in the  $\text{IC}_{50}$  value for ethacrynic acid for I71V hGST A1-1 the most noticeable change occurs at the H-site. This statement is confirmed by the results shown in Table 2, where the most noticeable changes occurred for the substrate CDNB, which binds at the H-site. The  $\text{IC}_{50}$  value taken together with the kinetic parameters for CDNB are in agreement with the notion that binding of CDNB in the reaction co-ordinate has been impacted upon for the I71V mutant.

Taking into account the structure of the active site located within the thioredoxin fold (Figure 2), this is an interesting result since the position of Ile71 is closer to the G-site than the H-site therefore any change at the active site was predicted to occur at the G-site. This result tells us that the function of the Ile71 residue has an effect on the cooperativity of the residues involved in catalysis and has long-range effects on the performance of the enzyme and that primarily the binding of CDNB in the reaction co-ordinate has been impacted upon for the I71V mutant.

#### 4.5 Conformational stability studies

The unfolding reaction was shown to be highly reversible thus allowing the calculation of thermodynamic parameters from the urea induced unfolding curves (Pace, 1989). Urea induced equilibrium unfolding was monitored using tryptophan fluorescence and ellipticity at 222 nm as probes. The unfolding transition curves of wildtype and I71V hGST A1-1 are characterised by single sigmoidal curves, suggestive of a two-state (folded dimer/unfolded monomer) transition. However, the single sigmoidal curve alone is not necessarily an indication of a two-state process. Although a two-state fitting model was used, the  $m$ -values obtained for I71V hGST A1-1 are lower than that of wildtype hGST A1-1. This suggests less surface area becomes exposed to solvent when I71V hGST A1-1 unfolds, thus indicating reduced cooperativity and suggests that I71V hGST A1-1 no longer follows a two-state transition.

Also evident from Figures 22 and 23 is the non-superimposability of the unfolding curves of wildtype and I71V hGST A1-1. There is a slight shift towards lower urea concentrations of the unfolding transition mid-point ( $C_m$  value) for I71V hGST A1-1 compared to wildtype hGST A1-1. The lower  $C_m$  value refers to reduced stability of the protein, but only when the  $m$ -value remains unchanged. A low  $m$ -value is not suggestive of a decreased stability but rather suggests the possible introduction of an intermediate (Myers *et al.*, 1995; Soulages, 1998). The  $m$ -value is related to the dependence of the free energy change of unfolding upon denaturant concentration where the broader the unfolding transition region, the lower the  $m$ -value (Pace, 1989). A comparison of wildtype and I71V hGST A1-1 unfolding transitions shows wildtype hGST A1-1 unfolds between 3.8 – 5 M urea whereas I71V hGST A1-1 unfolds in the urea range of 3 – 5 M urea. A decreased  $m$ -value is also suggestive of decreased cooperativity and the possible accumulation of an intermediate state (Soulages, 1998). The cooperativity of protein folding arises when hydrophobic and hydrophilic copolymer sequences collapse to states that are compact and also have good hydrophobic cores (Dill *et al.*, 1995). As mentioned in the introduction, Ile71 is found within a hydrophobic core of the thioredoxin fold. Mutation of Ile71 could result in a disruption of this hydrophobic core and thus account for the decreased cooperativity of the unfolding process of I71V hGST A1-1.

In most reported equilibrium unfolding studies, the transition between the native and unfolded states is assumed to proceed via a two-state mechanism (Soulages, 1998). To be consistent with a two-state model the unfolding curves should be indistinguishable when monitored by several independent techniques (Pace, 1986). Such is the case for wildtype hGST A1-1 where the unfolding transition monitored by both fluorescence and CD (Figure 24) are superimposable, suggesting the unfolding is highly cooperative under equilibrium conditions. This corresponds with previously published data which indicates that the urea induced equilibrium unfolding of wildtype hGST A1-1 occurs via a two-state transition and that the unfolded monomer and folded dimer are the only two species present in significant concentrations at equilibrium (Wallace *et al.*, 1998b; Wallace *et al.*, 1998a).

When looking at I71V hGST A1-1 unfolding transitions the fluorescence and CD unfolding curves are similar (Figure 25) but not superimposable. The non-superimposability of the unfolding transitions together with the decreased *m*-value for I71V hGST A1-1 suggest the introduction of an intermediate state and thus indicate the presence of a non-two-state unfolding process (Soulages, 1998). With this in mind a three-state model was fitted to the mutant equilibrium unfolding data. The three-state model did not fit well to the data. A possible explanation for this is that the probes used, namely fluorescence and CD, are low-resolution probes and did not reflect the structural changes that accompany the formation of the intermediate. Figure 26 shows plots of I71V hGST A1-1 fluorescence data. By varying the way in which data is plotted one can see whether the probes used were sensitive enough to give evidence of an intermediate. The single sigmoidal curves of both plots in Figure 26 do not show the presence of an intermediate yet when plotted together a possible intermediate becomes apparent. There is a greater degree of non-superimposability of the unfolding transitions between 2-3.5 M urea. this could indicate an intermediate, which was monitored by one probe to a greater extent than the other.

The results obtained for the  $\Delta G(\text{H}_2\text{O})$  indicate that the stability of I71V hGST A1-1 is reduced compared to that of wildtype hGST A1-1. The Gibbs free energy change in the



absence of denaturant ( $\Delta G(\text{H}_2\text{O})$ ) provides a measure of the conformational stability of a protein (Pace, 1989). This result corresponds to the results that were predicted since the removal of a methyl group results in the loss of direct interactions with hydrophobic residues and the destabilisation of an enzyme by a predicted 4.6 kJ/mol (1.1kcal/mol) (Eriksson, 1992). As has been previously stated, the mutation of Ile to Val results in the removal of a methyl group from the side chain of isoleucine and therefore a decrease in stability is expected. However the stability upon introduction of the mutation results in a decrease in stability of on average, 21 kJ/mol (5 kcal/mol), almost 5 times greater than the predicted decrease. This tells us that Ile 71 plays an important role in the stability of the protein and possibly in determining cooperativity within domain 1. Studies on rat GST A1-1 by Atkins *et al.* (1997) on  $\alpha$ -helix 9, have suggested the possible stabilising role of tertiary interactions between Phe220, a residue within  $\alpha$ -helix 9, and residues in domain 1. the replacement of Phe220 with either Ile or Leu enhanced the pressure induced conformational changes in helix 9 and a replacement of Phe220 with Tyr increased the stability of the helix, possibly via hydrogen bonding interactions between Try9 and Tyr220. The stability of I71V hGST A1-1 is most likely compromised due to the removal of hydrophobic interactions made between the methyl group of Ile71 and the residues occupying the hydrophobic pocket (Atkins *et al.*, 1997).

#### **4.6 Thermodynamic characterization of *S*-hexylglutathione binding to**

##### **I71V hGST A1-1**

The binding isotherms for both wildtype and I71V hGST A1-1 resemble sigmoidal plots and are useful in gaining accurate binding enthalpy ( $\Delta H$ ) and entropy ( $\Delta S$ ) values. For both wildtype and I71V hGST A1-1 integrated data for *S*-hexylglutathione binding fit well to a single-site binding model indicating one independent binding site per subunit. This correlates with previously published data stating *S*-alkylglutathione conjugates (such as *S*-hexylglutathione) bind GSTs from different gene classes exothermically with a stoichiometry of one inhibitor molecule bound per GST subunit (Ortiz-Salmeron *et al.*, 2001; Ortiz-Salmeron *et al.*, 2003). The binding stoichiometry indicated that one *S*-hexylglutathione molecule binds to each active site, consistent with the crystallographically determined stoichiometry (Kuhnert *et al.*, 2005).

The binding strength of the inhibitor (*S*-hexylglutathione) to a protein is seen in terms of  $K_d$ , where the lower the  $K_d$ , the tighter the binding. The ligand binds 5-fold more tightly to wildtype (0.07  $\mu\text{M}$ , 25°C) than I71V hGST A1-1 (0.37  $\mu\text{M}$ , 25°C). The Gibbs free energy change ( $\Delta G$ ) determines the binding affinity of a ligand to a particular protein (Luque *et al.*, 1998). The direct relationship between  $\Delta G$  and  $K_d$  is seen in the equation:

$$\Delta G = -RT \ln K_d \quad (15)$$

The  $K_d$  can be seen as an indication of the number of interactions that form when the ligand binds an enzyme. The results suggests that incorporation of the I71V mutation, resulting in the removal of a methyl group, removes some interactions that normally form in wildtype hGST A1-1 and thus resulted in less tight binding of the ligand. The  $\Delta G$  values are similar for all studies carried out at different temperatures. This is an example of the enthalpy-entropy compensation effect that is common to many binding processes (Lumry *et al.*, 1970; Sigurskjold *et al.*, 1991). The large and favourable enthalpy term is attributed to hydrogen bonding and van der Waals interactions in the complex formation and these overcome the unfavourable entropy change. This explains the overall favourable Gibbs free energy of binding. The results (25°C) indicate the reaction was enthalpically favourable (-74.01 kJ/mol) but entropically unfavourable (-0.125 J/mol/K) for I71V hGST A1-1. It is evident that the overall  $\Delta G$  is slightly more favourable for wildtype than I71V hGST A1-1.

The binding enthalpy of a reaction is due to a number of different contributions such as protein-ligand hydrogen bonds, salt bridges and van der Waals contacts as well as the loss of protein-solvent hydrogen bonds. The negative  $\Delta H$  refers to the formation of hydrogen bonds and van der Waals contacts formed when the ligand binds the protein (Sigurskjold *et al.*, 1991). The binding enthalpy is due to the fact that when bonds form, energy is released. Results in Table 5 show that interaction of the ligand with wildtype and I71V hGST A1-1 is enthalpically favourable (negative  $\Delta H$  values) and that the enthalpy of binding is the major driving force in the association (i.e., both proteins exhibit large, negative  $\Delta H^0$  values). Although the I71V mutation involves the removal of

a methyl group resulting in the loss of interactions with the ligand and therefore less tight binding, the enthalpy indicates that bonds formed when the ligand binds I71V hGST A1-1 are stronger than when binding wildtype hGST A1-1. There may be less interactions occurring in I71V hGST A1-1 binding but the bonds formed are tighter and this contributes towards the more negative  $\Delta H$ .

Entropy is viewed as the amount of freedom a system possesses to explore available conformational space. The major contributors to the entropy of binding are changes in conformational degrees of freedom ( $\Delta S_{\text{conf}}$ ) and changes in solvation ( $\Delta S_{\text{solv}}$ ) (Murphy, 1999). Given the large number of rotatable bonds compared to the total number of non-hydrogen atoms in a molecule of *S*-hexylglutathione, the free inhibitor is not conformationally constrained. The binding of *S*-hexylglutathione to hGST A1-1 would incur a high entropic penalty, because the highly flexible inhibitor will undergo a loss of conformational entropy upon complex formation (Kuhnert *et al.*, 2005). In order for the overall entropy change to contribute favourably to the binding, liberation of solvent molecules bound to the surface of the ligand and/or the binding site of the macromolecule must occur to an extent sufficiently high to overcome the entropy changes for the ligand and the macromolecule (Sigurskjold *et al.*, 1991).

The entropy term ( $T\Delta S$ ) at 25°C of *S*-hexylglutathione binding to wildtype hGST A1-1 (-19kJ/mol) (Kuhnert *et al.*, 2005) is largely more favourable than that of I71V hGST A1-1 (-63kJ/mol). The entropic advantage of complex formation with the wildtype protein could be due to greater desolvation of the active site (Kuhnert *et al.*, 2005). This would therefore imply that due to the I71V mutation there is less desolvation at the active site resulting in unfavourable entropy values. The unfavourable entropic costs of *S*-hexylglutathione binding to I71V hGST A1-1 (at temperatures higher than 10 °C) probably reflects the degree of immobilisation of the ligand, thus decreasing its flexibility and increasing its rigidity at the active site. It is also possible that the mutation results in a flexible protein being more ordered. The overall effect of the removal of the methyl group from the side chain of Ile71 is that the mutation is entropically destabilising but enthalpically stabilising at increasing temperatures. The presence of the Ile71 residue

found near the active site therefore stabilises wildtype hGST A1-1 entropically. At higher temperatures the unfavourable  $\Delta S$  are compensated for by favourable  $\Delta H$ .

Coupling of proton exchange to a binding event is a consequence of change in protonation state of groups on the protein and/or ligand upon complex formation (Brokx *et al.*, 2001). Previous studies by Kolobe (Kolobe *et al.*, 2004) showed that binding of Bromosulphophthalein to either site of hGST A1-1 is not coupled to any proton linkage effects and thus the experimentally measured enthalpy is the true enthalpy of binding, i.e.,  $\Delta H_{\text{obs}} = \Delta H_{\text{bind}}$ . The results indicated that the binding ITC only yields information on the energetics of ligand binding and the nature of the binding site (Kolobe *et al.*, 2004).

By performing identical experiments at different temperatures (5 – 25<sup>0</sup>C) it is possible to measure the heat capacity change ( $\Delta C_p$ ) of protein-ligand binding reactions. The  $\Delta C_p$  at constant pressure is defined as the temperature derivative of one of the basic thermodynamic parameters that describes the state of a macroscopic system, namely, the enthalpy (Makhatadze *et al.*, 1995). Heat capacity changes observed in protein unfolding experiments have been correlated to changes in solvent-accessible surface area and it has been shown that the heat capacity changes are directionally proportional to the difference in solvent accessible non-polar surface area between native and unfolded states (Spolar *et al.*, 1989; Livingstone *et al.*, 1991). It has long been said that the basis for the  $\Delta C_p$  observed in protein-ligand binding is related to the changes in the solvation of the protein and ligand during the binding process (Sturtevant, 1977; Eftink *et al.*, 1991). The temperature dependence studies yielded a  $\Delta C_p$  value of  $-1.71$  kJ/mol/K (Kuhnert *et al.*, 2005) for wildtype and  $-2.12$  kJ/mol/K for I71V hGST A1-1. The negative  $\Delta C_p$  is a good indicator of changes in hydrophobic interactions with binding, being negative if hydrophobic bonds are formed and positive if they are broken (Luque *et al.*, 1998). A negative  $\Delta C_p$  can be expected for the reduction of solvent access to non-polar surfaces (Loladze *et al.*, 2001). The binding processes observed for wildtype and I71V hGST A1-1 are characteristic of a binding process driven by the gain in solvent entropy associated with the burial of solvent-accessible hydrophobic surface area. The  $\Delta\Delta C_p = -0.41$  kJ/mol/K suggests the burial of solvent-accessible non-polar surface area occurs to a

larger extent in I71V hGST A1-1 than in wildtype hGST A1-1 since the more negative the  $\Delta C_p$  the more non-polar surface area becomes buried (Sturtevant, 1977; Spolar *et al.*, 1989; Livingstone *et al.*, 1991). A possible explanation for the result is that the I71V mutation involves the removal of a methyl group and therefore the introduction of a cavity into the hydrophobic core that could result in a better fit of the ligand into the active site. An alternate explanation is that there is a ligand induced conformational change in the protein, which results in more van der Waals contacts, a decrease in  $\Delta S$ , and an increase in the non-polar surface being buried.

#### 4.7 Conclusion

A topologically conserved isoleucine residue in hGST A1-1 was truncated by the removal of one methyl group with the mutation of Ile71  $\rightarrow$  Val. The detailed structure at the site of the mutation is unknown, however the non-disruptive nature of the mutation was confirmed by the absence of any significant changes in the proteins global structural properties. Any changes to the arrangement of side-chain residues to accommodate the formation of the cavity were small since the fluorescence emission wavelengths were similar to those of wildtype hGST A1-1 for both excitation at 280 nm and 295 nm. Intensity of the spectra were identical for excitation at 280 nm and for CD spectra with only a small increase in intensity upon denaturation of the I71V mutant when excited at 295 nm. The monomeric molecular mass was determined to be the same as the wildtype (26 kDa). Although non-disruptive to the global structure of hGST A1-1, the I71V mutation greatly increased the activity of the enzyme. The mutation also resulted in a decrease in the stability of the protein, which is expected due to the removal of the methyl group, however the decrease in stability was larger than predicted. This tells us that the Ile71 residue is important in the stability of the protein as well as in the cooperativity of folding.

The mutation had a noticeable impact on the kinetics of the enzyme with an increase in the values for all kinetic parameters determined, for both substrates, namely GSH and CDNB. Results showed that the mutation had a negative impact on substrate binding and a positive impact on the catalysis of the enzyme as seen by the increase in specific activity as well as an increase in the  $k_{cat}$  and  $k_{cat}/K_m$  values. A possible explanation for the

increase in specific activity is that the mutation helps to stabilise the transition state thereby allowing for a more efficient enzyme. The mutation could also have resulted in a more open active site therefore affecting the on/off rates of substrate binding.

Changes in the thermodynamic parameters were also observed due to the incorporation of the mutation. The  $K_d$  indicates a tighter binding of the substrate, *S*-hexylglutathione, to wildtype hGST A1-1. The binding enthalpy and entropy of the binding reaction suggested that although there may be less interactions occurring in I71V hGST A1-1, the bonds formed are tighter thus contributing towards the more negative  $\Delta H$ . The change in heat capacity of I71V hGST A1-1 when compared to the wildtype suggests the burial of solvent-exposed non-polar surface area occurs to a larger extent in I71V hGST A1-1 than in wildtype hGST A1-1 since the more negative the change in heat capacity the more non-polar surface area becomes buried

Although Ile71 is not directly involved in catalysis, its presence serves an important role nonetheless. The data suggests that Ile71 conservation is for the stability of the protein as well as playing a pivotal indirect role in catalysis and substrate binding.

## CHAPTER 5 REFERENCES

Allardyce, C.S., McDonagh, P.D., Lian, L., Wolf, C.R. and Roberts, G.C.K. (1999) The role of tyrosine-9 and the C-terminal helix in the catalytic mechanism of Alpha class glutathione S-transferases. *Biochem. J.* 343, 525-531

Anfinsen, C.B. (1973) Principles that govern the folding of protein chains. *Science* 181, 223-230

Armstrong, R.N. (1997) Structure, catalytic mechanism, and evolution of the glutathione transferases. *Chem. Res. Toxicol* 10, 2-18

Baldwin, E.P., Hajiseyedjavadi, O., Baase, W. A. and Matthews, B.W. (1993) The role of backbone flexibility in the accommodation of variants that repack the core of T4 lysozyme. *Science* 262, 1715-1718

Behe, M.J., Lattman, E.E. and Rose, G.D. (1991) The protein-folding problem: The native fold determines packing, but does packing determine the native fold? *Proc. Natl. Acad. Sci. U S A* 88, 4195-4199

Bico, P., Chen, C.Y., Jones, M., Erhardt, J. and Dirr, H. (1994) Class pi glutathione S-transferase: Meisenheimer complex formation. *Biochem. Mol. Biol. Int.* 33, 887-892

Bjornestedt, R., Stenberg, G., Widersten, M., Board, P.G., Sinning, I., Jones, T.A. and Mannervik, B. (1995) Functional significance of arginine 15 in the active site of human class Alpha glutathione transferase A1-1. *J. Mol. Biol.* 247, 765-773

Board, P.G. and Mannervik, B. (1991) The contribution of the C-terminal sequence to the catalytic activity of GST2, a human alpha class glutathione transferase. *Biochem. J.* 275, 929-935

Bousset, L., Belrhali, H., Melki, R., and Morera, S. (2001) Crystal structures of the yeast prion Ure2p functional region in complex with glutathione and related compounds. *Biochemistry* 40, 13564-13573

Bowie, J.U., Reidhaar-Olson, J.F., Lim, W.A. and Sauer, R.T. (1990) Deciphering the message in protein sequences: Tolerance to amino acid substitutions. *J. Mol. Biol.* 307, 721-735

Brokx, R.D., Lopez, M.M., Vogel, H.J. and Makhatadze, G.I. (2001) Energetics of target peptide binding by calmodulin reveals different modes of binding. *J. Biol. Chem.* 276, 14083-14091

Buckle, A.M., Cramer, P. and Fersht, A.R. (1996) structural and energetic responses to cavity-creating mutations in hydrophobic cores: Observation of a buried water molecule and the hydrophobic nature of such hydrophobic cavities. *Biochemistry* 35, 4298-4305

Cameron, A.D., Sinning, I., L'Hermite, G., Olin, B., Board, P.G., Mannervik, B., Jones, T.A. (1995) Structural analysis of human Alpha class glutathione transferase A1-1 in the apo-form and in complex with ethacrynic acid and its glutathione conjugate. *Structure* 3, 717-727

Di Nardo, A.A., Larson, S.M. and Davidson, A.R. (2003) The relationship between conservation, thermodynamic stability, and function in the SH3 domain hydrophobic core. *J. Mol. Biol.* 333 (3), 641-655

Dill, K.A. (1990) Dominant forces in protein folding. *Biochemistry* 29 (31), 7133-7151

Dill, K.A., Bromberg, S., Yue, K., Fiebig, K.M., Yee, D.P., Thomas, P.D. and Chan, H.S. (1995) Principles of protein folding: a perspective from simple exact models. *Protein Sci.* 4, 561-602



Dirr, H., Reinemer, P., and Huber, R. (1994) X-ray crystal structures of cytosolic glutathione S-transferases. Implications for protein architecture, substrate recognition and catalytic function. *Eur. J. Biochem.* 220, 645-661

Dirr, H.W., Little, T., Kuhnert, D.C. and Sayed, Y. (2005) A conserved N-capping motif contributes significantly to the stabilisation and dynamics of the C-terminal region of class Alpha glutathione transferases. *J. Biol. Chem* 280, 19480-19487

Dobson, C.M. and Karplus, M. (1999) The fundamentals of protein folding: bringing together theory and experiment. *Curr. Opin. Struct. Biol.* 9, 92-101

Eftink, M.R. and Anusiem, A.C. (1991) Fluorescence techniques for studying protein structure. *Methods Biochem. Anal.* 35, 127-205

Erhardt, J. and Dirr, H. (1995) Native dimer stabilizes the subunit tertiary structure of porcine class pi glutathione S-transferases. *Eur. J. Biochem.* 230, 614-620

Eriksson, A.E., Baase, W.A., Zhang, X.J., Heinz, D.W., Blaber, M., Baldwin, E.P., Matthews, B.W. (1992) Response of a protein structure to cavity-creating mutations and its relation to the hydrophobic effect. *Science* 255, 178-183

Fersht, A.R. (1997) Nucleation mechanisms in protein folding. *Curr. Opin. Struct. Biol.* 7, 3-9

Fersht, A.R. (1999) Structure and mechanisms in protein science: a guide to enzyme catalysis and protein folding. *W. H. Freeman and co, New York*

Friedberg, I. and Margalit, H. (2001) Persistently conserved positions in structurally similar, sequence dissimilar proteins: Roles in preserving protein fold and function. *Protein Sci.* 11, 350-360

Graminski, G.F., Zhang, P.H., Sesay, M.A., Ammon, H.L. and Armstrong, R.N. (1989) Formation of the 1-(S-glutathionyl)-2,4,6-trinitrocyclohexadienate anion at the active site of glutathione S-transferase: evidence for enzymic stabilization of sigma-complex intermediates in nucleophilic aromatic substitution reactions. *Biochemistry* 28, 6252-6258.

Green, R.F. and Pace, C.N. (1974) Urea and guanidine hydrochloride denaturation of ribonuclease, lysozyme,  $\alpha$ -chymotrypsin and  $\beta$ -lactoglobulin. *J. Biol. Chem.* 249, 5388-5393

Guex, N. and Peitsch, M.C. (1997) SWISS-MODEL and the Swiss-Pdb Viewer: an environment for comparative protein modeling. *Electrophoresis* 18, 2714-2723

Habig, W.H. and Jakoby, W.B. (1981) Assays for differentiation of glutathione S-transferases. *Methods Enzymol.* 77, 398-405

Harrop, S.J., DeMaere, M.Z., Fairlie, W.D., Reztsova, T., Valenzuela, S.M., Mazzanti, M., Tonini, R., Qiu, M.R., Jankova, L., Warton, K., Bauskin, A.R., Wu, W.M., Pankhurst, S., Campbell, T.J., Breit, S.N. and Curmi, P.M. (2001) Crystal structure of a soluble form of the intracellular chloride ion channel CLIC1 (NCC27) at 1.4-Å resolution. *J. Biol. Chem* 276, 44993-45000

Holmgren, A., Soderberg, B.O., Eklund, H. and Branden, C.I. (1975) Three-dimensional structure of Escherichia coli thioredoxin-S2 to 2.8 Å resolution. *Proc. Natl. Acad. Sci. USA* 72 (6), 2305-2309

Hornby, J.A., Luo, J.K., Stevens, J.M., Wallace, L.A., Kaplan, W., Armstrong, R.N. and Dirr, H. (2000) Equilibrium folding of dimeric class mu glutathione transferases involves a stable monomeric intermediate. *Biochemistry* 39, 12336-12344

Ji, X., Zhang, P., Armstrong, R. N. and Gilliland, G.L. (1992) A three-dimensional structure of a glutathione S-transferase from the Mu gene class. Structural analysis of the

binary complex of isoenzyme 3-3 and glutathione at 2.2 Å resolution. *Biochemistry* 31, 10169-10184

Kaplan, W., Husler, P., Klump, H., Erhardt, J., Sluis-Cremer, N. and Dirr, H. (1997) Conformational stability of pGEX-expressed *Schistosoma japonicum* glutathione S-transferase: a detoxification enzyme and protein affinity tag. *Protein Sci.* 6, 399-406

Kellis, J.T., Nyberg, K., Sali, D. and Fersht, A.R. (1988) Contribution of hydrophobic interactions to protein stability. *Nature* 333, 784-786

Kirk, W.R., Kurian, E. and Prendergast, F.G. (1996) Characterization of the sources of protein-ligand affinity: 8-anilino-1-naphthalene sulphonate binding to intestinal fatty acid binding protein. *Biophys. J.* 70, 69-83

Kolm, R.H., Sroga, G.E. and Mannervik, B. (1992) Participation of the phenolic hydroxyl group of Tyr-8 in the catalytic mechanism of human glutathione transferase P1-1. *Biochem. J.* 285, 537-540

Kolobe, D., Sayed, Y. and Dirr, H.W. (2004) Characterisation of bromosulphophthalein binding to human glutathione transferase A1-1: thermodynamics and inhibition kinetics. *Biochem. J.* 382, 703-709

Kuhnert, C.D., Sayed, Y., Mosebi, S., Sayed, M., Sewell, T. and Dirr, H.W. (2005) Tertiary interactions stabilise the C-terminal region of human glutathione transferase A1-1: a crystallographic and calorimetric study. *J. Mol. Biol.* 349, 825-838

Ladner, J.E., Parsons, J. F., Rife, C. L., Gilliland, G.L. and Armstrong, R.N. (2004) Parallel Evolutionary Pathways for Glutathione Transferases: Structure and Mechanism of the Mitochondrial Class Kappa Enzyme Rgstk1-1. *Biochemistry* 43 (352)

Laemmli, U.K. (1970) Cleavage of structural proteins during the assembly of the head of bacteriophage T4. *Nature* 227, 680-685

- Lakowicz, J.R. (1983) Principles of fluorescence spectroscopy. *Plenum Press, New York*
- Lakowicz, J.R. (1999) Principles of fluorescence spectroscopy. *Plenum Press, New York.*
- Levinthal, C. (1968) Are there pathways for protein folding? *J. Chim. Phys.* 65, 44-45
- Lim, W.A. and Sauer, R.T. (1989) Alternative packing arrangements in the hydrophobic core of lambda repressor. *Nature* 339, 31-36
- Livingstone, J.R., Spolar, R.S. and Record, M.T., Jr. (1991) Contribution to the thermodynamics of protein folding from the reduction in water-accessible nonpolar surface area. *Biochemistry* 30, 4237-4244
- Loladze, V.V., Ermolenko, D.N. and Makhatadze, G.I. (2001) Heat capacity changes upon burial of polar and nonpolar groups in proteins. *Protein Sci.* 10, 1343-1352
- Lumry, R. and Rajender, S. (1970) Enthalpy-entropy compensation phenomena in water solutions of proteins and small molecules: a ubiquitous property of water. *Biopolymers* 9, 125-1227
- Luque, I. and Freire, E. (1998) Structure-based prediction of binding affinities and molecular design of peptide ligands. *Methods Enzymol.* 295, 100-127
- Makhatadze, G.I. and Privalov, P.L. (1995) Energetics of protein structure. *Adv. Protein Chem.* 47, 307-425
- Mannervik, B. and Danielson, U.H. (1988) Glutathione Transferases: structure and catalytic activity. *CRC Crit. Rev. Biochem.* 23, 283-337
- Martin, J.L. (1995) Thioredoxin - a fold for all reasons. *Structure* 3, 245-250

- Matulis, D. and Lovrien, R. (1998) 1-Anilino-8-naphthalene sulfonate anion-protein binding depends primarily on ion pair formation. *Biophys. J.* 74, 422-429
- Michnick, S.W. and Shakhnovich, E. (1998) A strategy for detecting the conservation of folding-nucleus residues in protein superfamilies. *Folding and Design* 3, 239-251
- Milla, M.E., Brown, B.M. and Sauer, R.T. (1994) Protein stability effects of a complete set of alanine substitutions in Arc repressor. *Nat. Struct. Biol.* 1, 518-523
- Mirny, L. and Shakhnovich, E. (2001) Evolutionary conservation of the folding nucleus. *J. Mol. Biol.* 308, 123-129
- Mosebi, S., Sayed, Y., Burke, J. and Dirr, H.W. (2003) Residue 219 impacts on the dynamics of the C-terminal region in glutathione transferase A1-1: implications for stability and catalytic and ligandin functions. *Biochemistry* 42, 15329-15332
- Murphy, K.P. (1999) Predicting binding energetics from structure: looking beyond  $\Delta G$  degrees. *Med. Res. Rev.* 19, 333-339
- Murzin, A.G., Brenner, S.E., Hubbard, T. and Chothia, C. (1995) SCOP: a structural classification of proteins database for the investigation of sequences and structures. *J. Mol. Biol.* 247, 536-540
- Myers, J.K., Pace, C.N. and Scolz, J.M. (1995) Denaturant m-values and heat capacity changes: relation to changes in accessible surface areas of protein folding. *Protein Sci.* 4, 2138-2148
- Nathaniel, C., Wallace, L.A., Burke, J. and Dirr, H.W. (2003) The role of an evolutionarily conserved cis-proline in the thioredoxin-like domain of human class Alpha glutathione transferase A1-1. *Biochem. J.* 372, 241-246

Nilsson, L.O., Edalat, M., Pettersson, P.L. and Mannervik, B. (2002) Aromatic residues in the C-terminal region of glutathione transferase A1-1 influence rate-determining steps in the catalytic mechanism. *Biochem. Biophys. Acta.* 1597, 157-163

Ortiz-Salmeron, E., Nuccetelli, M., Oakley, A.J., Parker, M.W., Lo, B.M. and Garcia-Fuentes, L. (2003) Thermodynamic description of the effect of the mutation Y49F on human glutathione transferase P1-1 in binding with glutathione and the inhibitor S-hexylglutathione. *J. Biol. Chem* 278, 46938-46948

Ortiz-Salmeron, E., Yassin, Z., Clemente-Jimenez, M.J., Las Heras-Vazquez, F.J., Rodriguez-Vico, F., Baron, C. and Garcia-Fuentes, L. (2001) A calorimetric study of the binding of S-alkylglutathiones to glutathione S-transferase. *Biochim. Biophys. Acta* 1548, 106-113

Pace, C.N. (1986) Determination and analysis of urea and guanidine hydrochloride denaturation curves. *Methods Enzymol.* 131, 266-280

Pace, C.N., Shirley, B.A., and Thomson, J.A. (1989) Measuring the conformational stability of a protein. In Protein Structure: a Practical Approach.(Creighton, T.E. ed). *IRL Press, Oxford University Press, Oxford*, pp. 311-330

Pande, V.S., Grosberg, A.Y., Tanaka, T. and Rokhsar, D.S. (1998) Pathways for protein folding: is a new view needed? *Curr. Opin. Struct. Biol.* 8, 68-79

Perkins, S.J. (1986) Protein volumes and hydration effects. The calculations of partial specific volumes, neutron scattering matchpoints and 280-nm absorption coefficients for proteins and glycoproteins from amino acid sequences. *Eur. J. Biochem.* 157, 169-180

Plaxco, K.W., Larson, S., Ruczinski, I., Riddle, D.S., Thayer, E.C., Buchwitz, B., Davidson, A.R. and Baker, D. (2000) Evolutionary conservation in protein kinetics. *J. Mol. Biol.* 298, 303-312

Reinemer, P., Dirr, H.W., Ladenstein, R., Schaffer, J., Gallay, O. and Huber, R. (1991) The three-dimensional structure of class pi glutathione S-transferase in complex with glutathione sulfonate at 2.3 Å resolution. *EMBO J.* 10, 1997-2005

Rennell, D., Bouvier, S.E., Hardy, L.W. and Poteete, A.R. (1991) Systematic mutation of bacteriophage T4 lysozyme. *J. Mol. Biol.* 222, 67-88

Richards, F.M. (1977) Areas, volumes, packing density and protein structure. *Annu. Rev. Biophys. Bioeng.* 6, 151-175

Sacchetta, P., Aceto, A., Bucciarelli, T., Dragani, B., Santarone, S., Allocati, N. and Di Ilio, C. (1993) Multi phasic denaturation of glutathione transferase B1-1 by guanidinium chloride: role of the dimeric structure on the flexibility of the active site. *Eur. J. Biochem.* 215, 741-745

Sali, A. and Blundell, T.L. (1990) Definition of general topological equivalence in protein structures. A procedure involving comparison of properties and relationships through simulated annealing and dynamic programming. *J. Mol. Biol.* 212, 403-428

Sayed, Y., Hornby, J.A., Lopez, M. and Dirr, H. (2002) Thermodynamics of the ligandin function of human class Alpha glutathione transferase A1-1: energetics of organic anion ligand binding. *Biochem. J.* 363, 341-346

Sayed, Y., Wallace, L.A. and Dirr, H.W. (2000) The hydrophobic lock-and-key intersubunit motif of glutathione transferase A1-1: implications for catalysis, ligandin function and stability. *FEBS Lett.* 465, 169-172

Sheehan, D., Meade, G., Foley, V.M. and Dowd, C.A. (2001) Structure, function and evolution of glutathione transferases: implications for classification of non-mammalian members of an ancient enzyme superfamily. *Biochem. J.* 360, 1-16

Sigurskjold, B.W., Altman, E. and Bundle, D.R. (1991) Sensitive titration microcalorimetric study of the binding of Salmonella O-antigenic oligosaccharides by a monoclonal antibody. *Eur. J. Biochem.* 197, 239-246

Sinning, I., Kleywegt, G.J., Cowan, S.W., Reinemer, P., Dirr, H.W., Huber, R., Gilliland, G.L., Armstrong, R.N., Ji, X., Board, P.G., Olin, B., Mannervik, B. and Jones, T.A. (1993) Structure determination and refinement of human Alpha class glutathione transferase A1-1, and a comparison with the Mu and Pi class enzymes. *J. Mol. Biol.* 232, 192-212

Soulages, J.L. (1998) Chemical denaturation: potential impact of undetected intermediates in the free energy of unfolding and m-values obtained from a two-state assumption. *Biophys. J.* 75, 484-492

Spolar, R.S., Ha, J.H. and Record, M.T., Jr. (1989) Hydrophobic effect in protein folding and other noncovalent processes involving proteins. *Proc. Natl. Acad. Sci. USA* 86, 8382-8385

Stenberg, G., Björnstedt, R. and Mannervik, B. (1992) Heterologous expression of recombinant human glutathione transferase A1-1 from a hepatoma cell line. *Protein Exp. Purif.* 3, 80-84

Stenberg, G., Board, P.G. and Mannervik, B. (1991) Mutation of an evolutionarily conserved tyrosine residue in the active site of a human class Alpha glutathione transferase. *FEBS Lett.* 293, 153-155

Stevens, J.M., Hornby, J.A.T., Armstrong, R.N. and Dirr, H.W. (1998) Class Sigma glutathione transferase unfolds via a dimeric and a monomeric intermediate: impact of subunit interface on conformational stability in the superfamily. *Biochemistry* 37, 15534-15541



Stryer, L. (1965) The interaction of a naphthalene dye with apomyoglobin and apohemoglobin. A fluorescent probe of non-polar binding sites. *J. Mol. Biol.* 13, 482-495

Sturtevant, J.M. (1977) Heat capacity and entropy changes in processes involving proteins. *Proc. Natl. Acad. Sci. USA* 74, 2236-2240

Suckow, J., Markeiwicz, P., Kleina, L.G., Miller, J., Kisters-Woike, B. and Muller-Hill, B. (1996) Genetic studies of the Lac repressor, XV:4000 single amino acid substitutions and analysis of the resulting phenotypes on the basis of the protein structure. *J. Mol. Biol.* 261, 509-523

Ventura, S. and Serrano, L. (2004) Designing proteins from the inside out. *Proteins* 56, 1-10

Wallace, L.A., Blatch, G.L. and Dirr, H.W. (1998a) A topologically conserved aliphatic residue in alpha-helix 6 stabilizes the hydrophobic core in domain II of glutathione transferases and is a structural determinant for the unfolding pathway. *Biochem. J.* 336, 413-418

Wallace, L.A. and Dirr, H.W. (1999) Folding and assembly of dimeric human glutathione transferase A1-1. *Biochemistry* 38, 16686-16694

Wallace, L.A., Sluis-Cremer, N. and Dirr, H.W. (1998b) Equilibrium and kinetic unfolding properties of dimeric human glutathione transferase A1-1. *Biochemistry* 37, 5320-5328

Wang, R.W., Newton, D.J., Huskey, S.E.W., McKeever, B., Pickett, C.B. and Lu, A.Y. (1992) Site-directed mutagenesis of glutathione S-transferase YaYa. Important roles in tyrosine 9 and aspartic acid 101 in catalysis. *J. Biol. Chem* 267, 19866-19871

Wilce, M.C. and Parker, M.W. (1994) Structure and function of glutathione S-transferases. *Biochem. Biophys. Acta.* 1205, 1-18

Winder, A.F. and Gent, W.L. (1971) Correction of light-scattering errors in spectrophotometric protein determinations. *Biopolymers* 10, 1243-1251

Wiseman, T., Williston, S., Brandts, J.F. and Lin, L.N. (1989) Rapid measurement of binding constants and heats of binding using a new titration calorimeter. *Anal. Biochem.* 179, 131-137

Woody, R.W. (1995) Circular dichroism. *Methods Enzymol.* 246, 34-71

Xia, B., Vlamis-Gardikas, A., Holmgren, A., Wright, P.E. and Dyson, H.J. (2001) Solution structure of *Escherichia coli* glutaredoxin-2 shows similarity to mammalian glutathione-S-transferases. *J. Mol. Biol.* 310, 907-918